

DOKUZ EYLÜL UNIVERSITY
GRADUATE SCHOOL OF NATURAL AND APPLIED SCIENCES

**GEOHERMIC STUDIES AND NUMERICAL
MODELING HEAT TRANSFER IN WESTERN
TURKEY**

by

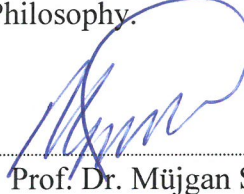
Elif BALKAN

March, 2017

İZMİR

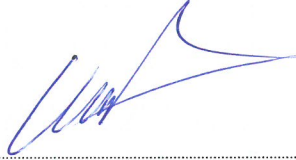
Ph.D. THESIS EXAMINATION RESULT FORM

We have read the thesis entitled “GEOTHERMIC STUDIES AND NUMERICAL MODELING OF HEAT TRANSFER IN WESTERN TURKEY” completed by **ELİF BALKAN** under supervision of **PROF. DR. MÜJGAN ŞALK** and we certify that in our opinion it is fully adequate, in scope and in quality, as a thesis for the degree of Doctor of Philosophy.



Prof. Dr. Müjgan ŞALK

Supervisor



Prof. Dr. Ünsal GEMİCİ

Thesis Committee Member



Prof. Dr. Gökhan GÖKTÜRLER

Thesis Committee Member



Prof. Dr. M. Nuri DOLMAZ

Examining Committee Member



Doç. Dr. Kamil ERKAN

Examining Committee Member



Prof. Dr. Emine İlknur CÖCEN
Director

Graduate School of Natural and Applied Sciences

**GEOHERMIC STUDIES AND NUMERICAL
MODELING HEAT OF TRANSFER IN WESTERN
TURKEY**

**A Thesis Submitted to the
Graduate School of Natural and Applied Sciences of Dokuz Eylül University
In Partial Fulfillment of the Requirements for the Degree of Doctor of
Philosophy in Geophysical Engineering**

by

Elif BALKAN

March, 2017

İZMİR

ACKNOWLEDGMENTS

This PhD thesis was completed with the great supports and helps of many people over the years. I would like to express my most heartfelt thanks to the following people.

First and foremost, I would like to express my deepest gratitude and special thanks to my advisor, Prof. Dr. Mjgan ŐALK for her valuable guidance, full support, motivation, endless patience at every stage throughout the study. Since the first day of my thesis I have learnt inestimable views from her for not only academic career but also my personal future.

I would like to express my gratefulness and thanks to Assoc. Prof. Dr. Kamil Erkan by heart. Without his support, wide knowledge, constructive feedback expertise and limitless patience, it would have been difficult for me to complete my thesis. It is always pleasure for me to work with him.

I would like to thank my thesis committee members, Prof. Dr. nsal GEMİCİ and Prof. Dr. Gkhan GKTRKLER. Their vast knowledge and insightful comments have guided me during my PhD study. I am really indebted to Prof. Dr. Gkhan GKTRKLER for his constructive criticisms about this study.

I really appreciate to Prof. Dr. O. Metin İLKİŐİK who introduced me heat flow studies and shared his valuable heat flow data set which constituted the starting point of this thesis. I am also thankful to Prof. Dr. A. Bahadır YAVUZ for helping me by providing all opportunities in his laboratory.

I am also grateful to geophysical engineer Cafer CIKCIK at State Hydraulic Works for providing well data for temperature-depth measurements.

I want to thank to the researchers Assoc. Prof. Dr. Bülent AKKOYUNLU and Mustafa Orkun İNAL who worked together during fieldworks as a part of TÜBİTAK project with the number of 113R019.

At last but not least, I would like to express my gratitude and special thanks to my wonderful family for their unlimited support and help with ultra-patience at every stage throughout the study.

This thesis is sported by research projects grants from the Scientific and Technical Research Council of Turkey (TÜBİTAK) No 113R019 and from Dokuz Eylül University, Graduate School of Natural and Applied Sciences, No. 2014.KB.FEN.022. I would like to thank the all researchers of TÜBİTAK project for sharing me collected data set.

Elif BALKAN

GEOHERMIC STUDIES AND NUMERICAL MODELING OF HEAT TRANSFER IN WESTERN TURKEY

ABSTRACT

The aim of this PhD thesis is to contribute to the understanding of the thermal state of western Turkey and its relationship to geology and regional tectonics. For this purpose new heat flow data are collected and combined with previously published data to obtain heat flow map of western Turkey. The completed investigations include temperature-depth measurements in wells, calculation geothermal gradient, evaluation thermal conductivity of major rock types, and determination of heat flow values. Analysis of these data sets after appropriate corrections yields us better picture of the regional distribution of subsurface temperature and heat flow within the study area. The mean thermal conductivity values for sedimentary, igneous and metamorphic rocks are computed for the entire study area as 2.43 ± 1.5 , 1.86 ± 0.7 and 3.08 ± 0.76 W/m/K. Statistical analysis shows that the range of the thermal conductivity values observed for sedimentary rocks is too wide to assign a constant thermal conductivity for heat flow and thermal modeling studies. The average conductive geothermal gradient and heat flow value are calculated to be 38 ± 12 °C/km and 74 ± 26 mW/m/m respectively in western Turkey.

In addition, finite elements method is used to calculate 2D steady-state temperature distribution and surface heat flow component induced by conductive heat transport for Gediz and Büyük Menderes grabens. Model predictions of Gediz graben are validated against the temperature measurements in two deep wells. The calculated surface heat flow values are in accordance with the regional heat flow trend in the regions. The significantly heat flow variations at the edges of grabens are resulted from the thermal conductivity contrast between the basement rock and sedimentary graben fill.

Keywords: Heat flow, geothermal gradient, thermal conductivity, numerical thermal modeling, Western Turkey

BATI TÜRKİYE'DEKİ JEOTERMİK ÇALIŞMALAR VE ISI TRANSFERİNİN SAYISAL MODELLENMESİ

ÖZ

Bu doktora tezinin amacı, Batı Türkiye'nin termal yapısının anlaşılmasına ve bunun bölgenin jeolojisi ve rejyonel tektoniği ile ilişkisine katkıda bulunmaktır. Bu amaçla, yeni toplanan ısı akısı veri seti önceden yayımlanmış veri seti ile birleştirilerek Batı Türkiye için bir ısı akısı haritası hazırlanmıştır. Tez süresi boyunca tamamlanan araştırmalar sondajlardan alınan sıcaklık-derinlik ölçümleri, sıcaklık gradyanı hesaplamaları, yaygın kayalara ait ısı iletim katsayılarının elde edilmesi ve ısı akısı değerlerinin belirlenmesini kapsamaktadır. Uygun düzeltmelerin ardından bu veri setinin analizi bize çalışma alanındaki bölgesel sıcaklık ve ısı akısı dağılımının daha iyi bir resmini vermiştir. Sonuçlarımıza göre bölgedeki sedimanter, magmatik ve volkanik kayaların ısı iletim katsayıları sırasıyla $2,43 \pm 1,4$, $1,86 \pm 0,7$ ve $3,08 \pm 0,76$ (W/m/K) olarak hesaplanmıştır. İstatistiksel analizler göstermiştir ki, gözlemlenen sedimanter kayaların ısı iletim katsayıları geniş bir değişim aralığına sahiptir. Bu nedenle ısı akısı ve modelleme çalışmalarında sıklıkla kullanılan sedimanter kayalar için sabit bir ısı iletim katsayısı kullanmak doğru değildir. Ayrıca Batı Türkiye için ortalama jeotermal gradyan ve ısı akısı değeri 38 ± 12 °C/km ve 74 ± 26 mW/m/m olarak hesaplanmıştır.

Bu çalışmalara ek olarak, Gediz ve Büyük Menderes grabenlerindeki konduktif ısı transferinin sebep olduğu, 2B kararlı-hal yeraltı sıcaklık dağılım ve yüzey ısı akısı bileşenleri sonlu elemanlar yöntemi kullanılarak hesaplanmıştır. Gediz grabeninde elde edilen model sonuçları, derin iki kuyudan alınan sıcaklık ölçümleriyle kıyaslanarak doğrulukları denetlenmiştir. Hesaplanan yüzey ısı akısı değerlerinin ise bölgenin rejyonel ısı akısıyla uyumlu olduğu görülmüştür. Graben kenarlarında gözlenen belirgin ısı akısı değişimleri, taban kayaç ve sedimanter graben dolgusu arasındaki ısı iletim katsayısı farkından ileri gelmektedir.

Anahtar kelimeler: Isı akısı, jeotermal gradyan, ısı iletim katsayısı, sayısal termal modelleme, Batı Türkiye.

CONTENTS

	Page
THESIS EXAMINATION RESULT FORM	ii
ACKNOWLEDGEMENTS	iii
ABSTRACT	v
ÖZ	vi
LIST OF FIGURES	x
LIST OF TABLES	xiii
CHAPTER ONE - INTRODUCTION	1
1.1 Scope of Thesis	1
1.2 A Brief History and Present Status of the Geothermic Studies in Western Turkey and Surrounding Area	3
1.3 Original Contributions of the Thesis	16
1.4 Outline of the Thesis	17
CHAPTER TWO - GENERAL GEOLOGY AND TECTONIC SETTINGS....	19
2.1 Gediz Graben.....	24
2.2 Büyük Menderes Graben.....	30
CHAPTER THREE- GEOTHERMOMETRY	34
3.1 Chemical Geothermometers	34
3.1.1 Silica Geothermometer	35
3.1.2 Cation Geothermometers	36
3.1.2.1 Na-K Geothermometer.....	36
3.1.2.2 Na-K-Ca Geothermometer.....	37
3.1.2.3 Na-Li Geothermometer	38
3.1.2.4 K-Mg Geothermometer.....	38

3.2 Geothermometry Applications	38
3.2.1 Geothermometry Results	39
3.2.2 Heat Flow Estimation from Silica Geo-temperatures.....	43
CHAPTER FOUR-THERMAL CONDUCTIVITY	45
4.1 Thermal Conductivity of Rocks	45
4.1.1 Anisotropy	46
4.1.2 Porosity	46
4.1.3 Texture and Mineral Composition.....	48
4.1.4 Temperature	49
4.1.5 Pressure.....	51
4.2 Thermal Conductivity Data Set.....	52
4.3 Data Analysis	52
4.4 Results	55
4.5 Discussion	60
4.6 Conclusion.....	62
CHAPTER FIVE-GEOTHERMAL GRADIENT	63
5.1 Geothermal Gradient Data Set	67
5.2 Data Analysis	67
5.2.1 Data Quality Classification.....	67
5.2.1 Topography Correction.....	73
5.2.3 Temperature Depth (T-D) Curves	74
5.3 Results	79
5.4 Discussion	81
5.5 Conclusion.....	83

CHAPTER SIX - HEAT FLOW.....	84
6.1 Energy Sources of the Earth.....	84
6.2 Heat Transfer Mechanisms in the Earth.....	85
6.3 Conductive Heat Flow.....	86
6.3.1 Heat Conduction Equation.....	86
6.3.2 Radioactive Heat Production.....	90
6.4 Continental Heat Flow.....	91
6.5 Heat Flow Data Set.....	92
6.6 Results.....	94
6.7 Correction of Sedimentation and Thermal Refraction Effect.....	96
6.8 Discussion and Conclusion.....	98
CHAPTER SEVEN-THERMAL MODELING.....	101
7.1 Finite Elements Approximation to Heat Conduction Equation.....	102
7.2 Applications.....	106
7.2.1 Thermal Model of Gediz Graben.....	109
7.2.1.1 Thermal Modeling Results of Gediz Graben.....	113
7.2.2 Thermal Model of Büyük Menderes Graben.....	119
7.2.2.1 Thermal Modeling Results of Büyük Menderes Graben.....	121
7.3 Discussion and Conclusion.....	123
CHAPTER EIGHT-CONCLUSION.....	125
8.1 Future Research Recommendations.....	127
REFERENCES.....	128

LIST OF FIGURES

	Page
Figure 1.1 Heat flow map of Aegean Sea	4
Figure 1.2 The first heat flow map of Turkey	5
Figure 1.3 500 m depth temperature distribution map of Turkey	6
Figure 1.4 Heat flow distribution map of western Anatolia from silica temperatures. 8	8
Figure 1.5 Heat flow map of Turkey.....	9
Figure 1.6 The preliminary heat flow map of western Anatolia	11
Figure 2.1 Simplified tectonic map of Turkey including major neotectonic structures and neotectonic provinces	19
Figure 2.2 Geological map of western Turkey.....	21
Figure 2.3 Simplified stratigraphic charts of some western Anatolian grabens	22
Figure 2.4 Simplified geology map of Gediz graben and surrounding areas	25
Figure 2.5 Geological map of Gediz graben around Alaşehir major structures geological units, location of the boreholes and seismic profiles.....	26
Figure 2.6 Neogene stratigraphy of the Gediz Graben based on the geological data around Alaşehir	27
Figure 2.7 2-D seismic reflection profile (S-12) (a) Uninterpreted profile (b) with interpretation of seismic stratigraphic units. Thick black line depicts the subsurface continuation of MGBF and thinner black lines illustrate some secondary hanging-wall faults offsetting the stratigraphic units.....	29
Figure 2.8 Transverse geologic cross section of the Gediz graben.....	29
Figure 2.9 Geological map of the Büyük Menderes Graben	30
Figure 2.10 Simplified stratigraphic section of the Büyük Mendres graben basin ...	31
Figure 2.11 (a) Location of the seismic section (b) A transverse seismic profile in association with (c) The interpreted cross-section showing the sequence stratigraphic units	33
Figure 3.1 Quartz geothermometry results for western Turkey	40
Figure 3.2 Na-K geothermometry results for western Turkey.....	42
Figure 3.3 Na-K-Ca geothermometry results for western Turkey.....	42

Figure 3.4 Heat flow distribuion map for western Anatolia esimated from silica geotemperatures	43
Figure 4.1 Thermal conductivity of limestone	47
Figure 4.2 Thermal conductivity of sandstone as a function of porosity and pore fluid at ambient temperature and pressure	48
Figure 4.3 Relationship between quartz content and measured thermal conductivity of rocks	49
Figure 4.4 Simplified geological map of study area	54
Figure 4.5 Histograms for saturated samples from western Turkey	56
Figure 4.6 Geology and tectonic structures of western Turkey	59
Figure 4.7 Histogram of the all saturated thermal conductivity values	60
Figure 4.8 Histograms of data set of western Turkey	61
Figure 5.1 Linear Temperature-depth log of Kite from Bursa.....	64
Figure 5.2 T-D curve from eastern Kansas and generalized stratigraphy encountered in the hole.....	65
Figure 5.3 Intra-borehole effects a) up flow and b) down flow on temperature-depth curves	66
Figure 5.4 Effect of lateral flow on T-D curve	66
Figure 5.5 Data locations with the corresponding quality classes	69
Figure 5.6 Topography correction model.....	73
Figure 5.7 Temperature–depth (T–D) curves for Aydin, Kütahya and Uşak	75
Figure 5.8 Temperature–depth (T–D) curves for Balıkesir and Çanakkale.....	76
Figure 5.9 Temperature–depth (T–D) curves for İzmir	77
Figure 5.10 Temperature–depth (T–D) curves for Manisa	78
Figure 5.11 Histogram of geothermal gradients in the western Anatolia	79
Figure 5.12 Distribution of the geothermal gradients in western Anatolia.....	80
Figure 5.13 Contour map of geothermal gradient.....	82
Figure 6.1 Conductive transfer of heat through an infinitely long layer.....	86
Figure 6.2 Control volume for one-dimensional conduction.....	87
Figure 6.3 Heat flow versus heat production	91
Figure 6.4 Histogram of heat flow data located in study area.	94

Figure 6.5 Regional Distribution of new heat flow data together with the previous heat flow data form Pfister et al. (1998) and Erkan (2015).	96
Figure 6.6 Changes in the surface heat flow in Menderes Massif with increasing rate of sedimentation and erosion	97
Figure 6.7 Heat flow map of study area using the results of this study	100
Figure 7.1 Finite element modeling and shape functions for linear interpolation of temperature field	103
Figure 7.2 Histogram of heat flow in Menderes Massif	109
Figure 7.3 Transverse geological cross section of Gediz graben.....	110
Figure 7.4 The boreholes drilled in Gediz graben.....	111
Figure 7.5 a) Interpreted seismic reflection profile S-12 b) geological cross section of Gediz graben	112
Figure 7.6 Simplified thermal model of Gediz Graben.....	112
Figure 7.7 Measured and modeled temperatures for BH-1 and BH-1 with RMS values for the scenario A.....	114
Figure 7.8 Measured and modeled temperatures for BH-1 and BH-1 with RMS values for the scenario B	115
Figure 7.9 Measured and modeled temperatures for BH-1 and BH-1 with RMS values for the scenario C	115
Figure 7.10 a) Vertical distribution of temperature at the range (at 2 km) for each scenario b) vertical distrivution in the middle of the basin (at 11km) for the same varying q_b values	117
Figure 7.11 a) The calculated 2D subsurface temperature distribution for scenario (B) and b) surface heat flow variation for each scenario.....	118
Figure 7.12 a) Interpreted seismic reflection profile b) geological cross section of Büyük Mүйük Menderes graben	120
Figure 7.13 Simplified thermal model for Büyük Menderes graben	121
Figure 7.14 a) Calculated 2D subsurface temperature for Büyük Menderes Graben b) surface heat flow variation	122

LIST OF TABLES

	Page
Table 1.1 Summary of geothermic studies in Turkey	13
Table 3.1 Quartz geothermometry equations	36
Table 3.2 Cation geothermometry equations	37
Table 3.3 Measured BHTs and estimated reservoir temperatures for the wells located in the region.....	41
Table 4.1 Thermal conductivity of pore-filling fluids	47
Table 4.2 Thermal conductivity of some rock-forming minerals	49
Table 4.3 Correction models for temperature effects on thermal conductivity	51
Table 4.4 Numbers of the data for western Anatolia	54
Table 4.5 Thermal conductivity values for dry and saturated conditions in western Anatolia.....	56
Table 5.1 Definitions of the data quality classes	68
Table 5.2 Geothermal gradients evaluated in this study	70
Table 5.3 Geothermal gradient data reported in Erkan (2015)	71
Table 5.4 Geothermal gradient data reported in Pfister et al. (1998).....	72
Table 6.1 Class (A/B/C/D/G) type data used in this study along with gradients thermal conductivities heat flow values and their respective errors	93
Table 7.1 Scenarios for RHP distribution	108
Table 7.2 Thermal conductivity values in Gediz Graben model	113
Table 7.3 Calibrated model parameters for Gediz Graben	114
Table 7.4 Thermal conductivity values used in Büyük Menderes graben model	121

CHAPTER ONE

INTRODUCTION

1.1 Scope of Thesis

Geothermics, deals with the thermal state of the Earth's interior and heat transport mechanisms. Several processes that form the Earth's crust such as earthquakes, volcanoes, mountain building etc. are controlled by the transfer and generation of heat. Knowledge of the heat flow density on the Earth's surface allows us to predict thermal condition of the deeper parts which are not accessible for temperature measurements. There are several interfering factors make the direct heat flow measurement impossible. Thus heat flow can be determined by measuring vertical geothermal gradient along with thermal conductivity of related rock where the temperature measurements are taken.

Numerous studies show that surface heat flow can be affected by several reasons in the different regions on the Earth (Lee & Uyeda, 1965; Pollack & Chapman, 1977; Cermak & Rybach, 1979, Jaupart & Mareschal, 2007). Lithology, surface topography, ground water (cold or thermal) circulation, young volcanism, variable radiogenic heat generation content, mantle heat flow, sedimentation effect at basins, basement structure and tectonic activity are the most predominant factors. To find out their relative contribution to surface heat flow density and to characterize these process are therefore of special interest for recent geothermic studies. Many geological and geophysical studies have been applied in sedimentary basins due to their economic values in geothermal exploration. However, density of heat flow and temperature data is still very limited. If constrained by measured data and observations, numerical models help us to arrive at estimation about first order aspects and processes, despite the complexity of the problem at hands.

This thesis presents results of geothermic studies obtained from western Turkey which is one of the tectonically active continental regions in the world. Due to its intense plate tectonic activity the study area has mentioned with high heat flow

previous studies (Tezcan & Turgay, 1991; İlkışık, 1995; Erkan, 2015). Significant extension and relatively little volcanism are responsible for the thermal structure of the region. The bottom hole temperatures (BHTs) in geothermal wells reach up the 287 °C in Gediz graben and 247 °C in Büyük Menderes graben (Baba, 2012; Karakuş & Şimşek, 2012). Even though exploration based studies demonstrate that there is a significant geothermal resource base in western Turkey, conventional heat flow studies have been very limited in the region. In this study, the new heat flow data (Temperature-depth and thermal conductivity measurements) from western Turkey are collected. After correcting for effects of the ground water flow, sedimentation, erosion and paleo climatic changes, they are analyzed together with the published data for local and regional variations. Heat flow map of western Turkey is presented and compared with earlier studies. Evaluated values are also used in numerical 2D thermal modeling along with the seismic and well data for the Gediz and Büyük Menderes grabens. The knowledge of heat production distribution of the common rocks types of the study area is not available so radiogenic heat production rate is assigned from literature. We compared calculated model approaches against measured temperatures observed from two deep wells in the Gediz graben. Finally, results are interpreted with respect to the regional tectonic pattern of study area. Therefore the novelty of this thesis stem from generation systematical data and modeling subsurface temperatures to describe the thermal pattern of western Turkey.

1.2 A Brief History and Present Status of the Geothermic Studies in Western Turkey Surrounding Area

Western Turkey is characterized in Europe Heat flow map (Cermak et al., 1977) by high values. According to the heat flow measurements in Europe and the surrounding areas, the eastern Mediterranean Sea has low and uniform heat flow values in contrast to the western Mediterranean Sea (Erickson, 1970; Cermak et al., 1977; Eckstein, 1978). The difference was also observed in geophysical data which strongly suggest a significant difference in the crustal structure and tectonics of the eastern and western Mediterranean Seas. The average heat flow for eastern Mediterranean Sea ($31 \pm 8 \text{ mWm}^{-2}$) is lower than the world average even if corrected for sedimentation. It was also underlined the apparent lower heat flow values observed in Black Sea. The rapid sedimentation rate at the Black Sea was the main reason of the low heat flow values. After correction of sedimentation effect, the average heat flow value of 115 mWm^{-2} was obtained for Black Sea but how realistic is the correlation has still being discussed (Erickson, 1970). In the Aegean Sea, while the boundary of the African and European plates characterized with low heat flow values, at the chains of the volcanic islands behind the Crete Island shows high heat flow anomaly (Figure 1.1). The highest heat flow value ($\sim 120 \text{ mWm}^{-2}$) was observed through the Paleogonian-Parnos zone (interior side of the Hellenic island arc) (Fytikas, 1980). This high heat flow zone is intersected with Bodrum-Karaada at the east. The second highest zone, exceeds 100 mWm^{-2} , is located around the central Aegean related with the İzmir-Ankara zone. At the northern Aegean islands and Biga and Gelibolu peninsulas, Jongsma (1974) emphasized the third high heat flow zone interpreted as andesitic volcanism with the age of Oligocene-Miocene. In Marmara Sea, Pfister et al. (1998) reported the results of high resolution temperature logs and thermal conductivity measurements from surface rocks. Surface heat flow varies from 35 mWm^{-2} to 115 mWm^{-2} with the average of 60 mWm^{-2} in the area. Heat flow distribution in Marmara Sea summarized as high heat flows around the southern part and relatively lower values for the eastern and northern part of the region.

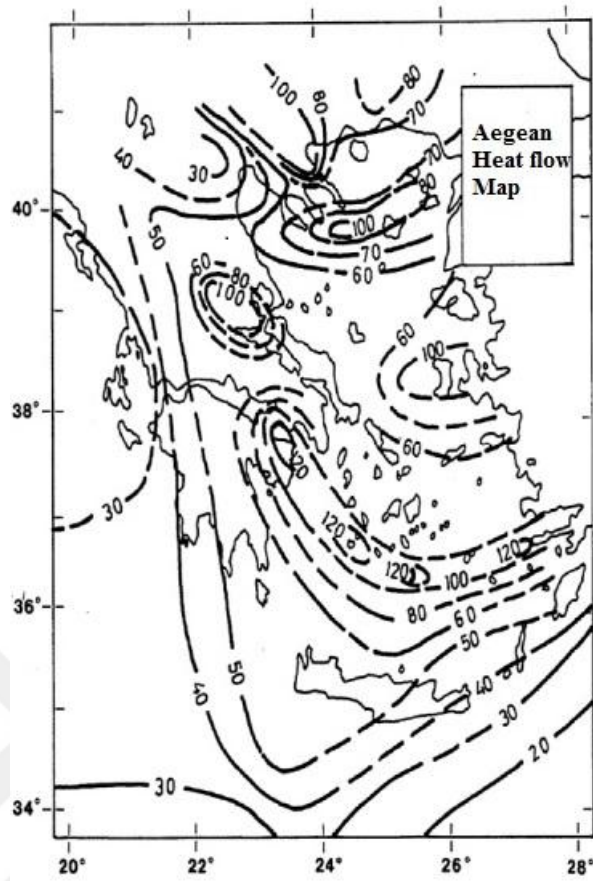


Figure 1.1 Heat flow map of Aegean Sea (Fytikas, 1980).

The history of geothermic investigations in Turkey dated back to foundation of the Kandilli Geophysical and Astronomical Observatory as a meteorological station in 1911. Ground temperatures for the maximum depth of 1 m were measured at 193 stations located throughout the Turkey for the agricultural purposes after the establishment of the State Meteorological Services. As a geophysical tool, the first ground temperature measurement was evaluated in Balçova geothermal field in 1962. Since then, geothermal gradient method was applied to almost all geothermal, natural gas and petroleum fields (Kızıldere-Denizli in 1963, Gonen-Balıkesir in 1964, Aydın in 1982 etc.) explored by the General Directorate of Mineral Research and Exploration and Turkish Petroleum (Tezcan, 1995). Many of them were conducted for limited fields and specific purposes of these organizations. Thus, results of them were not published. They were just stored in the archives of these companies. All these measurements would be the data set of the first heat flow map of Turkey.

As a local scale, the first heat flow map of Turkey (Tezcan, 1979) was prepared in 1976 and firstly published in as a part of Heat flow map of Southern Europe and the Mediterranean Region (Cermak et al., 1977). It was also reported in combined with geothermal potential of Turkey as a chapter in Terrestrial Heat flow in Europe (Cermak & Rybach, 1979). Tezcan & Turgay (1989) prepared preliminary heat flow map for Turkey using temperature data from coal wells. His map also took place in European Heat Flow Map prepared by Hurting et al. (1992). Tezcan & Turgay (1991) revised this map (Figure 1.2) and prepared subsurface temperature maps for five different depths. In Tezcan (1995), the original first heat flow and subsurface temperature distribution maps completely edited with the inclusion of new temperature data from 204 oil and coal wells. In these studies, statistical relationship between data point and isotherms were not revealed thus it is assumed that linear interpolations technique was used. In the all of these studies, the constant thermal conductivity of $2.1 \text{ Wm}^{-1}\text{K}^{-1}$ was taken for calculation of the heat flow. Tezcan, (1995) indicated that the high flow anomalies are associated with the well known metamorphic massifs; Menderes Massif, Kazdağ Massif and Kırşehir Massif and large granitic intrusions occurred in these Massifs.

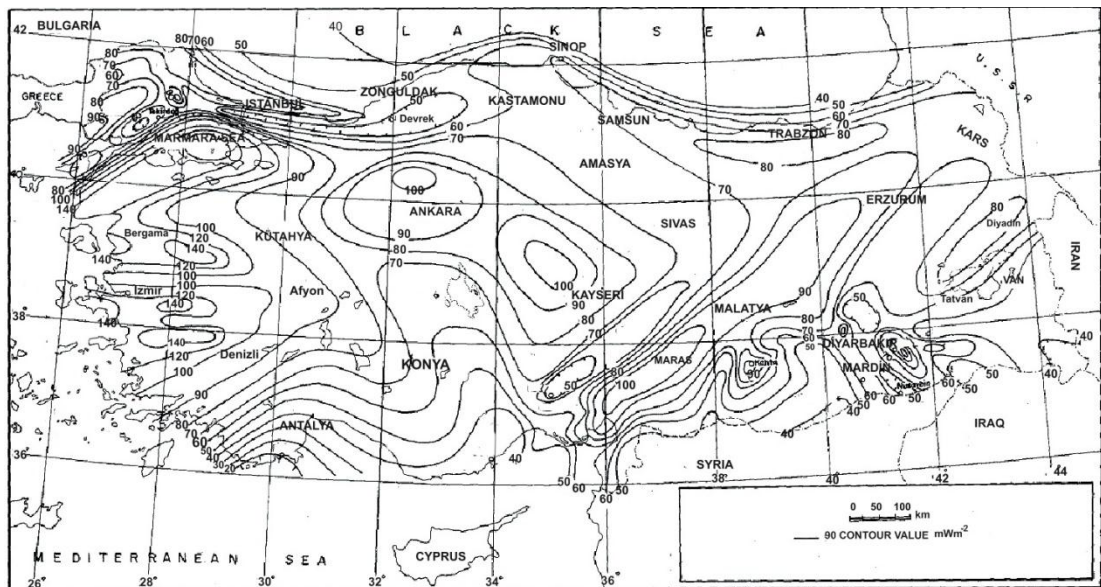


Figure 1.2 The first heat flow map of Turkey (Tezcan & Turgay, 1991)

Subsurface temperature distribution and temperature gradient studies were started with Ünalán & Öngür (1979). They generated the first temperature gradient maps for Trakya, Adana and some basins of southeastern Anatolia. They fixed the surface temperature to 15 °C and used the bottom hole temperatures (BHTs) measured at deeper than 400m to estimate the temperature distribution at 1000m. Tezcan & Turgay (1991) published the temperature distribution contour map at 1000m and Turkey and Tezcan (1995) revised it with new additional data. Serpen & Mihçakan (1999) conducted a study of the geothermal resource base using stochastic modeling techniques and data from heat-flow maps that had been drawn based on geothermometer and temperature gradient information. Finally, the first temperature gradient map of Turkey was prepared using meteorological data and 487 BHTs (Mihçakan et al., 2006) instead of temperature-depth measurements. Subsurface temperature distribution maps for 500m (Figure 1.3) and 1000m depths were built for assessment of geothermal sources of Turkey using geostatistical methods (Başel et al., 2010).

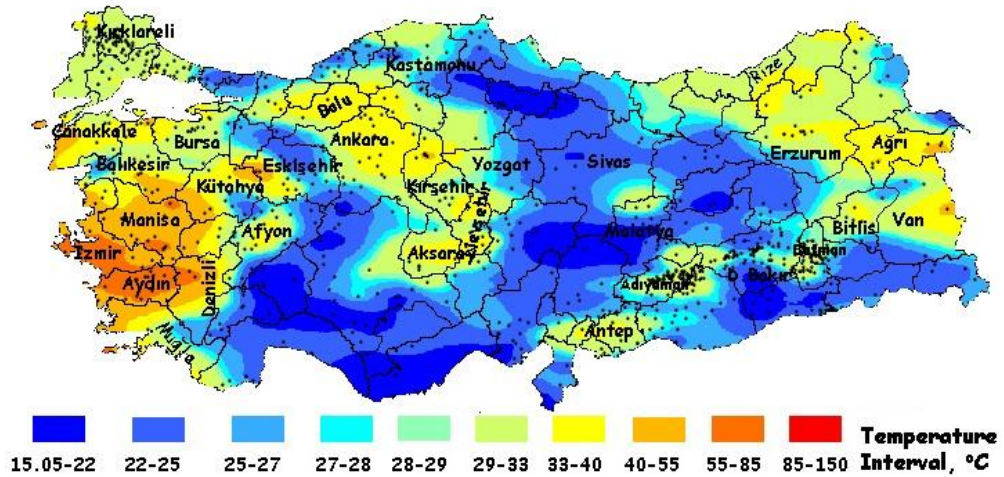


Figure 1.3 500 m depth temperature distribution map of Turkey (Başel et al., 2010).

Alternatively to conventional method, heat flow can be estimated using by silica temperature of thermal waters. İlkisik (1989), as a pioneer, used the silica estimator to find out the regional heat flow pattern of the northwestern Anatolia. Alptekin et al. (1990) pointed out a relationship between the high heat flow values, the high seismic activity and geological structures in western Turkey. The highest value of 247 mWm^{-2} was measured in Gediz (Simav Graben) and a mean heat flow anomaly of 150 mWm^{-2} followed the Eocene aged collision zone which is seismically very active. A mean heat flow value of $107 \pm 45 \text{ mWm}^{-2}$ was obtained by İlkışık (1995) at the western part of Anatolia (Figure 1.4). He calculated heat flow using silica temperature on 187 thermal springs. Results of his study stated that heat flow in western Anatolia is approximately 50-60% higher than the world average. He pointed out that the areas with high heat flow values are related with Tertiary and younger volcanism and prevalent geological structures such as Gediz and Büyük Menderes grabens. Heat flow values derived from silica temperatures were interpreted together with seismological data for western Anatolia by Yolsal et al., (2005). Their results indicated that heat regime in the area is associated with active tectonics.

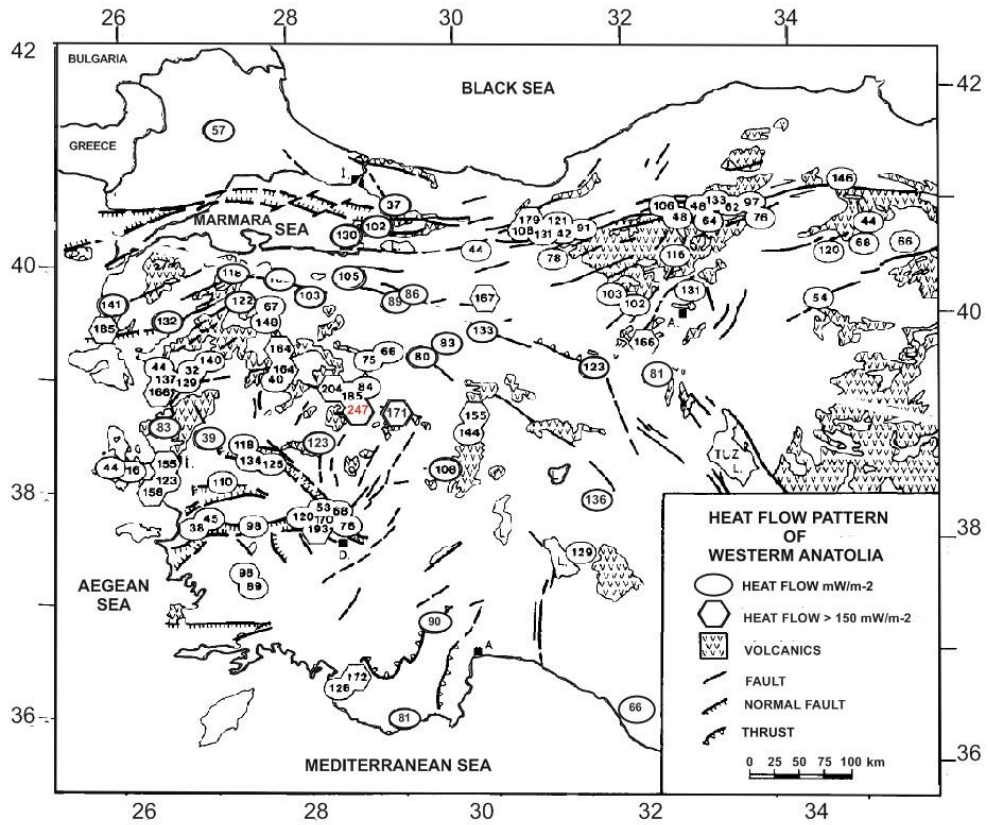


Figure 1.4 Heat flow distribution map of western Anatolia from silica temperatures (İlkişik, 1995)

From 1995 to 1999, The Directorate of Mineral Research and Exploration (MTA) and The Scientific and Technical Research Council of Turkey (TUBITAK) together with some universities carried out “The Heat flow map of Turkey” project to evaluate detailed heat flow map of Turkey, starting from western Turkey (İlkişik et al, 1996a, 1996b). The data collection was realized by a team at MTA under the leadership of H. M. Yenigün. In this project temperature depth (T-D) measurements were made in shallow wells drilled for water explorations (which are not in use). For thermal conductivity measurements, surface rocks samples were collected from outcrops in the vicinity of each measurement site. Thermal conductivity measurements of rock samples collected from western Anatolia were made on dry condition using QTM-500 devices and they need to correction to saturated condition before calculating heat flow but any correction was made by researchers. The rest of the measurements were conducted on saturated condition and they do not need any correction. Yemen (1999), in his master thesis, evaluated the heat flow map of İzmir, Aydın and Manisa provinces using data set from mentioned project without any

correction and analysis. This is the main reason of the negative values calculated in the southern part of the Gediz graben. Unfortunately, the heat flow map of Turkey (Figure 1.5) of scale 1:10000000 is also revealed using the same raw data set by MTA (Karlı et al., 2006).

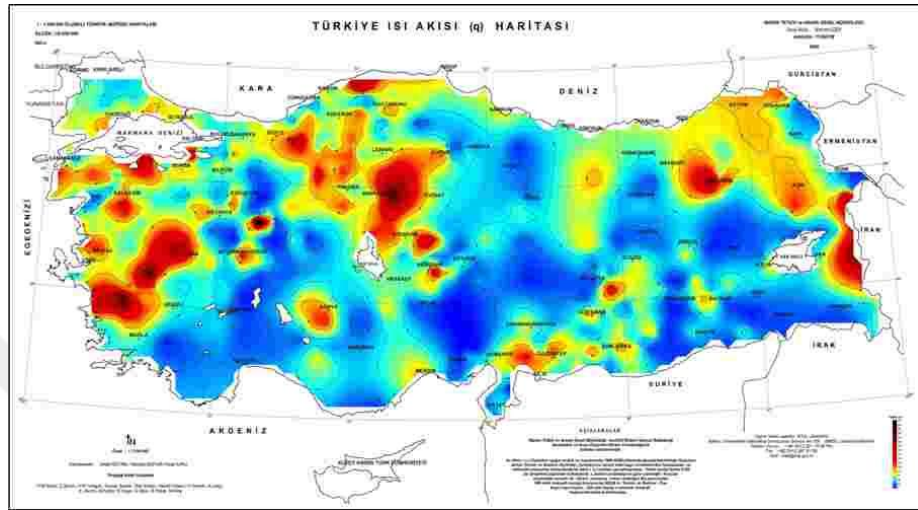


Figure 1.5 Heat flow map of Turkey (Karlı et al., 2006).

Heat flow can be estimated from spectral analysis of magnetic data (Bhattacharyya, 1965; 1966 Spector & Bhattacharyya, 1966). The power spectrum method is commonly used to find Curie point depth at which the Curie temperature is reached. Lots of local and large-scale attempt was made to estimate heat flow values from curie depths in Turkey (Hisarlı, 1995; Ateş et al., 2005; Dolmaz et al., 2005a; Bektaş et al., 2007; Maden, 2010; Akın & Çiftçi, 2011, Akın et al., 2014; Maden et al., 2015). Using spectral analysis Şalk et al. (2005) were reported heat flow values for western Anatolia derived from Magsat magnetic data. A constant thermal conductivity of $2 \text{ W m}^{-1} \text{ K}^{-1}$ was used in calculation of heat flow for the region. Their study demonstrated the relationship between high heat flow and shallow curie depth. Calculated curie depths were also in accordance with the results of Aydın et al, (2005). Dolmaz et al. (2005a) constructed the heat flow map of Western Anatolia from Curie point depths constituted by using aeromagnetic data. Differ from Şalk et al. (2005), they correlated the estimated Curie point depths with geothermal gradient values and thermal conductivity measurements (Yemen, 1999) and heat flow data

(Tezcan & Turgay, 1989; İlkısık, 1995). They used mean thermal conductivity of $2.127 \text{ Wm}^{-1}\text{K}^{-1}$ in their calculations. Akın et al. (2014) estimated the Curie point depths of Turkey applying the power spectrum to aeromagnetic data of Turkey. Instead of constant thermal conductivity, they used uncorrected thermal conductivity data from Karlı et al. (2006) for heat flow calculations. According to this study, mean heat flow value of Turkey was obtained as 74 mWm^{-2} . They showed that the highest heat flow values of $\sim 229 \text{ mWm}^{-2}$ obtained between Uşak and Afyon have the minimum depth at the same time. This anomaly was also previously mentioned in Dolmaz et al., (2005a).

Although Turkey has several geothermal areas and generally many of these areas are located around the graben systems, thermo-mechanical models of them have not been developed. The study of Göktürkler et al. (2003) is the unique work presenting the crustal-scale conductive heat model of grabens in western Anatolia. They mentioned about the relatively higher temperatures in grabens and regions under them than those in the surrounding areas. Temperature at the bottom of their model called as crust was calculated as $1075\text{-}1100 \text{ }^\circ\text{C}$.

Erkan (2015) has prepared a preliminary heat flow map of western Anatolia (Figure 1.6). He used the data set from aforementioned project (İlişik et al., 1996a; 1996b) and Pfister et al. (1998). High resolution temperature logs and thermal conductivities obtained from outcrops or literature related rock type were analyzed for determination of the conductive heat flow of the study area. The average heat flow of the study area was suggested as $73\pm 22 \text{ mWm}^{-2}$ in his study. The highest heat flow anomalies ($> 100 \text{ mWm}^{-2}$) were recorded at the western part of Çanakkale and central part of the Menderes Massif near Kula volcanic center.

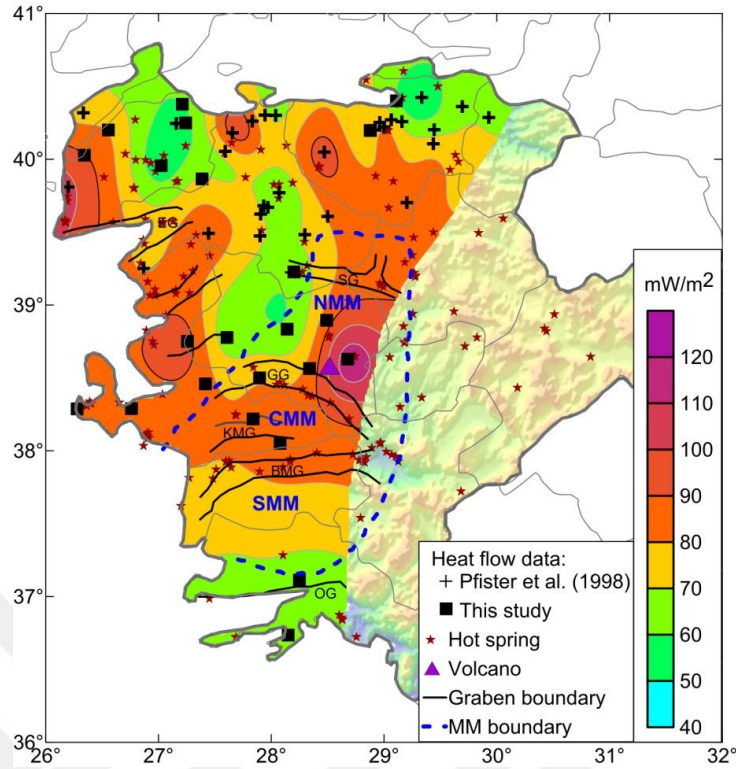


Figure 1.6 The preliminary heat flow map of western Anatolia (Erkan, 2015).

In addition to all these studies, researchers worked through on estimation of geothermal resource potential of Turkey (Serpen & Mihçakan, 1999; Mihçikan & Öcal, 1998; Satman, 2007; Başel et al., 2008; Serpen et al., 2009; Başel et al., 2010; Korkmaz et al., 2014). Accessible stored heat energy values of Turkey were calculated (Serpen & Mihçakan, 1999) using stochastic modeling techniques with information from heat flow maps (Tezcan, 1979; İlkışık, 1995). They also predicted the accessible geothermal energy resource and convertible energy using Monte Carlo Simulator and estimation approach. Serpen et al. (2010) estimated the accessible geothermal potential of Büyük Menderes graben as $5.22 \cdot 10^{19}$ J using stochastic and risk analysis methods. Geothermal resource assessment of Turkey was predicted by Korkmaz et al. (2014) using three approaches. Turkey's geothermal resource base between surface and 3 km depth was evaluated as 3.96×10^{23} J and geothermal capacity of currently indentified 290 geothermal fields was determined to be 10.576 MW. Using the reference temperature of 15 °C at surface they estimated the thermal potential of 135 fields of Turkey as 38.2 GW_t.

Ahlatçı (2005) estimated the heat flow, transferred from the earth surface to the atmosphere, over the entire Turkey using geothermal gradient data and rock thermal conductivities. The study indicated that the heat being released amounted to 84.2GW and that the average heat flux was 109 mWm^{-2} (Serpen, 2006). These values for Turkey are in agreement with those of other studies (İlkışık, 1995; Serpen & Mihçakan, 1999).

All summarized publications, tabulated in Table 1.1, show that western Turkey has remarkable heat flow values related to its tectonic position. The lack of the thermal conductivity and the geothermal gradient data are the main reasons of the limited number of detailed heat flow studies in the area. Thermo-mechanical modeling studies are crucial importance on determining the geothermal potential. In particular, detailed modeling investigation will bring a new perspective to Enhanced Geothermal Systems (EGS) resource estimations in the region.

Table 1.1 Summary of geothermic studies in Turkey

<i>Purpose</i>	<i>Method</i>	<i>Region</i>	<i>Reference</i>	<i>Explanations</i>
Heat flow	Conventional methods	Mediterranean and Black Sea	Erickson, 1970	Low HF in Mediterranean sea
		Aegean Sea	Jongsma, 1974	High HF at margins of Black sea
		Southern Europe and Mediterranean	Cermak et al., 1977	High HF in the northern and central Aegean
		Eastern Mediterranean	Eckstein, 1978	Turkey located in Europe HF map with high HF values
		Europe	Cermak & Rybach, 1979	Using λ of sea floor sediments
		Western Anatolia	Tezcan, 1979; Tezcan & Turgay, 1989; 1991	Using Tezcan, 1979's HF data
		Europe	Tezcan, 1995	Using constant $\lambda=2.1 \text{ Wm}^{-1}\text{K}^{-1}$
		Marmara Sea Region (NW Turkey)	Hurting et al., 1990	European heat flow map (For Turkey Tezcan, 1979's HF data was used)
		İzmir, Aydın, Manisa	Pfister et al., 1998	Mean HF value of 60 mWm^{-2}
		Turkey	Yemen, 1999	Raw data set was used in HF determination
		Karlı et al., 2006	Raw data set was used in HF determination	
		Western Anatolia	Erkan, 2015	The primarily HF map for study area using İlkışık et al. (1996a;1996b)'s data after applying required corrections
Silica temperatures		Northwest Anatolia	İlkışık, 1989	The maximum HF value was obtained along the Gulf of Edremit-Gönen-M.kemalpaşa zone
		Western Anatolia	Alptekin et al., 1990	Depth of heat generation in the crust was calculated as 10-15 kilometers.
		Western Anatolia	İlkışık, 1995	Relation between high heat flow values and high seismic activity
		Western Anatolia	Yolsal et al., 2005	The max HF value of 247 mWm^{-2} was estimated in Gediz (Simav graben) and mean HF was calculated as $107\pm 45 \text{ mWm}^{-2}$

HF: Heat flow; λ : Thermal conductivity; CPD: Curie Point Depth.

Table 1.1 Summary of geothermic studies in Turkey (continue)

<i>Purpose</i>	<i>Method</i>	<i>Region</i>	<i>Reference</i>	<i>Explanations</i>
Heat flow	By means of CDPs evaluated from spectral analysis of magnetic data	Edremit-Susurluk	Hisarlı, 1995	HF values were calculated for both constant $\lambda=2$ and $3 \text{ Wm}^{-1}\text{K}^{-1}$
		Aydın-İzmir	Bal, 2004	HF values range between $60\text{-}180 \text{ mWm}^{-2}$ using constant $\lambda=2$ and $3 \text{ Wm}^{-1}\text{K}^{-1}$
		Western Anatolia	Şalk et al., 2005	HF values change between $40\text{-}140 \text{ mWm}^{-2}$ constant $\lambda=2 \text{ Wm}^{-1}\text{K}^{-1}$ was used
			Dolmaz et al., 2005a	HF values change between $62\text{-}150 \text{ mWm}^{-2}$ $\lambda= 2.50 \text{ Wm}^{-1}\text{K}^{-1}$ for plutonic rocks $\lambda= 2.75 \text{ Wm}^{-1}\text{K}^{-1}$ for metamorphic rocks $\lambda= 1.87 \text{ Wm}^{-1}\text{K}^{-1}$ for volcanic rocks and $\lambda= 2.06 \text{ Wm}^{-1}\text{K}^{-1}$ for sedimentary rocks
		Kırşehir Massif	Akın&Çiftçi, 2011	
		Turkey	Akın et al., 2014	Mean heat flow value of Turkey is estimated as 74 mWm^{-2}
		Eastern Anatolia	Bektaş et al., 2007	Using $\lambda= 2.5 \text{ Wm}^{-1}\text{K}^{-1}$
		Erzurum	Maden N, 2010; Maden et al., 2015	Asthenospheric heat flow is 68 mWm^{-2} without intrusions and 42 mWm^{-2} with intrusion (constant $\lambda=2 \text{ Wm}^{-1}\text{K}^{-1}$)
		Menderes Massif	Bilim et al., 2015	Heat flow values vary between $105\text{-}252 \text{ mWm}^{-2}$ (constant $\lambda= 2.5$ and $2.7 \text{ Wm}^{-1}\text{K}^{-1}$)
		Central Anatolia	Ateş et al., 2005 Dolmaz et al., 2005b	CDP of Central Anatolia varies from 7.9 km and 22.6 km
Tukey	Aydın et al., 2005	Deepest cruie isotherm depths range between 20 and 29 km		
Kütahya-Denizli	Bilim, 2007	Generally shallow curie point depth		
Central Anatolia	Bilim et. al., 2015	Estimated CDPs vary from 11 to 22 km with mean of 16.7 km		
Menderes Massif and Aegean Region	Bilim et al., 2016	Estimated CDPs vary from 6.21 to 12.41 km with mean of 9.29km Radiogenic heat production calculated between 0.38 and $0.80 \mu\text{Wm}^{-3}$		

HF: Heat flow; λ : Thermal conductivity; CPD: Curie Point Depth

Table 1.1 Summary of geothermic studies in Turkey (continue)

<i>Purpose</i>	<i>Method</i>	<i>Region</i>	<i>Reference</i>	<i>Explanations</i>
Deep temperature distribution	Numerical Modeling	Western Anatolia	Göktürkler et al., 2009	2D steady state conductive heat transfer model was used
Subsurface temperature distribution mapping	Stochastic methods	Turkey	Ünalın&Öngür, 1979; Serpen&Mıkçakan, 1999; Mihçikan&Öcal, 2000; Başel et. al., 2008;2010	Temperature distribution maps at 1 m 500m and 1000m depths
	Volumetric heat content model	Europe	Hurter& Schellschmidt, 2003	Temperature distribution at 1000m depth
Geothermal potential estimation	Stochastic basin analysis methods	Turkey	Başel et al., 2008; 2010; Korkmaz et al., 2014 Serpen et. al., 2009,	

HF: Heat flow; λ : Thermal conductivity; CPD: Curie Point Depth.

1.3 Original Contributions of the Thesis

The original contributions to the geothermic studies in western Turkey are summarized as follow:

- Silica heat flow map of western Turkey is updated using the new chemical data obtained from Inventory of Turkey Geothermal Resources (Akkuş et al., 2005).
- Thermal conductivity data set for the major rock types located in western Turkey is evaluated.
- High precision new T-D measurements were acquired from abandoned water wells as a part of TUBITAK project with the number of 113R019. After classified according the quality criteria given in the chapter 5 geothermal gradient of each data point is determined. If necessary topography correction is applied on related geothermal gradient data.
- Geothermal gradient distribution of western Turkey is mapped using the new data set together with the previously published.
- New heat flow values are calculated using the new geothermal gradients and thermal conductivity data set.
- Sedimentation and thermal refraction effects are eliminated from the new heat flow data set.
- The heat flow map of western Turkey is updated using the new high quality heat flow data set together with published data.
- 2D steady-state temperature distribution within the Gediz and Büyük Menderes grabens are modeled using finite elements method under the assumption of conductive heat transfer.

1.4 Outline of the Thesis

The rest of this thesis includes seven chapters. This first chapter is devoted to presentation of the introduction, purpose and the present status of the study area. The remaining chapters of this thesis are organized as follows:

Chapter 2 presents the general geologic and tectonic settings of study area. Geological cross sections obtained from previously published geologic and geophysical studies for Gediz and Büyük Menderes graben are also summarized in subsections.

In Chapter 3, firstly the geothermometers used in geothermic studies are briefly explained. Secondly the most common geothermometers are applied to the thermal waters from western Anatolia to estimate reservoir temperature and compare with measured reservoir temperatures if they are available. Finally heat flow values estimated from Silica geothermometers are mapped for the region.

In Chapter 4 the raw thermal conductivity data reported in İlkışık (1996a; 1996b) is initially classified according to the lithologic types encountered in western Turkey. Then, the mean thermal conductivities of the lithologies are calculated for both dry and saturated conditions. Finally, the significance of the results is discussed by comparing with the general geologic and tectonic settings.

In Chapter 5, the new temperature depth measurement data are analyzed, firstly classified in order to eliminate intensively disturbed by local hydrogeological effects. Then, these new data are combined with the existing published data to generate geothermal gradient distribution map of western Turkey.

In Chapter 6, the heat flow map of western Turkey is updated using the results of Chapter 4 and Chapter 5.

In Chapter 7, 2D thermal models of Gediz and Büyük Menderes grabens are investigated using the finite element method (FEM) under the assumption of conductive heat transfer.

Finally, Chapter 8 is the conclusion chapter that covers main conclusions and contributions of this thesis and offers new insights in to the future studies.



CHAPTER TWO

GENERAL GEOLOGY AND TECTONIC SETTINGS

Turkey is located within the Mediterranean Earthquake Belt where the complex deformation occurs due to the continental collision between African and Eurasian plates (Figure 2.1). This collision causes the westward extrusion of Anatolian plate along the along the North Anatolian Fault Zone (NAFZ) and East Anatolian Fault Zone (EAFZ) (Bozkurt, 2001). On the other hand, convergence between African and Anatolia plates result in a subduction zone along the Aegean and Cyprean arcs calls as Aegean Subduction Zone (ASZ) (Papazachos & Comninakis, 1971; McKenzie, 1978; Mart & Wooside, 1994) and African plate is descending beneath the Anatolian plate. Ongoing deformation of the region has resulted in the generation of four different neotectonic provinces in Turkey: (1) East Anatolian Contractional Province, (2) North Anatolian Province, (3) Central Anatolian ‘Ova’ Province and (4) West Anatolian Extensional Province (Şengör et al., 1985). Each province shows unique structural components and tectonic features (Figure 2.1).

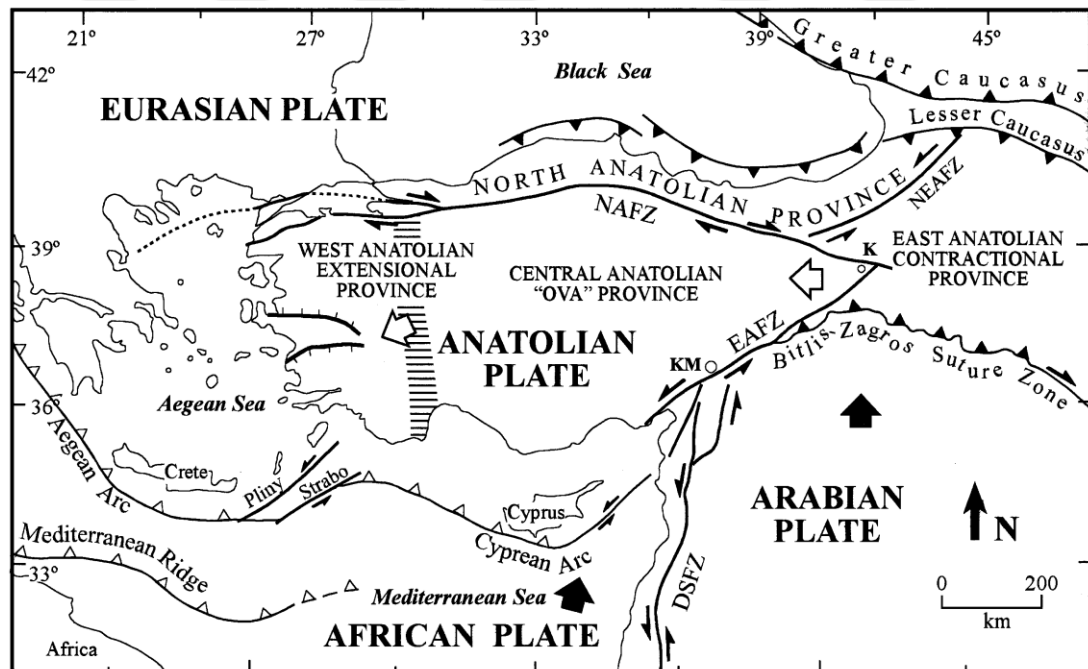


Figure 2.1 Simplified tectonic map of Turkey including major neotectonic structures and neotectonic provinces (Bozkurt, 2001).

Western Anatolia region noted for its long and complicated geological history. Tectonic evidence suggests that, the area has experienced Cenozoic extensional tectonics (Şengör & Yılmaz, 1981; Okay & Tüysüz, 1999; Rimmelé et al., 2003; van Hinsbergen et al., 2005, 2010; Çemen et al., 2006; Ring et al., 2010; Jolivet et al., 2013). The reasons and the initial time for this extension are open to interpretation. Currently, five different models of the regional extension are common: (1) the westward escape or lateral extrusion of the Anatolian microplate along the its wedges (the North Anatolian and East Anatolian Fault zones) due to the collision between the Arabian and Eurasian plates along the Bitlis-Zagros suture zone (Dewey & Şengör, 1979; Şengör, 1979, 1980, 1987; Şengör & Yılmaz, 1981; Şengör et al., 1985; Görür et al., 1995; Çemen et al., 1999); (2) back-arc spreading (rifting) behind a Tethyan subduction zone to the south and subduction rollback accompanied by the subduction along the Aegean-Cyprian trench (Mc Kenzie, 1978; Le Pichon & Angelier, 1979, 1981; Meulenkamp et al., 1988, 1994; Spakman et al., 1988; Jolivet & Brun, 2010; Jolivet et al., 2013) (3) Orogenic collapse caused by the spreading and thinning of over-thickened crust following the latest Paleocene collision across Neotethys during the latest Oligocene–Early Miocene (Seyitoğlu & Scott, 1992; Seyitoğlu et al., 1992); (4) A three-stage continuous shear extensional mechanism as a result of the mechanisms listed above (1), (2) and (3) (Çemen et al., 2006; Gessner et al., 2013); (5) combination of the mechanism (1) and (3) called as Episodic model. In this model extension is induced by orogenic collapse at the first stage and second phase is defined by the westward escape of the Anatolian block (Sözbilir & Emre, 1996; Koçyiğit et al., 1999; Bozkurt, 2000, 2001, 2003; Işık & Tekeli, 2001; Lips et al., 2001; Sözbilir, 2001, 2002; Bozkurt & Sözbilir, 2004; Koçyiğit, 2005). Each models listed above predicted a different timing for the inception of extension. Some of them suggested that the Cenozoic extensional tectonics in the western Anatolian began in Middle Miocene (Yılmaz et al., 2000) or earliest Miocene (Seyitoğlu et al., 1992) while other studies suggested that the extension has begun in Late Oligocene (Lips et al., 2001; Catlos & Çemen, 2005; Çemen et al., 2006), or in Early Eocene in the Rhodope region (Jolivet & Brun, 2010; Ersoy et al., 2014).

Numerous graben basins and their basin bounding active normal faults are the response of the prevalent extensional regime in the area. These basins can be classified in to two groups as E-W trending (e.g. Edremit, Bakırçay, Kütahya Simav, Gediz, Küçük Menderes, Büyük Menderes and Gökova) and NE-SW trending (Soma, Gördes, Demirci, Selandi and Uşak-Güre) (Figure 2.2). The age of these grabens is also controversial. Three different views are suggested in several studies. Firstly researchers proposed that the grabens began to form during Tortonian (Şengör & Yılmaz, 1981; Şengör et al., 1985; Şengör, 1987). According to the Seyitoğlu & Scott 1991 the basins started to form during Early Miocene and continued their evolution since then. However, the recent studies revealed that the grabens are Plio-Quaternary structures located in west Anatolian extensional province (Koçyiğit et al., 1999; Bozkurt, 2000; Sarıca, 2000; Yılmaz et al., 2000).

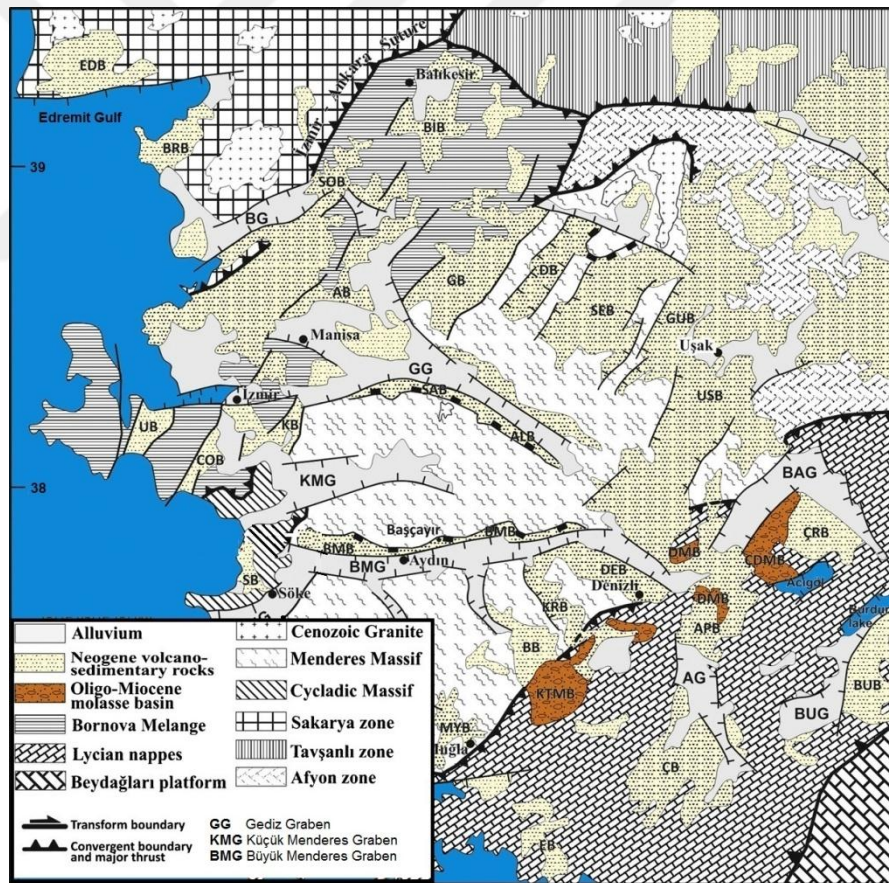


Figure 2.2 Geological map of western Turkey (Sümer et al., 2013).

Grabens are filled with volcano-sedimentary sequences dissecting Menderes Metamorphic Complex (MMC) in western Anatolia. Continental collision between African and Eurasian plates provides proper temperature-pressure condition for occurrence of MMC. MMC is the oldest on Anatolian plate and one of the largest metamorphic terrains in the world which began to develop during the Late Oligocene–Early Miocene (Bozkurt & Park, 1994; Çemen et al., 2006; Emre, 1996; Işık & Tekeli, 2001; Lips et al., 2001). MMC, as a basement unit, is exposed approximately 200×100 km in the area. It has been proposed that the massif consist of a Precambrian/Cambrian core overlain by a cover comprising sediments. It includes much kind of metamorphosed rocks from high to low grade including gneiss, mica schists, phyllites, quartz schists, marbles and granodiorites. Initially, the age of the MMC was determined as Paleozoic-Mesozoic (Şengör et al., 1984; Yılmaz et al., 2000; Güngör & Erdoğan, 2002), recent studies indicated that it ups to Eocene (Özer & Sözbilir, 2003). The fill of the basins overlying MMC are generally composed of two main, lower and upper, volcano-sedimentary successions. The basic difference between two units is origin of the conglomerate content. While the upper volcano-sedimentary conglomerates contain clasts from MMC, in lower volcano-sedimentary successions lacks these clasts (Ersoy et al., 2014). Sedimentary parts of the successions consist of generally limestone, sandstone, conglomerate, shale and marl (Innocenti et al., 2005). Andesite, tuff, basalt and rhyolite are the common volcanic rocks within typical sections (Ersoy et al., 2014). As shown in Figure 2.3 volcanic rock content of the sedimentary fills decreases from north to south in the region.

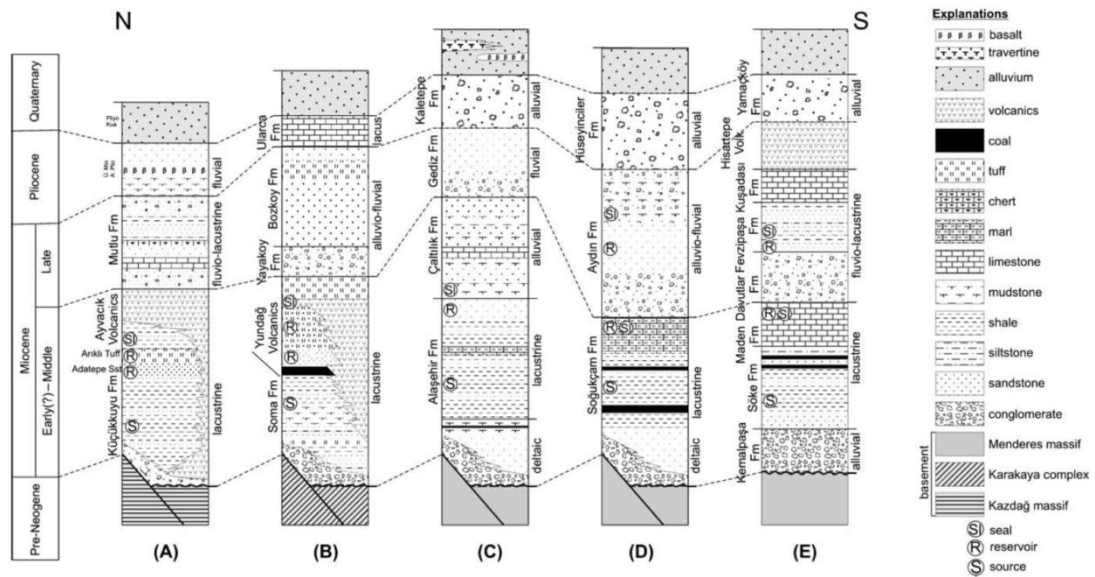


Figure 2.3 Simplified stratigraphic charts of some western Anatolian grabens. (A) Edremit graben (Çiftçi et al., 2004); (B) Bakırçay graben (Yılmaz et al., 2000); (C) Alaşehir graben (Çiftçi and Bozkurt, 2009a); (D) Büyük Menderes graben (Yazman et al., 2004); and (E) Söke graben (Gürer et al., 2001). Dotted lines approximately depict the correlation of the stratigraphic charts in time. Formation names and depositional environments are illustrated on the left and right-hand side of each column, respectively.

Gediz and Büyük Menderes grabens are the most prominent features of the region. They are the largest grabens compared with others basins. High heat flow values and medium-to-high enthalpy geothermal systems are encountered along and within these grabens (Serpen et al., 2009; 2010). In parallel with tectonic effects the young volcanic activity lasting from the upper Miocene to recent time may probably the origin of the heat source in the region (Çağlar, 1961; Demirel & Şentürk, 1996). The heat transferred to the shallower depths by the helps of tectonics activities related with volcanism. According to the Karakuş (2013) young volcanism is limited in the area and most of the geothermal systems have nonmagnetic heat source. He correlated the intense thermal activity with enhancement of second permeability in hard and brittle lithologies due to active extensional tectonic regime. Fractured rocks of MMC such as gnesis and quartz-schist units act as a reservoir rock for geothermal systems. Volcano-sedimenraty sequences with high clay content have very low permeability and act as a cap rock while thermal waters circulate within the major faults and fractured zones. Therefore geothermal gradient is high in these regions.

Generally geothermal fields follow the major grabens of the MMC such as Gediz, Küçük Menderes and Büyük Menderes. Salihli-Kurşunlu, Tugutlu-Urganlı and Alaşehir-Kavaklıdere are the most important geothermal fields in Gediz graben. The maximum resource temperatures reach up to 287 °C in the wells of Alaşehir. Kızıldere, Yenice, Salavatlı-Sultanhisar, Gölemezli, Aydın and Germekcik are the main geothermal fields located in Büyük Menderes graben. Kızıldere-Denizli is also the first geothermal field discovered in Turkey. The bottom temperatures in Kızıldere rise to 242 °C and this value is the maximum temperature obtained in Büyük Menderes graben. There are also lots of hot springs in these grabens with the discharge temperature between 25 and 100 °C (Baba, 2012; Karakuş & Şimşek, 2012).

2.1 Gediz Graben

Gediz Graben is the most important structural element of the western Anatolian extensional province. It was firstly term as Alaşehir Graben by Seyitoğlu & Scott (1996) and after Gediz River, which runs through much of the basin, it is also known as Gediz Graben. It extends more than 150 km along the Gediz River and has approximately 40 km width at its western end, but becomes narrow eastward until it dies out (Figure 2.4.).

Gediz graben evolved as an asymmetric graben bounded by normal faults dominantly active at the southern margin through the entire Miocene, developing into a graben as a result of post-Miocene faulting of the northern margin (Ciftçi & Bozkurt, 2009a). The southern master graben-bounding fault (MGBF) plays critical role in its deformation and deposition (Figure 2.6). Structurally two types of normal faults are observed in Gediz. The first type, low-angle normal fault called as Gediz detachment that separates metamorphic rocks in the footwall from sedimentary fill in the hanging wall (Cohen et al., 1995; Hetzel et al., 1995a, 1995b; Emre, 1996; Koçyiğit et al., 1999; Yılmaz et al., 2000; Lips et al., 2001; Sözbilir 2001, 2002; Işık et al., 2003; Bozkurt & Sözbilir, 2004). High-angle normal faults are the second type that dominates deformation in the graben fill. High-angle faults are active both

southern and northern borders of the Gediz graben and low angle normal faults are cut by the high angles faults (Çiftçi et al., 2010; Bozkurt & Sözbilir, 2004; Purvis & Robertson, 2005; Çiftçi & Bozkurt, 2009b).

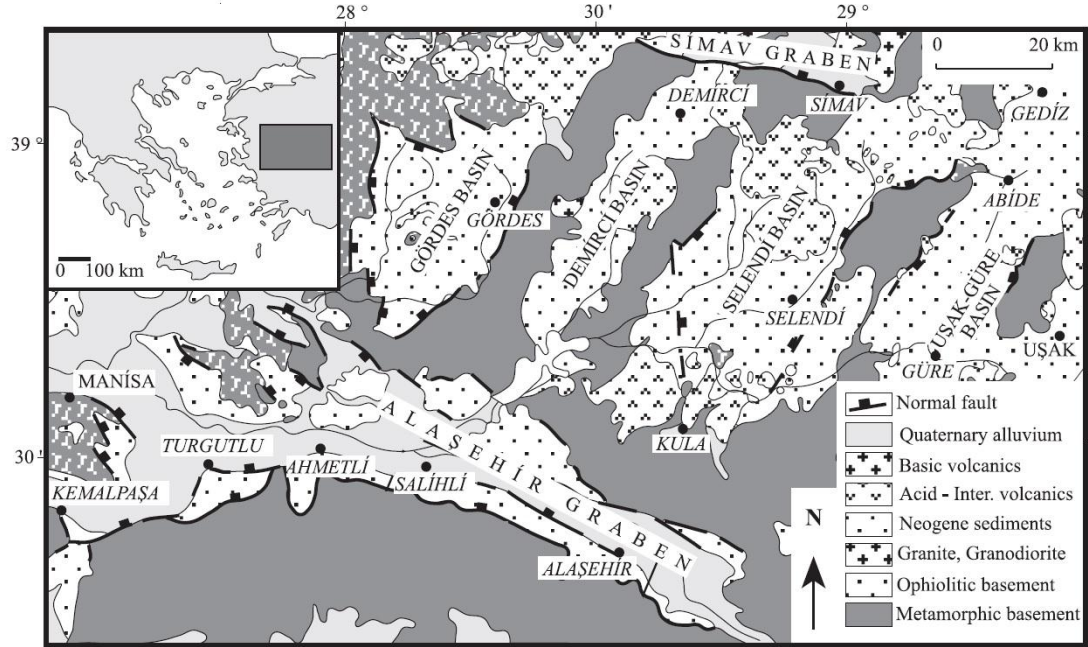


Figure 2.4 Simplified geology map of Gediz graben and surrounding areas (Seyitoğlu, 1997).

Metamorphic rocks of the Menderes Massif which composed of mainly schists, marbles, quartzites and phyllites represent the basement unit in Gediz graben. Estimated thickness of the graben fills ranges between 1.5-4 km (Akçığ, 1983; Paton, 1992; Gürer et al., 2002; Sarı & Şalk, 2006; Özyalın et al., 2012). Generally, fill of the graben consist of continental clastic rocks of mainly alluvial, lacustrine, and fluvial origin. It classified into five different formations; Miocene Alaşehir, Çaltılık and Gediz formations, and post-Miocene Kaltepe and Bintepele formations underlying Quaternary alluvium (Çiftçi & Bozkurt, 2009a) (Figure 2.5). These Miocene and post-Miocene formations are separated by an angular unconformity

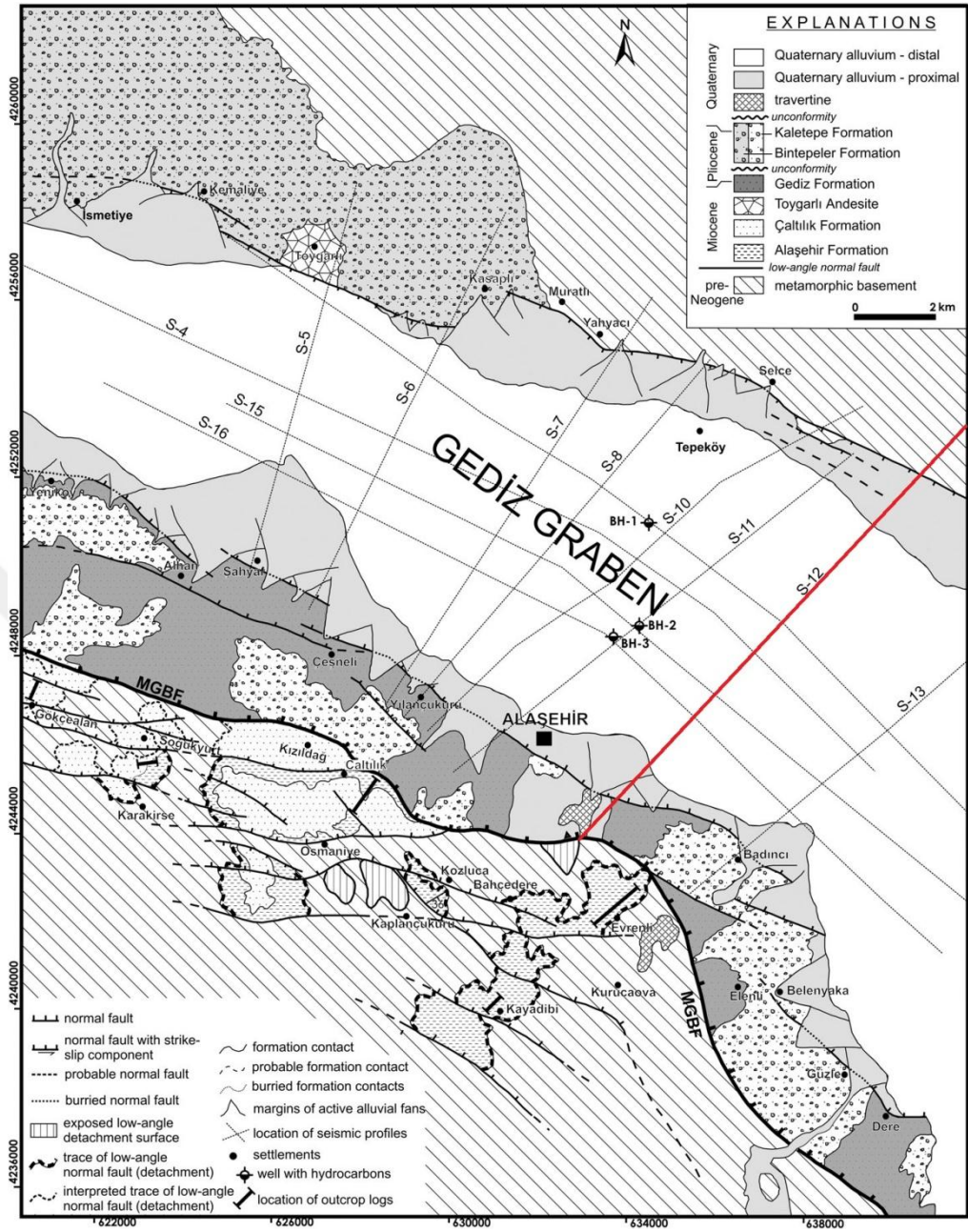


Figure 2.5 Geological map of Gediz graben with geological units, location of the boreholes and seismic profiles. MGBF, master graben bounding fault; BH, borehole and red line refines seismic profile (S-12) (Çiftçi & Bozkurt, 2009a).

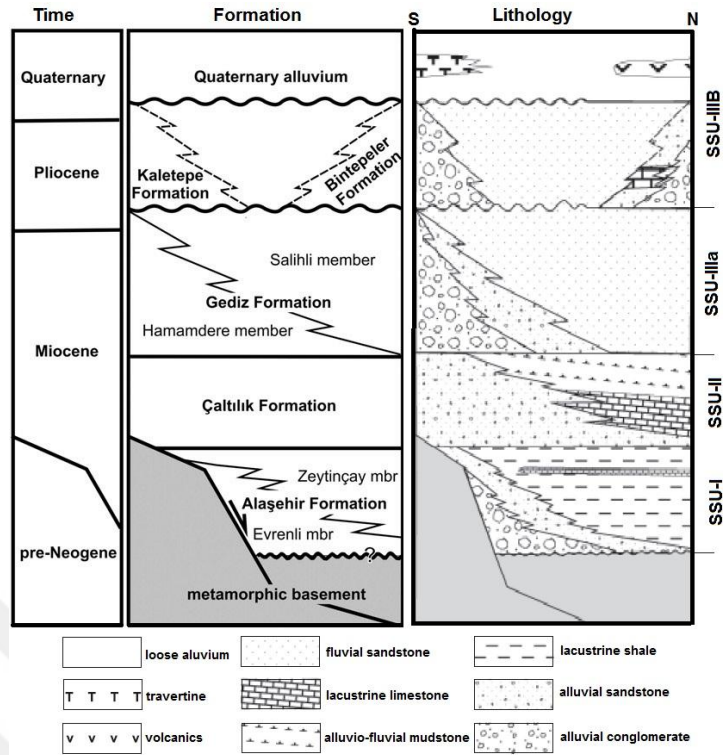


Figure 2.6 Neogene stratigraphy of the Gediz Graben based on the geological data around Alaşehir. (Çiftçi & Bozkurt, 2009a).

Depositional geometry of Gediz graben was provided Çiftçi & Bozkurt (2009a), using totally 270 km length 2D seismic reflection data interpreted with logs from three boreholes (Figure 2.5) and outcrops. There is a good match between the lithostratigraphic formations and the seismic stratigraphic units identified by Çiftçi & Bozkurt (2009a) (Figure 2.6 and Figure 2.7).

Seismic stratigraphic unit I (SSU-I) overlying metamorphic basement is in a good match with Alaşehir formation. Alaşehir formation is the oldest unit exposed along the southern margin of the Gediz graben (Çiftçi & Bozkurt, 2009b). It starts with conglomerates at the base (Yazman & İztan, 1990; İztan & Yazman, 1991; Yazman et al., 1998; Yılmaz et al., 2000) and continues with alteration of conglomerates to sandstone, siltstone and shales to the top edge. (Yazman & İztan, 1990; İztan & Yazman, 1991; Cohen et al., 1995; Yazman et al., 1998; Purvis & Robertson, 2005). Seismic stratigraphic unit II (SSU-II) lies above the SSU-I with an explicit change. SSU-II correlates with the Çaltılık Formation and it can be interpreted that disorganized conglomerates of alluvial fans dominate the proximal part of the unit

near MGBF. Towards north to more distal area, more organized and water driven deposits (e.g., lacustrine carbonates of the Çaltılık Formation) become dominant to produce parallel and continuous reflection responses. Seismic stratigraphic unit III (SSU-III) overlies the SSU-II and is characterized by almost horizontal reflectors onlapping onto the underlying unit SSU-III correlates to more than one formation. Together with the Quaternary alluvium, Gediz, Kaletepe and Bintepele formations (or their basinward equivalents) are all included within the SSU-III (Çiftçi & Bozkurt, 2009a) (Figure 2.7b).

Geological cross section in Figure 8 shows the geometry and bounding structure of Gediz graben and emphasizes its asymmetric nature. Cross section also illustrates the role on the southern margin in generating sedimentary fill. Thus, thickness of the Miocene units is decreasing towards the north and post Miocene units are more uniform suggested the limited motion of the north margin during the post Miocene (Yusufoğlu, 1996; Çiftçi & Bozkurt, 2009b). Three boreholes reached to the Neogene clastics with BH-1 reaching all the way to the basement metamorphic. Geothermal gradients are higher at the BH-3 and BH-2 drilled in closer proximity to southern margin than BH-1 due the convectational transportation of the heat.

Consequently, Figure 2.8 will be the base for our thermomechanical modeling studies for Gediz graben in the Chapter 7.

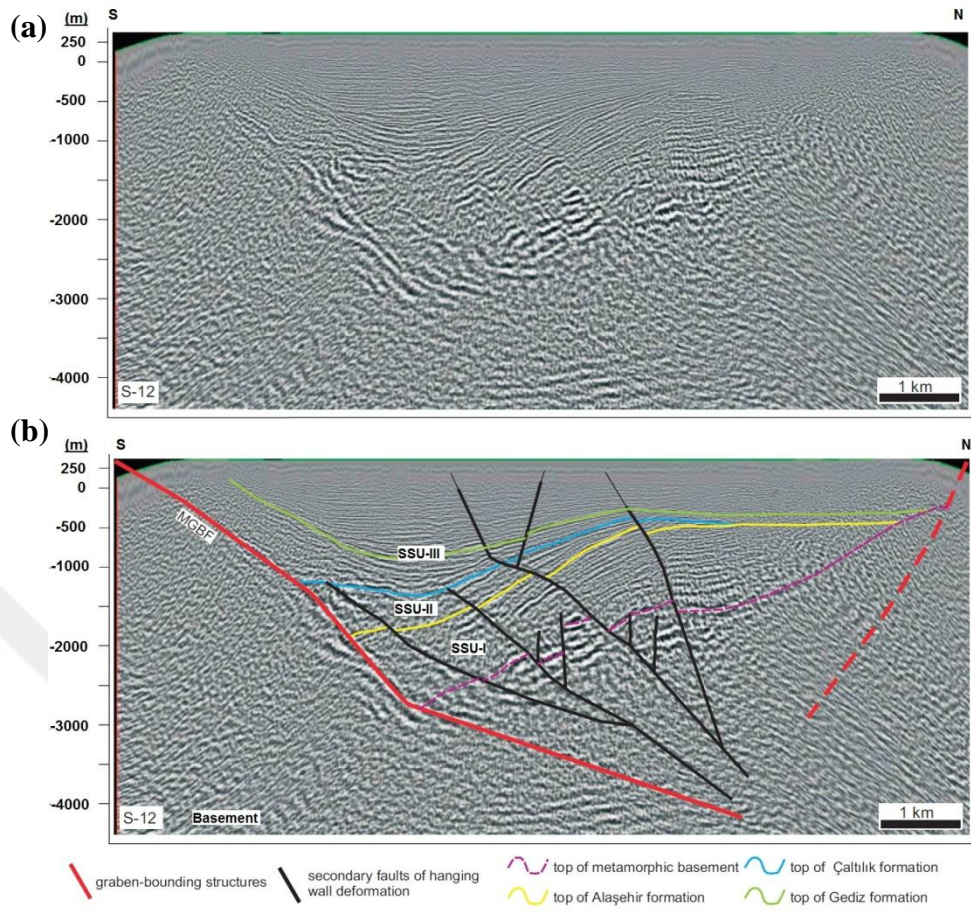


Figure 2.7 2-D seismic reflection profile (S-12) (a) Uninterpreted profile (b) with interpretation of seismic stratigraphic units. Thick black line depicts the subsurface continuation of MGBF and thinner black lines illustrate some secondary hanging-wall faults offsetting the stratigraphic units (Çiftçi & Bozkurt, 2010). See Figure 2.5 for location of the seismic profile.

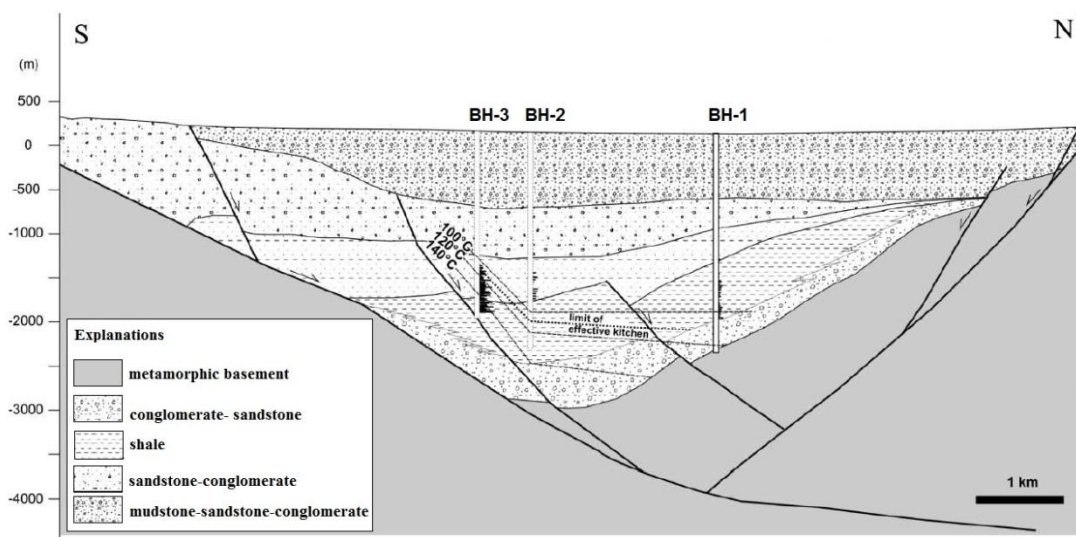


Figure 2.8 Transverse geologic cross section of the Gediz graben. BH:borehole (Çiftçi et al., 2010).

2.2 Büyük Menderes Graben

The Büyük Menderes graben is the other prominent graben after Gediz with its great extension and sedimentary thickness in western Anatolia. It extends from Ortaklar in the west to Sarayköy in the east containing Büyük Menderes River. It has approximately 150 km length and 2.5-14 km width. The width of the graben increases from east to west. In contrast to Gediz, northern margin with well developed fault systems is active at Büyük Menderes (Figure 2.9). The northern margin of the Buyuk Menderes graben has a South-dipping low-angle normal fault (the Buyuk Menderes detachment fault) that separates a sequence of high-grademetamorphic gneisses and a Neogene sedimentary rock succession in its hangingwall from the marble-intercalated mylonitized schists in its footwall (Emre & Sözbilir, 1997; Lips et al., 2001; Gessner et al., 2001; Çemen et al., 2006).

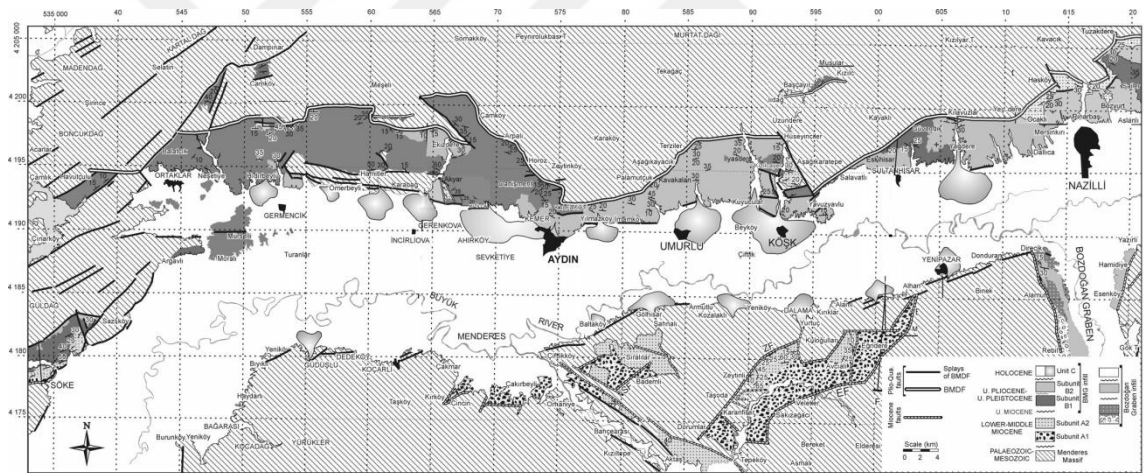


Figure 2.9 Geological map of the Büyük Menderes Graben. BDMF – Büyük Menderes Detachment Fault, EF – Egridere fault, ZF – Zeytinli fault, SF – Sıralılar fault (gürer et al., 1999).

Two major rock units are described in Büyük Menderes graben and surroundings; pre-Neogene basement units and Neogene-Quaternary sedimentary fill up to 2.5 km thick (Gürer et al., 2009). Metamorphic rocks of Menderes massif constitute the pre-Neogene basement of the graben (Bozkurt, 2000) and consist of three lithological successions; (1) core (mostly augen gneiss) at the base, (2) Palaeozoic low-grade metasediments (schist cover), and (3) Cenozoic marble-dominated sequence (marble cover). The intensity of metamorphism increases toward the core (Bozkurt, 2004).

The fill of Büyük Menderes graben is well encountered particularly along the northern margin of the graben. Simplified stratigraphic section (Figure 2.10) of graben indicated that three litho-stratigraphic units termed A, B and C, are present in the Büyük Menderes Graben region. All these units rest on the basement metamorphics rocks (Gürer et al., 2009).

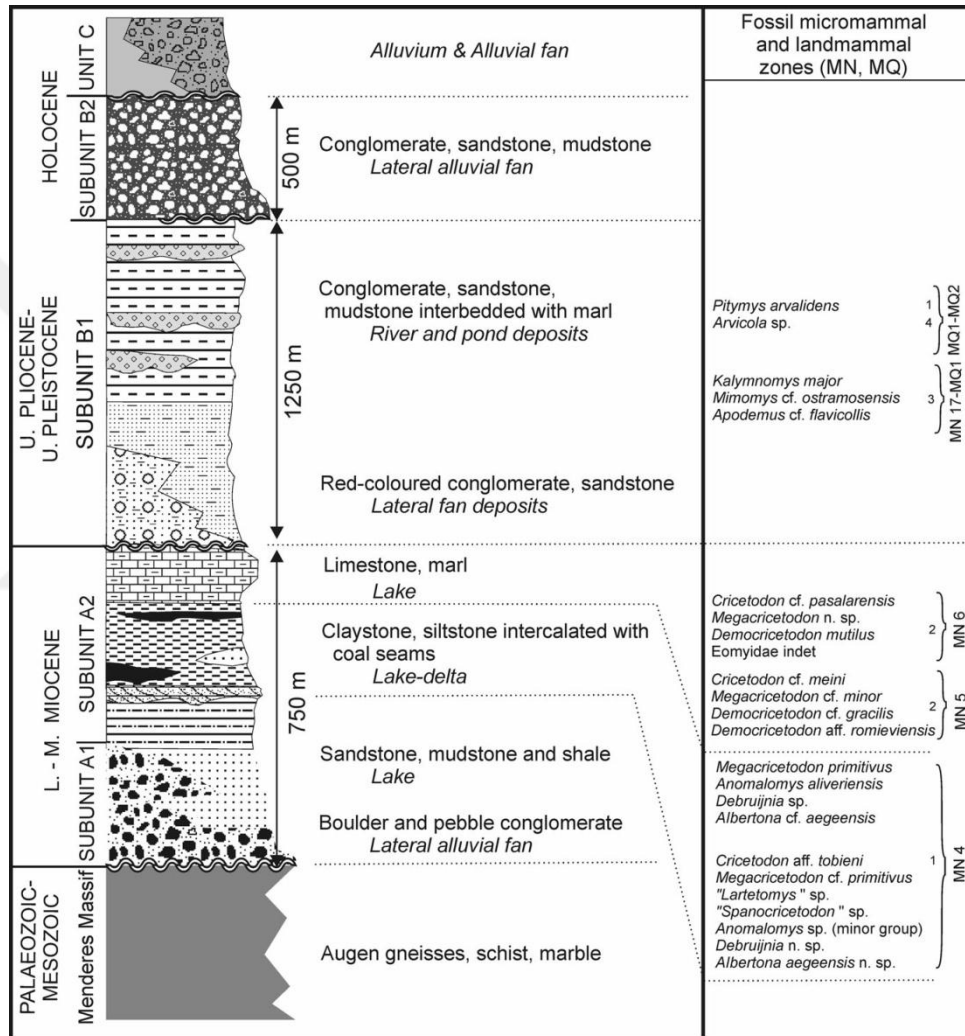


Figure 2.10 Simplified stratigraphic section of the Büyük Mendres graben basin-fill (from Gürer et al., 2009).

The unit A is mainly consisted of northwards tilted continental clastic sediments lie between the metamorphic rocks of the Menderes Massif in the north This unit comprises a broadly coarsening-upwards sequence with a total thickness of 2 km (Cohen et al., 1995). At the basement, lithology is reddish, coarse-grained, well cemented, poorly sorted, polygenetic conglomerate composed of clasts derived from the underlying metamorphics. Above the conglomerates, siltstone, mudstone and shale alternations, together with conglomerates and pebbly sandstones are present (Bozkurt, 2000). Alternations of sandstone, siltstone, mudstone and claystone with approximately horizontal, massive, cobble to boulder conglomerates draw the Unit B. It has east-west trending, high-angle normal faults along its contacts, both with the deformed sediments of unit A to the north and the younger basin-fill sediments (unit C) to the south (Bozkurt, 2000). Unit C forms from generally alluvial fan and graben floor sediments. The source of these alluvial fan sediments is the metamorphic basement, unit A and B sediments. Grain sizes of the alluvial fans are getting smaller along the Büyük Menderes River. These sediments, with the present-day configuration of the Büyük Menderes Graben, are juxtaposed with unit B sediments along high-angle graben-bounding normal faults (Bozkurt, 2000).

The contact between graben fill and basement is clearly seen the seismic reflection section (Çifçi et al., 2011). They classified the graben fill in to four sedimentary sequences using seismic data (Figure 2.11). According to the N–S compiled seismic and geological data, the deepest detachment fault governs the region, and the other faults operate on it. This fault splits the sedimentary and the metamorphic rocks and forms the boundary.

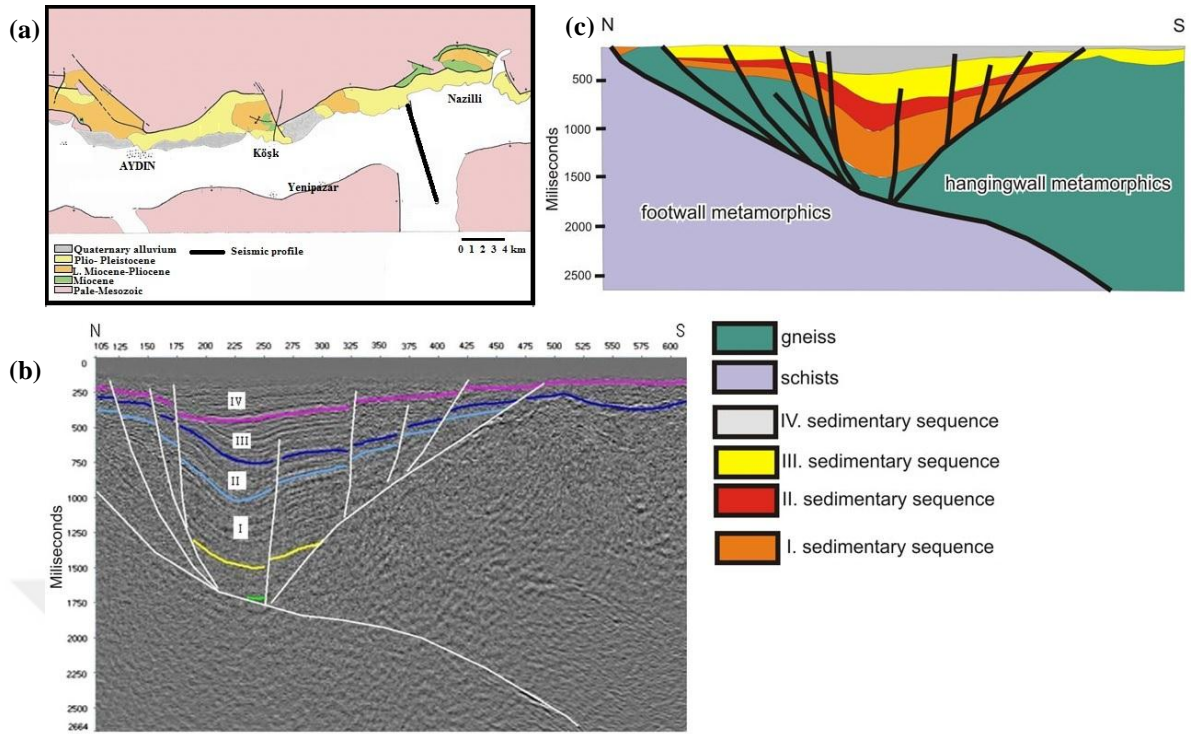


Figure 2.11 (a) Location of the seismic section (b) A transverse seismic profile in association with (c) The interpreted cross-section showing the sequence stratigraphic units (Çifçi et al., 2011).

CHAPTER THREE

GEO THERMOMETRY

Geothermometry is one of the essential tools in geothermal exploration, development and monitoring studies. It is possible to estimate of the reservoir (subsurface) temperatures with geothermometry equations using the chemical and isotopic composition of surface discharges from wells and/or natural springs/fumaroles. The geothermometers depend on one or more dissolved constituents in the thermal water whose concentrations vary depending on the temperatures of the water. The constituents may be solutes gases or isotopes and according their constituents geothermometers can be classified in to three groups as (a) Water or solute geothermometers, (b) Isotope geothermometers, (c) Steam or gas geothermometers. Generally type (a) and (c) named as Chemical Geothermometers (Arnórsson, 2000).

3.1 Chemical Geothermometers

Chemical geothermometers are based on temperature-dependent, water-rock reactions that control the chemical compositions of the thermal waters. All geothermometry equations rely on the assumption that the water preserves its chemical composition during its ascent from the reservoir to the surface. Assumption of the preservation of water chemistry may not always hold because the water composition may be affected by physical processes such as cooling and mixing with waters from different reservoirs. Cooling processes can be actualized by conductive heat loss or adiabatic way. Conductive cooling does not by itself change the composition of the water but may affect its degree of saturation with respect to several minerals thus; it may bring about a modification in the chemical composition of the water by mineral dissolution or precipitation. Adiabatic cooling causes changes in the composition of ascending water these changes include degassing, and hence the increase in the solute content as a result of steam loss (Arnórsson, 2000).

Generally, two types of chemical geothermometers are commonly used in geothermal studies are based on mineral solubility (silica-SiO₂) and ion exchange reactions (Na/K, Na-K-Ca, Na-Li, K-Mg and etc.). These chemical geothermometers refer to silica and cation geothermometers.

3.1.1 Silica Geothermometer

Silica geothermometer is the most reliable geothermometer in estimation reservoir temperature. They are based upon temperature dependent water solubility of various form of silica. Silica can be found in geothermal water in many phases including quartz, cristobalite, chalcedony, opal, moganite, amorphous silica (Dress et al., 1989). Quartz is the most stable phase with lowest solubility while amorphous silica is the least stable phase with highest solubility within them. They represent the two extreme points of silica geothermometer. The solubility of the others phases will be between them.

The first silica geothermometers equation was derived by Fournier (1977) from quartz solubility data than several different silica geothermometers have been proposed and improved by different scientists. In this study quartz geothermometry equations given in Table 3.1 are applied on the water samples collected from Gediz and Büyük Menderes grabens.

It is also possible to estimate heat flow using the silica temperatures. Swanberg & Morgan (1978, 1980) showed a linear correlation between silica temperature and heat flow. This allows the estimation of heat flow from silica geotemperatures in region where traditional heat flow measurements are unavailable. This correlation is represented by:

$$T(\text{SiO}_2) = mq + b \quad (3.1)$$

where $T(\text{SiO}_2)$ is the temperature of the reservoir (°C), q is the heat flow (mWm^{-2}) and b is the long term mean annual surface temperature. The slope m is the thermal resistance and if multiplied by thermal conductivity ($\text{Wm}^{-1}\text{K}^{-1}$), reflects the mean

depth (m) to which ground water may circulate. İlkışık (1995) used the values of m as 0.7 for the calculation of heat flow in western Turkey.

Table 3.1 Quartz geothermometry equations

Equation to obtain temperatures	Reference
$T = [1309/(5.19 - \log S)] - 273.15$	Fournier, (1977)
$T = [1522/(5.75 - \log S)] - 273.15$	Fournier, (1977)
$T = -42.198(\pm 1.345) + 0.28831(\pm 0.01337)S - 3.6686 \times 10^{-4}(\pm 3.152 \times 10^{-5})S^2 + 3.1665 \times 10^{-7}(\pm 2.421 \times 10^{-7})S^3 + 77.034(\pm 1.216)\log S$	Fournier & Potter, (1982)
$T = \{-44.119(\pm 0.438)\} + \{0.24469(\pm 0.00573)\}S - \{1.7414 \times 10^{-4}(\pm 1.365 \times 10^{-5})\}S^2 + \{79.305(\pm 0.427)\}\log S$	Verma & Santoyo, (1997)
$T = -55.3 + 0.3659S - 5.3954 \times 10^{-4}S^2 + 5.5132 \times 10^{-7}S^3 + 74.360 \log S$	Arnorsson, (2000)
$T = \{[1175.7(\pm 31.7)]/[4.88(\pm 0.08) - \log S]\} - 273.15$	Verma, (2000)

S is SiO_2 concentration in mg/l; temperature (T) is in $^\circ\text{C}$

3.1.2 Cation Geothermometers

The cation geothermometry is based on ion-exchange reactions that have temperature-dependent equilibrium constants. These are Na-K, Na-K-Ca, Na-Li, Li-Mg, K-Mg, and Na-K-Mg geothermometers. We used Na-K, Na-K-Ca, Na-Li, K-Mg geothermometers in this study and their equations are given in Table 3.2.

3.1.2.1 Na-K Geothermometer

The low Na/K ratios in geothermal water are the indicators of high temperatures in the depths (D'Amore & Arnorsson, 2000). Na/K ratio is probably controlled by ion exchanges between them and alkali feldspars in geothermal water (Ellis & Wilson, 1960; Nicholson, 1993). The advantage of this geothermometer include that it is less affected by dilution or steam loss given that it is based on a ratio. The Na-K geothermometer is applicable up to 350°C , as the re-equilibration is slower than that of the silica-quartz geothermometer. Therefore, the Na-K geothermometer may give indications regarding the deeper part of the system in comparison to the silica geothermometer, depending on the system's hydrology.

Unfortunately, below the 100°C the Na-K geothermometer gives poor results. It is also unsuitable if the waters contain high concentration of calcium (Ca) as is the case for springs depositing travertine.

Table 3.2 Cation geothermometry equations

Type	Equation to obtain temperatures	Reference
Na-K	$T = 777 / [\log(\text{Na}/\text{K}) + 0.700] - 273$	Fournier & Truesdell, (1973)
Na-K	$T = 856 / [\log(\text{Na}/\text{K}) + 0.857] - 273$	Truesdell, (1976)
Na-K	$T = 1217 / (\pm 93.9) / [\log(\text{Na}/\text{K}) + 1.483] - 273.15$	Fournier, (1979)
Na-K	$T = 883 / [\log(\text{Na}/\text{K}) + 0.780] - 273$	Tonani, (1980)
Na-K	$T = 933 / [\log(\text{Na}/\text{K}) + 0.993] - 273$	Arnorsson et al., (1983)
Na-K	$T = 1319 / [\log(\text{Na}/\text{K}) + 1.699] - 273$	Arnorsson et al., (1983)
Na-K	$T = 1178 / [\log(\text{Na}/\text{K}) + 1.470] - 273$	Nivea & Nivea, (1987)
Na-K	$T = 1390 / [\log(\text{Na}/\text{K}) + 1.750] - 273$	Giggenbach, (1988)
Na-K	$T = 1289 / (\pm 76) / [\log(\text{Na}/\text{K}) + 0.615] - 273.15$	Verma-Santoyo, (1997)
Na-K	$733.6 - 770.551 [\log(\text{Na}_m/\text{K}_m)] + 378.189 [\log(\text{Na}_m/\text{K}_m)]^2 - 95.753 [\log(\text{Na}_m/\text{K}_m)]^3 + 9.544 [\log(\text{Na}_m/\text{K}_m)]^2$	Arnorsson, (2000)
Na-K	$T = 1052 / [1 + \exp(1.714 \log(\text{Na}/\text{K}) + 0.252)] + 76$	Can, (2002)
Na-K	$T = \{883 (\pm 15) / [\log(\text{Na}/\text{K}) + 0.894 (\pm 0.032)]\} - 273$	Díaz-González et al., (2008)
Na-K	$T = 833 / [\log(\text{Na}/\text{K}) + 0.908] - 273.15$	Díaz-González et al., (2008)
K-Mg	$T = 4410 / [14.0 - \log(\text{K}^2/\text{Mg})] - 273.15$	Giggenbach, (1988)
K-Mg	$T = 2330 / [7.35 - \log(\text{K}^2/\text{Mg})] - 273.15$	Fournier, (1991)
K-Mg	$T = 1077 / [4.033 + \log(\text{K}^2/\text{Mg})] - 273.15$	Fournier, (1997)
Na-Li	$T = 1000 (\pm 47) / [\log(\text{Na}_m/\text{Li}_m) + 0.38 (\pm 0.11)] - 273.15$	Fouillac & Michard, (1981)
Na-Li	$T = 1195 (\pm 75) / [\log(\text{Na}_m/\text{Li}_m) - 0.19 (\pm 0.25)] - 273.15$	Fouillac & Michard, (1981)
Na-Li	$T = 1590 / [\log(\text{Na}/\text{Li}) + 0.779] - 273.15$	Kharaka & Mariner, (1989)
Na-Li	$T = 1049 (\pm 44) / [\log(\text{Na}_m/\text{Li}_m) + 0.44 (\pm 0.10)] - 273.15$	Verma & Santoyo, (1997)
Na-Li	$T = 1267 (\pm 35) / [\log(\text{Na}_m/\text{Li}_m) + 0.07 (\pm 0.10)] - 273.15$	Verma & Santoyo, (1997)
Na-K-Ca	$T = 1647 / [\log(\text{Na}_m/\text{K}_m) + \beta (\log((\text{Ca}_m)0.5/\text{Na}_m) + 2.06) + 2.47] - 273.15$	Fournier & Truesdell, (1973)
Na-K-Ca	$T = 1120 / [\log(\text{Na}/\text{K}) + \beta (\log(\text{Ca}0.5/\text{Na}) + 2.06) + 1.32] - 273.15$	Kharaka & Mariner, (1989)

Concentrations of Na, K, Li, Ca and Mg are in mg/kg (elements symbols are used for this purpose).

Concentrations in molar units are indicated by the subscript m, i.e. Na_m , K_m , Ca_m . T is temperature (T) in °C.

3.1.2.2 Na-K-Ca Geothermometer

Na-K-Ca geothermometer was developed by Fournier & Truesdell (1973) for the application to waters with high concentration of calcium (Ca). It gives less erroneous results than the Na-K geothermometer for low-temperature geothermal waters (Fournier & Truesdell, 1973; Karingithi, 2009) and non-equilibrated waters. Both Na-K and Na-K-Ca geothermometers are not applicable the acidic waters which would not be in equilibrium with feldspars (D'Amore & Arnorsson, 2000). An empirical correction is applied to Na-K-Ca geothermometer results if water contains high dissolved Mg.

3.1.2.3 Na-Li Geothermometer

The Na-Li geothermometer was firstly formulated by Fouillac & Michard (1981) by the help of statistic study about granitic and volcanic ground waters. Two other Na-Li geothermometers were documented in Kharaka et al., (1982) and Verma & Santoyo (1997) are used in this study.

3.1.2.4 K-Mg Geothermometer

K-Mg geothermometers is used in the cases where dissolved Na and Ca have not equilibrated between water and rock. Giggenbach (1988) and Fournier (1991) developed and applied the geothermal fluids. By assuming only geothermal fluids in formations of the sedimentary cover, which consist of carbonate, evaporite, and detrital deposits, the K-Mg geothermometers cannot be applied. Actually, these formations are poor in feldspars indicating another origin for these elements such as dolomite dissolution and leaching of seawater brines (Sonney & Vuataz, 2010). K-Mg geothermometers are applicable from 50 to 300 °C, and are of greatest use in the study of low to intermediate enthalpy systems when equilibrium has not been attained between the fluid and the complete mineralogical assemblage of the host rock (Nicholson, 1993).

3.2 Geothermometry Applications

In this thesis, geothermometric equations are applied to calculate and compare geotemperature estimates from different cation and silica geothermometers. Chemical data used in this study is obtained from Inventory of Turkey Geothermal Resources, reported by Mineral Research & Exploration General Directorate (MTA) in 2005. This data set consists of surface temperature, Na, K, Ca, Cl, Mg, Li contents of thermal water and their locations. Collected samples were analyzed at the MTA laboratories. Na and K concentrations were determined by flame photometry and atomic absorption spectrometry. Titration methods were used for Ca, Mg, Cl analyses. Due to the deficiency of Mg and Li concentrations, K-Mg and Na-Li geothermometers are not applied on our data set.

Before applying geothermometers on data sets, the degree of water–rock equilibrium attained in the reservoir is evaluated by determining the Maturity Index (MI) of thermal waters proposed by Giggenbach (1988).

$$MI = 0.315 * \log(K^2/Mg) \log(K/Na) \quad (3.2)$$

MI values less than 2.0 mean that thermal water and reservoir rock are not in equilibrium. If the MI value is between 2.0-2.66, thermal water and reservoir rock are partially balanced. MI values more than 2.66 indicate that thermal waters have attained water–rock equilibrium. Cation geothermometers (generally Na–K geothermometers) are not reliable for the nonequilibrium waters. In this case, reservoir temperatures calculated from silica geothermometers are generally used as dependable results.

3.1.1 Geothermometry Results

Aquifer temperatures of all thermal water in the study area are estimated using SolGeo computer program (Verma et al., 2008). The program used the geothermometry equations given in Table 3.1 and Table 3.2 including their respective applicability constraints. Mean geotemperature values are used to map the results of each geothermometers. In Figure 3.1 distribution of silica geothermometers is given. The mean reservoir temperatures estimated by Quartz geothermometers vary between 66 and 265°C for water samples. The maximum temperatures are calculated for water samples located around Denizli Kızıldere geothermal area. Estimated temperatures from Quartz geothermometers fit best with the bottom hole temperatures (BHTs) located in Sandıklı (AF-1, AF-6 etc.) and Urganlı (U-1) (Table 3.3).

SiO₂ (Quartz) Geothermometers

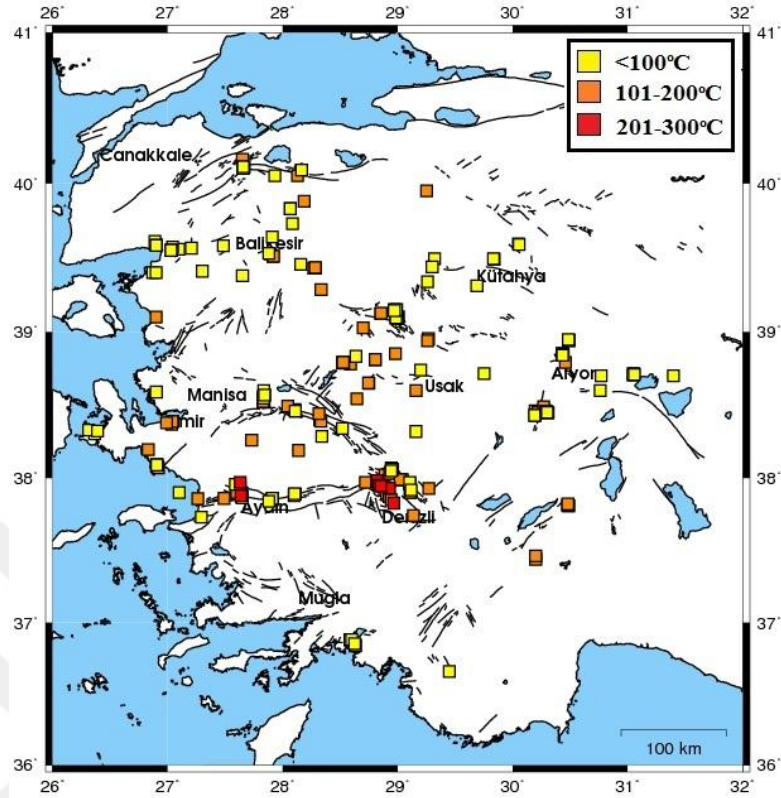


Figure 3.1 Quartz geothermometry results for western Turkey

The Na-K geothermometer is generally thought to take longer to reach equilibrium at a given temperature than other commonly used geothermometers. Therefore, the Na/K ratio is commonly used to estimate possible highest temperatures in deeper parts of a system where waters reside for relatively long time periods, and other geothermometers are used to estimate lower temperatures that occur in shallower reservoirs where waters reside for relatively short periods of time (Fournier, 1989). Generally, reservoir temperatures computed from the Na-K geothermometers are about 20–30 °C higher than those of Quartz geothermometers in this study (Figure 3.2). Na-K geothermometers yield reservoir temperatures agreeing well with BHTs in Öberbeyli (ÖB-2 and ÖB-3) and Kızıldere (R-2) geothermal area (Table 3.3).

Table 3.3 Measured BHTs and estimated reservoir temperatures for the wells located in the region.

<i>Name</i>	<i>Region</i>	<i>Measured</i>	<i>SiO₂</i>		
		<i>T (°C)</i>	<i>Quartz</i>	<i>Na-K</i>	<i>Na-K-Ca</i>
AF-1	Afyon	98	106	154	191
R-260	Afyon	92	128	134	178
AF-3	Afyon	97	118	149	193
AF-4	Afyon	95	129	156	192
AF-5	Afyon	79	96	151	185
AF-6	Afyon	92	124	154	186
AF-7	Afyon	93	131	159	100
AF-8	Afyon	91	95	160	188
AF-9	Afyon	50	136	N/A	112
AF-10	Afyon	96	127	153	101
G-3	Afyon	74	98	181	120
AYTER-1	Aydın	78	100	175	106
AYTER-2	Aydın	80	109	202	118
ÖB-1	Aydın	203	157	157	152
ÖB-2	Aydın	231	166	235	260
ÖB-3	Aydın	230	107	229	254
ÖB-4	Aydın	213	105	213	225
ÖB-5	Aydın	221	186	226	118
ÖB-6	Aydın	221	95	185	131
ÖB-7	Aydın	203	188	203	229
ÖB-9	Aydın	223	212	195	210
GÖNEN-1	Balıkesir	82	104	119	157
GÖNEN-2	Balıkesir	78	84	115	154
GÖNEN-3	Balıkesir	78	112	126	161
GÖNEN-4/A	Balıkesir	71	73	127	166
KD-1	Denizli	198	193	202	322
KD-2	Denizli	119	198	170	113
KD-4	Denizli	172	183	188	N/A
KD-6	Denizli	196	215	197	250
KD-16	Denizli	207	232	206	252
R-2	Denizli	205	207	204	282
B-1	İzmir	114	117	166	173
B-6	İzmir	93	110	117	80
B-7	İzmir	115	139	154	94
B-9	İzmir	122	130	146	93
GI-1/A	Kütahya	78	107	137	157
GI-2	Kütahya	97	104	163	170
GI-3	Kütahya	78	106	219	202
U-1	Manisa	62	66	162	191
K-1	Manisa	96	151	198	198
K-2	Manisa	96	146	205	210
K-3	Manisa	96	141	202	211

N/A: not available chemical data

Na-K-Ca temperatures are in accordance with the Na-K temperatures. The maximum temperatures are calculated around Uşak in Na-K-Ca geothermometers applications (Figure 3.3).

The thermal waters of western Anatolia are located along the tectonically active zones (faults and grabens). The geothermometry applications reveal that Denizli is the most promising region in terms of geothermal energy potential. Among the all geothermometers applied to the region, Quartz and Na-K geothermometers yield reservoir temperatures agreeing well with each other and measured BHTs.

NaK Geothermometers

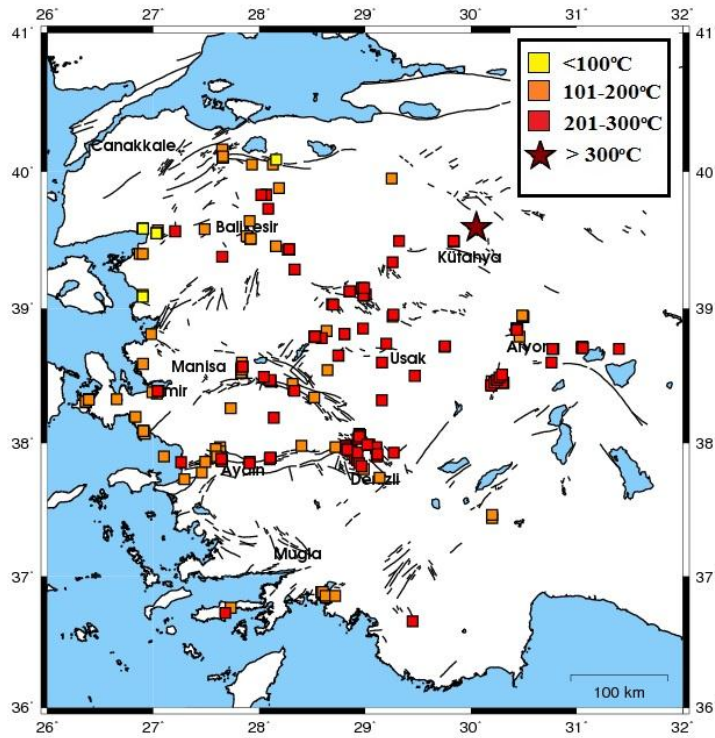


Figure 3.2 Na-K geothermometry results for western Turkey.

NaKCa Geothermometers

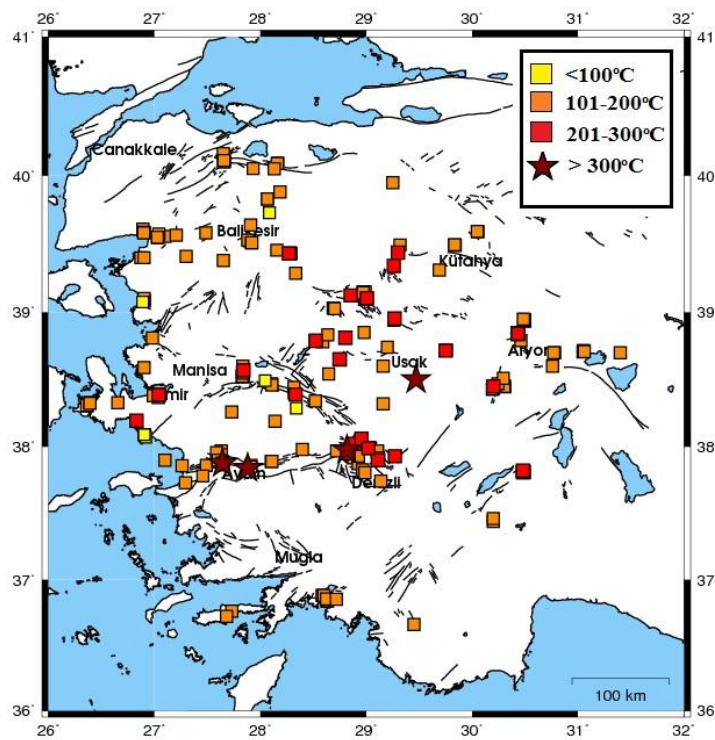


Figure 3.3 Na-K-Ca geothermometry results for western Turkey.

3.2.2 Heat Flow Estimation from Silica Geo-Temperatures

The heat flow distribution map estimated from silica temperatures for western Turkey was presented by İlkışık (1995) as mentioned in Chapter 1. The mean heat flow value was calculated as $107 \pm 45 \text{ mWm}^{-2}$ using 187 thermal waters from western Anatolia and some regions from central Anatolia. In this thesis this map is updated for western Anatolia region by using 90 new chemical data obtained from Inventory of Turkey Geothermal Resources, reported by Mineral Research & Exploration General Directorate (MTA) (Akkuş et al., 2005).

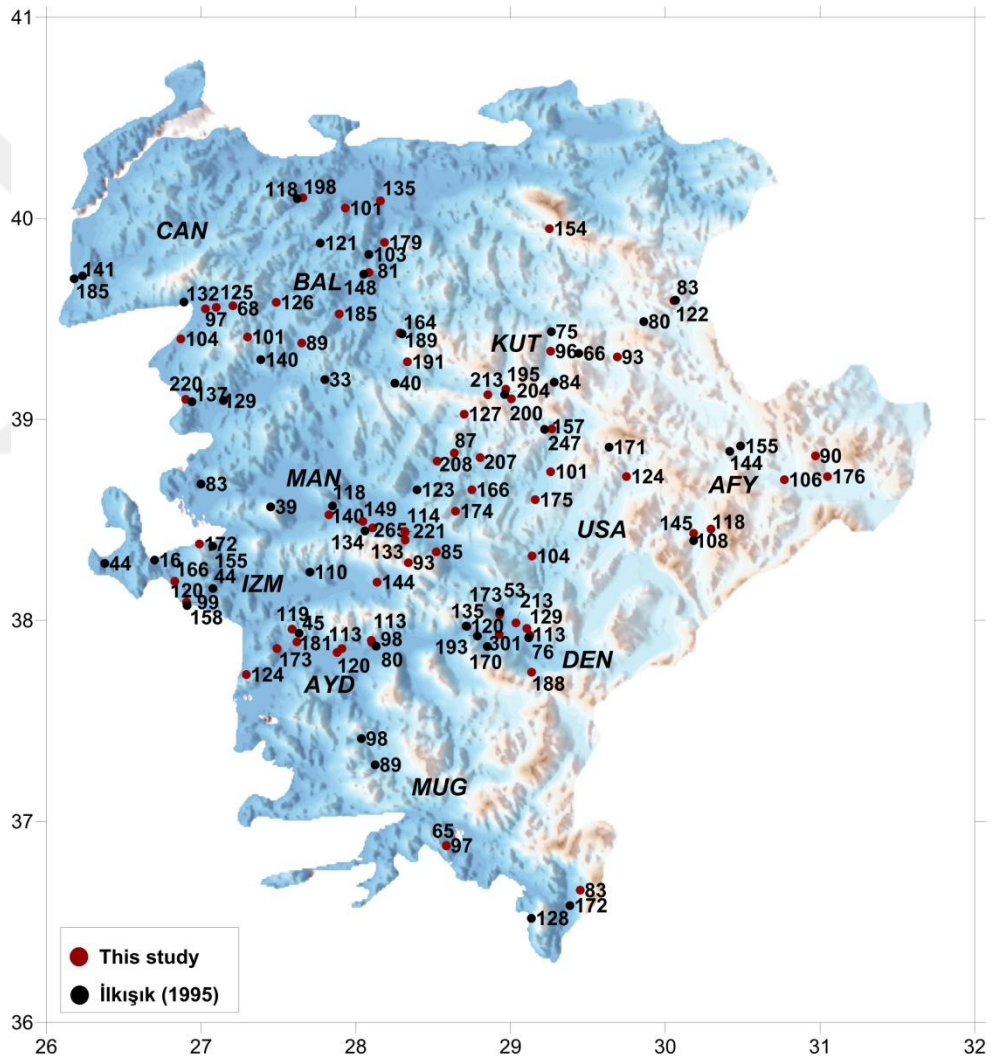


Figure 3.6 Heat flow distribution map for western Anatolia estimated from silica geotemperatures. Heat flow values are given in mWm^{-2} . AYD:Aydın; AFY: Afyon; BAL: Balıkesir; CAN: Çanakkale; DEN:Denizli; IZM: İzmir; KUT: Kütahya; MAN: Manisa; MUG:Muğla; USA:Uşak.

Different from İlkışık study, our results include only western Anatolia region. As seen in Figure 3.6 maximum heat flow value of 301 mWm^{-2} is calculated for Kızıldere geothermal field in Denizli. Additionally, in Gediz graben the value of 265 mWm^{-2} is calculated for the Kurşunlu. Our results indicate that the average heat flow value for the area is $131 \pm 45 \text{ mWm}^{-2}$. These extremely high values refer to geothermal systems where the heat energy mainly transfers by convection. This is the main reason of the differences between silica heat flow value and heat flow values obtained by conventional method. It should not be forgotten that silica geotemperatures and heat flow values are the indicators of the geothermal systems, they can not be used in conduction based thermal investigation studies.



CHAPTER FOUR

THERMAL CONDUCTIVITY

Thermal conductivity is a physical property that characterizes the ability of a material to conduct heat. The knowledge of thermal conductivity is required in heat flow determinations as the heat flow is calculated by multiplying the geothermal gradient with the thermal conductivity (Jaeger, 1965). Thermal conductivity is also an essential input parameter in thermal modeling investigations as it controls the steady-state temperature distribution within the earth (Blackwell & Steele, 1989). In particular, the contrast in thermal conductivity between sediments and basement rocks may lead to significant temperature changes even if the regional heat flow is constant (Thakur et al., 2012; Erkan & Blackwell, 2008; Balkan & Şalk, 2014).

Although western Turkey is well-known to have medium-to-high enthalpy geothermal systems (Başel et al., 2010), detailed thermal models have not been developed due to lack of direct thermal conductivity measurements beside insufficient geothermal gradient data. In particular, thermal conductivity information is necessary for estimating the Enhanced Geothermal System (EGS) potential of an area (Tester et al., 2006). This study aims to accommodate the gap in the knowledge of thermal conductivities of the major lithologic units in western Anatolia.

4.1 Thermal Conductivity of Rocks

The thermal conductivity of rocks depends on various parameters including anisotropy, mineral composition, porosity, temperature, pressure and properties of pore-filling fluids. This leads to a large variability in thermal conductivities within each rock type (sedimentary, volcanic, plutonic, and metamorphic rocks).

4.1.1 Anisotropy

Some of physical properties such as density or heat capacity of a rock are independent with measuring direction, they are scalar properties. But this not always the case, thermal conductivity of a material varies with the direction within the rock. Anisotropy of thermal conductivity can be defined as ratio between thermal conductivity parallel to the layering and thermal conductivity perpendicular to layering. Anisotropy of thermal conductivity depends on the structure and texture of a rock. Therefore thermal conductivity must be defined in relation to a direction in a crystal, and the magnitude of the thermal conductivity may be different in different directions. Simmons (1961) emphasized that the thermal conductivity calculated in a single borehole through anisotropic rock will not match to the thermal conductivity parallel to the borehole. Generally if a rock is layered the parallel thermal conductivity (parallel to bedding) is greater than the perpendicular thermal conductivity (Robertson, 1988). Anisotropy ratio for sedimentary rocks can be reaches up to 2.5 (Kappelmeyer & Hänel, 1974; Gretener, 1981; Popov et al., 1995).

4.1.2 Porosity

Thermal conductivity of rocks depends strongly on its porosity. The effect of the porosity is to decrease considerably the bulk thermal conductivity as pore-filling fluids (water, air, gas etc.) have lower thermal conductivity (Table 4.1) than the rock forming minerals (Table 4.2) (Brigaud & Vasseur, 1989). Figure 4.1 shows that thermal conductivity of limestone decreases with increasing porosity but it increases if the pores fill with water instead of air.

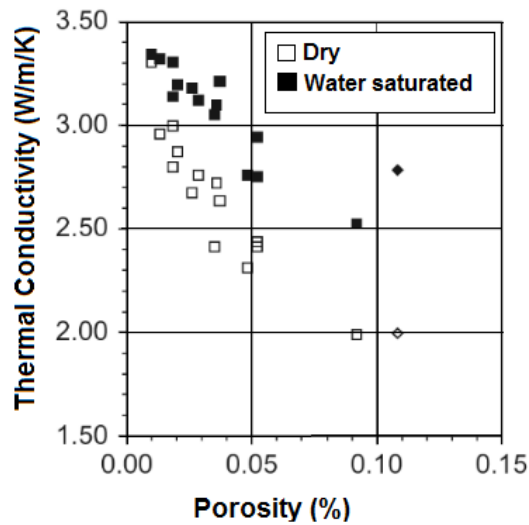


Figure 4.1 Thermal conductivity of limestone Poulsen et al. (1982)

Table 4.1 Thermal conductivity of pore-filling fluids (Schön, 2011)

Pore Fluid	T (°C)	λ (Wm ⁻¹ K ⁻¹)
Air		0.025
Gas		0.027
Water (mean)		0.50-0.59
	0	0.5602
	20	0.5992
	40	0.6281
	70	0.6619
	100	0.6789
Oil	20	0.14-0.15
Crude oil	20	0.13-0.14

The influence of pore-filling fluid on thermal conductivity depends on porosity ratio of the rock and texture. If porosity is low, the effect of pore-filling fluids on bulk thermal conductivity is small, because rocks matrix materials conduct the heat much better than the fluids. However, if the porosity is high, the bulk thermal conductivity of rock will decrease. Therefore, increase in ratio of solid phase per unit volume (decreasing the porosity) will result in an increase in the bulk thermal conductivity of the rock. The effect of the pore-fluid type on thermal conductivity of sandstone is given Figure 4.2. Thermal conductivity of water is higher than other possible pore fluids. Thus a higher thermal conductivity for water saturated sandstone and lower conductivity for gas-bearing sandstone can be expected.

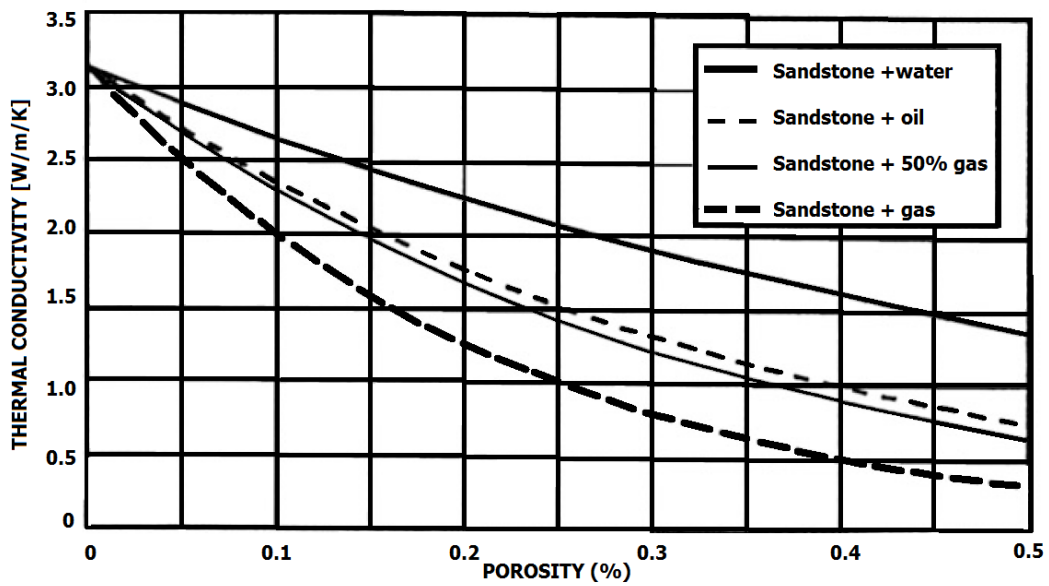


Figure 4.2 Thermal conductivity of sandstone as a function of porosity and pore fluid at ambient temperature and pressure (Poelchau et al., 1997).

4.1.3 Texture and Mineral Composition

Thermal conductivity of a rock is influenced by directly texture and which consist of mineralogical assemblages. Crystal structure and grain boundaries of the rocks may change the amount of the heat it has been exposed to. Heat can easily transfer between in a dense grain texture than in a loosely packed one. Thermal conductivities of possible rock-forming rocks are given in Table 4.2. Among the rock-forming minerals quartz and hematite have a high thermal conductivity as clay, gypsum and organic materials have low thermal conductivity. This originates the dependence of thermal conductivity on mineral composition of rocks (Schön, 2011). Minerals with high thermal conductivity cause an increase on bulk thermal conductivity. Therefore, for metamorphic rocks, high values for quartzite (high quartz content) and low values for quartz-mica schist and gneiss (low quartz content) are expected (Clauser, 2006). Figure 4.3 shows the linear correlation between quartz content and thermal conductivity of 35 rocks samples from Posiva Oy field in Finland (Kukkonen & Lindber, 1998).

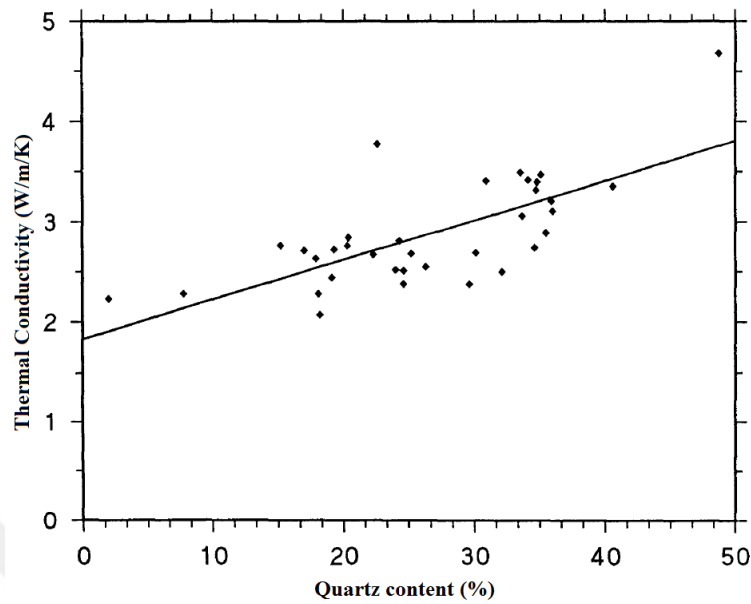


Figure 4.3 Relationship between quartz content and measured thermal conductivity (Kukkonen & Lindber, 1998).

Table 4.2 Thermal conductivity of some rock-forming minerals

Mineral	λ ($\text{Wm}^{-1}\text{K}^{-1}$)	Mineral	λ ($\text{Wm}^{-1}\text{K}^{-1}$)
Quartz- α	7.69 (CH), 7.69 (CR) 7.7 (B)	Magnetite	5.10 (CH), 4.7-5.3(M), 5.1(CR)
Quartz-mean	6.5 (C)	Hematite	11.28 (CH), 11.2-13.9 (M)
Zircon	5.54 (CH), 5.7 (M)	Calcite	3.59 (CH), 3.25-3.9 (M)
Serpentine	3.53 ± 1.28 (CH), 1.8-2.9 (M)	Dolomite	5.51(CH), 5.5 (CR), 5.3 (B)
Clay minerals	2.9 (Q), 1.7 (C)	Anhydrite	4.76 (CH), 4.76 (CR), 5.4 (C)
Feldspar	2.3 (H), 2.0 (DJ)	Gypsum	1.26 (CH), 1.0-1.3 (M)
Apatite	1.38 ± 0.01 (CH), 1.4 (M)	Organic materials	0.25 (Q), 1.0 (B)

B: Brigaud et al. (1989, 1992); C: Clauser (2006); CH: Clauser & Huenges (1995); CR: Cermak & Rybach (1982); DJ: Drury & Jessop (1983); M: Melnikov et al. (1975); Q: Quiel (1975).

4.1.4 Temperature

Thermal conductivity is a temperature dependent physical property. Temperature dependence of a material is characterized by the structure of itself. Thermal conductivity of crystalline solid materials decreases with temperature based on Debye's theory. Amorphous materials are characterized by an increase with increasing temperature (Schön, 2011).

Thermal conductivity of a rock tends to decrease with increasing temperature. Heat conductivity in rocks is mainly due to lattice vibration and free electrons. As the temperature rise, lattice vibrations impede the motion of free electrons. However, thermal conductivity increases with the cube of temperature in radiation driven case. Thus, generally thermal conductivity first shows a decrease with temperature until heat radiation becomes significant at temperature above about 1200 °C (Clauser, 2009).

In heat flow studies, thermal conductivity measurements are conducted at room temperatures thus they need to extrapolate to in situ temperatures using some kind of corrections. Correction models, evaluated by different researchers, are tabulated in Table 4.3. Lee & Deming (1998) compared this correction models on 117 temperature dependent thermal conductivity measurements. The equation derived by Somerton (1992) has the lowest mean absolute relative error within them and the magnitude of the error rise up with increasing temperature.

In the study of Kukkonen et al. (1998), temperature dependence of the thermal conductivity was classified in to two groups according to the quartz content of rocks. The rocks with high quartz content have high thermal conductivity and a rapid decrease recorded on them with increasing temperature. Low quartz content results in a low thermal conductivity value and exhibit much smaller temperature dependence.

Table 4.3 Correction models for temperature effects on thermal conductivity.

Functional forms of models	Reference	Explanation
$\lambda(T) = \lambda_m + \left[\frac{T_0 T_m}{T_0 - T_m} (\lambda_0 \lambda_m) \left(\frac{1}{T} - \frac{1}{T_m} \right) \right]$	Chapman et al., 1984	T in degrees Celsius
$\lambda(T) = \lambda_{20} - 10^{-3} (T - 293) (\lambda_{20}^{-1.38}) [\lambda_{20} (1.8 \times 10^{-3} T)^{-0.25 \lambda_{20}} + 1.28] \lambda_{20}^{-0.64}$	Sekiguchi, 1984	T in Kelvins
$\lambda(T) = A \frac{B}{350 + T}$	Zoth & Haenel, 1988	T in degrees Celsius, A and B are the constants which depend on rock type
$\lambda(T) = \frac{\lambda_{25} \left[1.007 + 25(0.0037 - \frac{0.0074}{\lambda_{25}}) \right]}{1.007 + T(0.0036 - \frac{0.0074}{\lambda_{25}})}$	Somerton, 1992	For the rocks with thermal conductivities less than 9.0 W/m/K at 20°C
$\lambda(T) = \frac{\lambda_{25} \left[1.007 + 25(0.0037 - \frac{0.0074}{\lambda_{25}}) \right]}{\lambda_{25} \left[1.007 + 25(0.0037 - \frac{0.0074}{\lambda_{25}}) \right]}$	Sass et al., 1992	For crystalline rock with thermal conductivity higher than 2.0 W/m/K at 25 °C
$\lambda(T) = \lambda_{20} \frac{293}{273 + T}$		T in degrees Celsius, valid up to 300 °C
$\lambda(T) = \frac{\lambda_{20}}{1 + b(T)} + c(T + 273.15)^3$	Kukkonen & Jöeleht, 1996	T in degrees Celsius, b and c are the experimental constants.
$\lambda(T) = \lambda_{20} \frac{1}{1 + 0.00005(T - 20)}$	Funnell et al., 1996	T in degrees Celsius
$\lambda(T) = \frac{1}{B(T - 532 \pm 45)} + 0.448 \pm 0.014$	Seipold, 1998	T in degrees Celsius B is a constant which depends on rock type

$\lambda(T)$; is the estimated thermal conductivity in W/m/K at estimated temperature, λ_m ; measured thermal conductivity, T_m ; absolute temperature, T_0 =room temperature, λ_0 =thermal conductivity at room temperature, λ_{20} ; Thermal conductivity in $\text{Wm}^{-1}\text{K}^{-1}$ at 20 °C, λ_{25} ; Thermal conductivity in $\text{Wm}^{-1}\text{K}^{-1}$ at 25 °C.

4.1.5 Pressure

The influence of pressure on thermal conductivity is relatively small when compared with the influence of temperature. Pressure effect on thermal conductivity is directly related with the porosity of rock. In homogeneous rock with little or no porosity pressure dependence of thermal conductivity is small because very large pressure are required to change the form of the rock material (Sweet, 1978). The dependence upon pressure was postulated by Hänel, (1976) as;

$$\lambda(P) = \lambda_0(1 + \alpha P) \quad (4.1)$$

where λ_0 is thermal conductivity at atmospheric pressure, P is the pressure in kg/cm^2 and α is the pressure coefficient in $\text{cm}^2\text{kg}^{-1}$ which depends on rock type (Birch & Clark, 1940). Using equation 4.1 Bridgman (1922) and Clark (1966) show that the effect of pressure on thermal conductivity of homogenous rock is small at pressure below 100 MPa.

In porous rock, generally, thermal conductivity varies as pressure increases because pressure causes to a decrease on the porosity ratio of a rock. It is believed that under the pressure pore filling fluids disappear which have significantly lower thermal conductivity than its homogenous part. Thus we would expect an increase on thermal conductivity as the rock is under high pressure (Sweet, 1978).

4.2 Thermal Conductivity Data Set

The dataset used in this study is obtained from two government-funded projects in Turkey (İlkişik et al., 1996a, 1996b), which were dedicated to construct the heat flow map of western Turkey. Data collection was carried by Mineral Research and Exploration General Directorate of Turkey (MTA). In these projects, thermal conductivity measurements were made and reported without further analyses and corrections. The measurements were carried out using a QTM-500 device in the laboratory of MTA (Karlı et al., 2006). Locations of the rock samples are given in Figure 4.4.

In this thesis, the raw thermal conductivity data is initially sorted according to the lithologic types encountered in western Anatolia. Then, the mean thermal conductivities of the lithologies are calculated for both dry and saturated conditions. Finally, the significance of the results is discussed by comparing with the general geologic and tectonic setting.

4.3 Data Analysis

The data consists of 136 thermal conductivity measurements performed by QTM-500 (Quick Thermal conductivity Meter) thermal conductivity device in the laboratory of MTA. QTM-500 is based on ASTM C 1113-90 hot wire method. It is an effective and reliable technique for measuring thermal conductivity (Grubbe et al., 1983; Sass et al., 1984). The thermal conductivity of a material is calculated by measuring the temperature as a function of time between two specified locations. The measurement range of QTM is 0.023–12 W/m/K, and minimum sample dimensions

required for measurement are 100×50×20 mm. QTM-500 is widely used in thermal conductivity determinations due to the advantage of rapid sampling time (Grubbe et al., 1983; Thienprasert & Raksaskulwong, 1984; Demirboğa, 2003; Çanakçı et al., 2007).

The samples were initially classified according to lithological descriptions given in the data set. Lithologic names were defined by reference to the Geological Map of Turkey (MTA, 2011). A summary of the entire dataset is given in Table 4.4. Measurements were conducted on dry samples, so they required corrections to saturated conditions for determinations of the bulk thermal conductivities (Hasan M. Yenigün 2011, personal communication).

For our dataset, porosity measurements are not available, so for corrections to saturated conditions, a mean porosity value for each lithology was assigned based on the published data (Fuchs et al., 2013; Baeyens & Bradbury, 1994; Manger, 1963; Yavuz et al., 2005; JICA, 1987; Ma & Daemen, 2006). In order to account for the uncertainty in the porosity estimations, a constant standard deviation of 20% of the mean porosities was assumed for all lithologic types. The effects of this uncertainty on saturated conditions were calculated by propagating the error in the measurements of dry conditions and the error in porosity estimations.

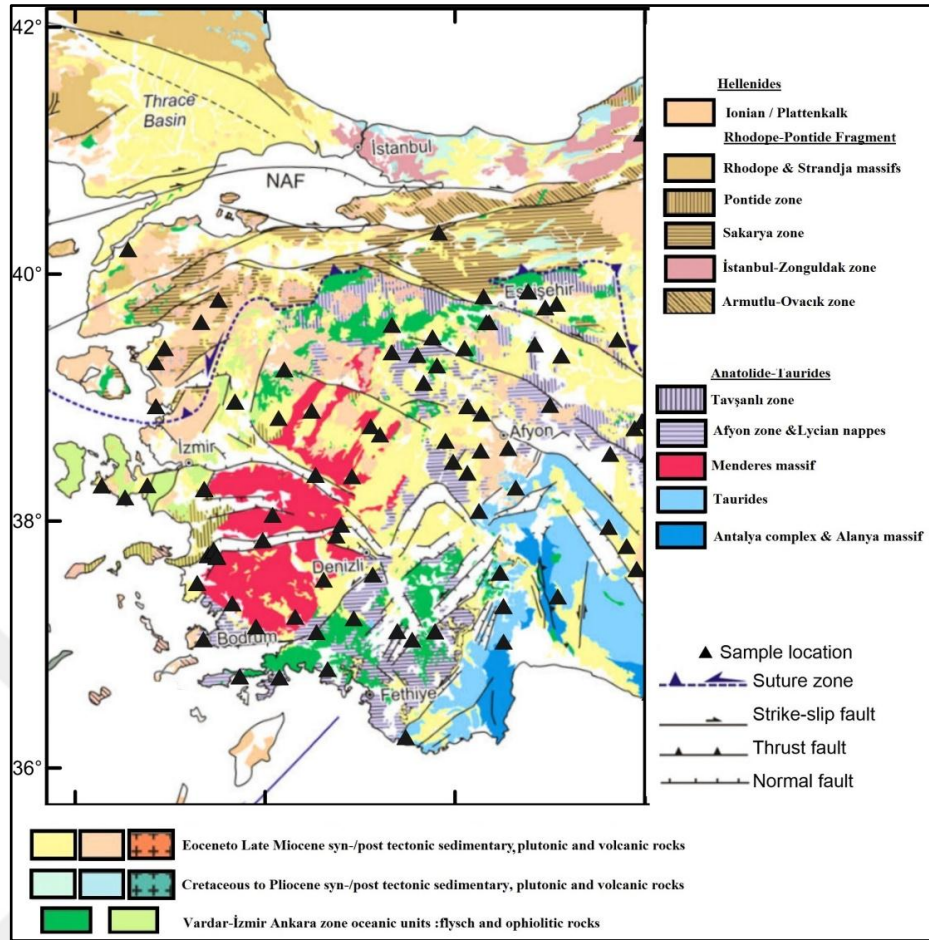


Figure 4.4 Simplified geological map of study area modified from Çemen et al., (2014) and location of rock samples. Note that more than one type of lithologic units were collected at same locations.

Table 4.4 Numbers of the data for western Anatolia

Lithology	Western Anatolia
Clastic Rocks	16
Claystone	20
Crystallized Limestone	6
Limestone	33
Lacustrine	18
Neritic	7
Pelagic	3
Marl	8
Marble	9
Schist	11
Andesite	19
Peridotite	3
Tuff	11
Total	136

The saturated thermal conductivities were determined using the geometric mean model (Fuchs et al., 2013). The relationship between dry (λ_d) and saturated (λ_s) thermal conductivity can be written as

$$\lambda_s = \lambda_d \left(\frac{\lambda_w}{\lambda_a} \right)^\phi \quad (4.2)$$

where $\lambda_a = 0.025 \text{ Wm}^{-1}\text{K}^{-1}$ and $\lambda_w = 0.59 \text{ Wm}^{-1}\text{K}^{-1}$ are the thermal conductivities of air, and water, respectively. Here, ϕ represents the porosity ratio.

4.4 Results

Table 4.5 lists the mean thermal conductivities of the rocks for western Anatolia. In addition to the mean values for dry and saturated conditions, ranges of expected values are also given by taking the standard deviation of the assigned porosity. Ten different representative rock types were analyzed in western Anatolia. The most of the rock samples belongs to limestone units followed by claystone units.

In western Anatolia, thermal conductivities of dry conditions vary between $0.7 \text{ Wm}^{-1}\text{K}^{-1}$ and $3.09 \text{ Wm}^{-1}\text{K}^{-1}$ (Table 4.5). Histograms for saturated thermal conductivity of certain lithologies are shown in Figure 4.5. Thermal conductivities increase considerably after corrections to saturated conditions (Table 4.5). Due to the high porosity rate for clastic rocks, a significant difference between dry and saturated condition is observed. The thermal conductivity varies considerably for each rock type. Claystone has the lowest thermal conductivity within all rocks. Especially, clastic rocks (which are mainly sandstone units) show a wide range of conductivities as a result of variations in quartz contents as well as high porosity values. For metamorphic rocks, the thermal conductivity of schist and marble are $3.19 \pm 0.93 \text{ Wm}^{-1}\text{K}^{-1}$ and $2.95 \pm 0.4 \text{ Wm}^{-1}\text{K}^{-1}$, respectively. In igneous rocks, the mean thermal conductivity of peridotite is $2.86 \pm 0.51 \text{ Wm}^{-1}\text{K}^{-1}$, followed by andesite with a mean of $1.99 \pm 0.68 \text{ W/m/K}$ and tuff of $1.30 \pm 0.57 \text{ Wm}^{-1}\text{K}^{-1}$. In this study the mean thermal conductivity of igneous rocks is lower than that of metamorphic rocks.

Table 4.5 Thermal conductivity values for dry and saturated conditions in western Anatolia

Lithology	N	λ_d (Wm ⁻¹ K ⁻¹)	ϕ_e (%)	λ_s (Wm ⁻¹ K ⁻¹)	$\lambda_{s,min} - \lambda_{s,max}$ (Wm ⁻¹ K ⁻¹)
Clastic Rocks (Sandstone)	16	1.57±1.10	25.0	3.08±2.05	2.5-4.8
Claystone	20	0.70±0.26	12.0	1.02±0.38	0.9-1.2
Crystallized Limestone	6	3.08±1.21	4.0	3.49±1.38	3.3-3.7
Limestone	33	2.62±0.77	4.0	2.98±0.86	2.8-3.1
Lacustrine	18	2.53±0.82	4.0	2.87±0.93	2.7-3.0
Neritic	7	2.91±0.60	4.0	3.30±0.68	3.1-3.5
Pelagic	3	3.09±0.04	4.0	3.51±0.04	3.3-3.7
Marl	8	1.35±0.52	1.5	1.52±0.50	1.4-1.5
Marble	9	2.93±0.40	0.2	2.95±0.40	2.9-3.0
Schist	11	2.80±0.82	4.0	3.19±0.93	3.0-3.3
Andesite	19	1.70±0.61	5.0	1.99±0.68	1.9-2.1
Peridotite	3	2.52±0.45	4.0	2.86±0.51	2.7-3.0
Tuff	11	1.11±0.48	5.0	1.30±0.57	1.2-1.4

N: number of the data, λ_d : mean thermal conductivity of dry rocks with their standard deviations, ϕ_e : estimated mean porosity from Fuchs et al. (2013), Baeyens & Bradbury (1994), Manger (1963), Yavuz et al. (2005), JICA (1987), Ma & Daemen (2006). λ_s : mean thermal conductivity of saturated rocks with their standard deviations. Standard deviation for porosity is assumed to be 20% of the mean porosity for range calculation. Ranges of expected values are also given for the saturated conditions.

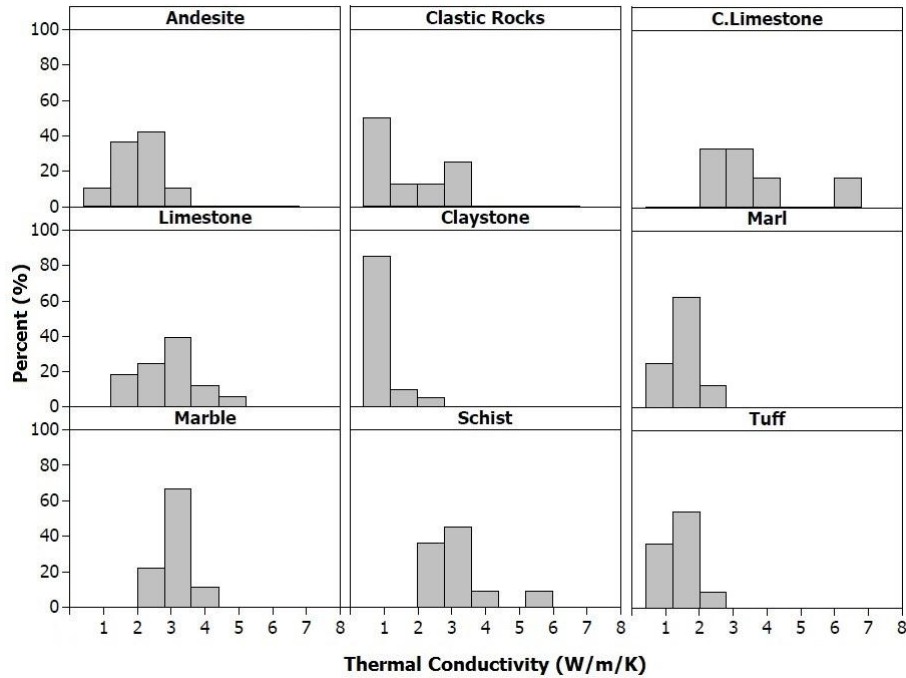


Figure 4.5 Histograms for saturated samples from western Turkey

Western Turkey province includes numerous grabens filled with volcano-sedimentary sequences dissecting Menderes Metamorphic Complex (MMC) (Figure 4.6). The collision between African and Eurasian plates provides proper temperature-pressure condition for occurrence of MMC. MMC is the oldest metamorphic terrain on Anatolian plate, and one of the largest metamorphic terrains in the world, which began to develop during the Late Oligocene–Early Miocene (Bozkurt & Park, 1994; Emre, 1996; Işık & Tekeli, 2001; Lips et al., 2001; Çemen et al., 2006). It includes many kinds of metamorphosed and ingenious rocks from high-to-low grades, including gneiss, mica schists, phyllites, quartz schists, marbles and granodiorites. We sampled two types of metamorphic rocks which are schist and marble (Table 4.5). According to our results, marbles stands out with a high thermal conductivity of $2.95\pm 0.4 \text{ Wm}^{-1}\text{K}^{-1}$. Marbles located in Menderes massif generally have high dolomite content (Yavuz et al., 2005), which directly increases the thermal conductivity of the marble. Western Turkey is characterized by a number of suture zones (Figure 4.6) which bears wide areas of peridotite units. In our dataset, three peridotite samples from these suture zones show a mean value of $2.86\pm 0.5 \text{ Wm}^{-1}\text{K}^{-1}$.

MMC is dissected by three major graben structures (Figure 4.6). The fills within the grabens are generally composed of two main, lower and upper, volcano-sedimentary successions. The basic difference between two units is the origin of the conglomerate content. While the upper volcano-sedimentary conglomerates contain clasts from MMC, they are absent in the lower volcano-sedimentary successions (Ersoy et al., 2014). Sedimentary parts of the successions consist of generally limestone, sandstone, conglomerate, shale and marl (Innocenti et al., 2005). Andesite, tuff, basalt and rhyolite are the common volcanic rocks within typical sections (Ersoy et al., 2014). As a part of sedimentary successions limestone, sandstone and marl units were sampled while andesite and tuff units were sampled from volcanic successions (Table 4.5).

In this study, we report results for three types of limestone sublithologies based on the geological map of Turkey (MTA, 2011). Among the three types, pelagic limestone by far shows the highest ($3.51\pm 0.04 \text{ Wm}^{-1}\text{K}^{-1}$) thermal conductivity values compared to the lacustrine and neritic limestone. It is followed by the crystallized limestone with $3.49\pm 1.38 \text{ Wm}^{-1}\text{K}^{-1}$. Assuming that limestones generally show similar low porosity values, thermal conductivity variations may be related to the clay contents of the sublithologies.

For volcanic rocks, porosity is the main contributor of thermal conductivity variations. Typical porosity rate of tuff ranges from %5 to %35. Age of the rock directly control the porosity ratio. With the increasing age, the length of time of exposure to hydrothermal alteration of the rock gets longer decreasing the porosity of the volcanic rock. Volcanic rocks older than 5Ma have typically low porosity rate (Blackwell et al., 1982, 1996). In Western Anatolia, volcanic rocks have ages from Oligocene to present (Fytikas et al., 1984). In our dataset, the ages of volcanic rocks are Miocene and older. As a result of this, relatively low porosity values were assigned for the volcanic rocks in western Anatolia (see Table 4.5).

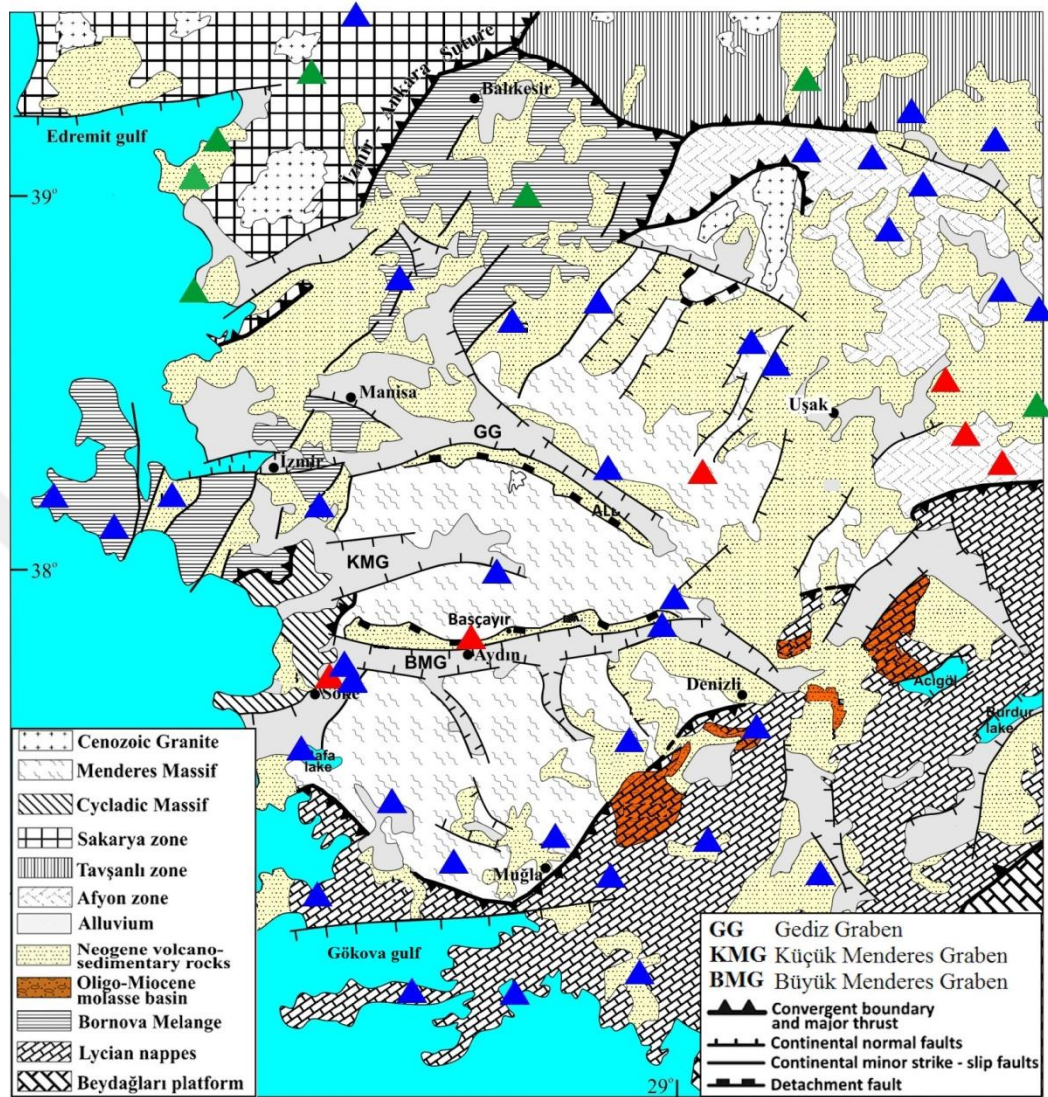


Figure 4.6 Geology and tectonic structures of western Turkey (Sümer et al., 2013). Blue, green and red triangles symbolize measurement points of sedimentary, volcanic and metamorphic rocks respectively.

4.5 Discussion

Histogram of the all data set is given in Figure 4.7. This figure confirms that the range of thermal conductivity values is too wide to assign a constant thermal conductivity value for heat flow and thermal modeling studies. A histogram of all data shows two peaks around the values of 1.5 and 3 $\text{Wm}^{-1}\text{K}^{-1}$, which refer to the basin filling sediments and basement rocks, respectively.

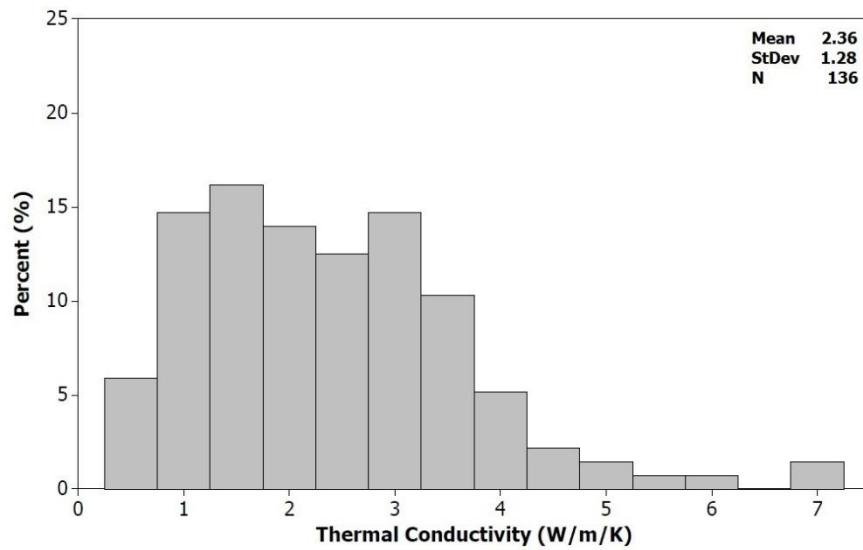


Figure 4.7 Histogram of the all saturated thermal conductivity values.

All data for the entire study area are divided into three mega groups as; sedimentary, metamorphic and igneous rocks. The histograms of thermal conductivity values of each group are given in Figure 4.8. This representation enables us to see the thermal characteristics of these mega groups individually. According to the histograms, it is possible to assign a single mean thermal conductivity for volcanic and metamorphic rocks. Mean thermal conductivity values for igneous and metamorphic rocks are assigned for the entire study area as 1.86 and 3.08 ($\text{Wm}^{-1}\text{K}^{-1}$), respectively. On the other hand, assigning a single mean thermal conductivity for sedimentary rocks is difficult. This is expected by the fact that thermal conductivity of the sedimentary rocks show wide range related to their physical properties. Thermal conductivities ranging from 0.61 to 7.11 ($\text{Wm}^{-1}\text{K}^{-1}$) is observed. The lowest values belong to claystones of alluvial units and the high values are derived from sandstone of neogene volcano-sedimentary rocks.

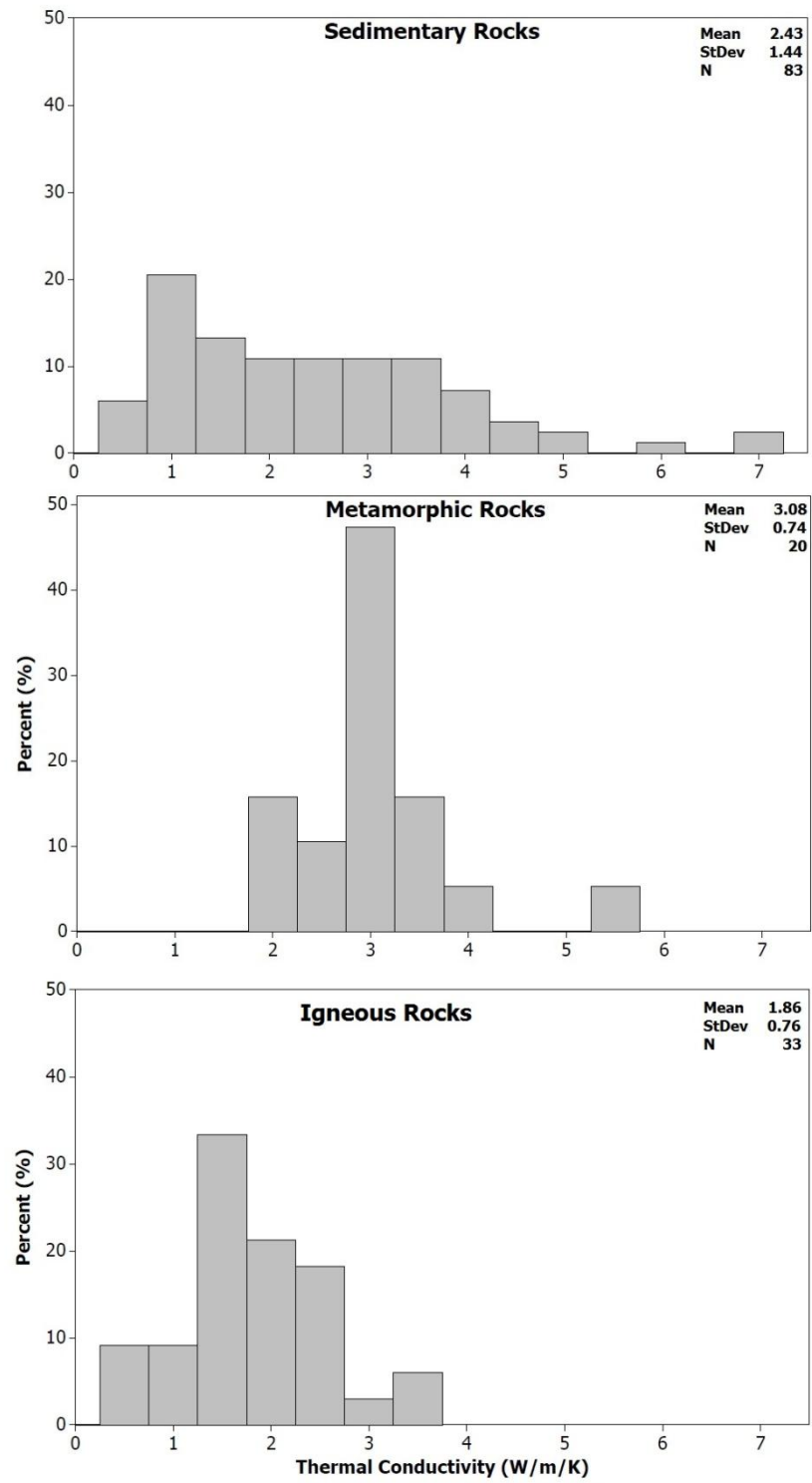


Figure 4.8 Histograms of data set of western Turkey.

4.6 Conclusion

In this thesis, we analyzed thermal conductivity measurements from 136 rock samples collected in western Turkey region. The samples were initially classified according to lithological descriptions given in the data set. Lithologic units were defined by reference to the geological map of Turkey (MTA, 2011). Data were corrected from dry to saturated conditions using the geometric mean model. Statistical analysis were applied both for dry and saturated conditions.

Limestone, the most common lithological unit in western Anatolia, is analyzed with its subunits namely the neritic, lacustrine and pelagic limestones. In general, neritic limestone shows higher thermal conductivity value compared to lacustrine limestone, and they are the two most common types of limestone found in Turkey.

Mean thermal conductivity values for igneous and metamorphic rocks are assigned for the entire study area as 1.86 and 3.08 ($\text{Wm}^{-1}\text{K}^{-1}$), respectively. Thermal conductivity of sedimentary rocks shows a wide range of values due to a wide variety of physical properties. The high thermal conductivity of sandstones is linked with the high quartz content whereas high thermal conductivity of crystallized limestones is linked with dolomitization.

The range of the thermal conductivity values observed for sedimentary rocks is too wide to assign a constant thermal conductivity value for heat flow and thermal modeling studies. Results of this study may be a valuable input for the future heat flow and thermal modeling studies in Turkey.

CHAPTER FIVE

GEOTHERMAL GRADIENT

The geothermal gradient is the rate of change of the temperature with depth in the earth. It is directly associated with the thermal conductivity of rocks, and affected by the heat flow. Heat always tends to transfer from the higher to lower temperatures. So if we find out temperature differences between two places in the Earth we know that heat is moving between them.

Continuous temperature-depth (T-D) logs, recorded under equilibrium conditions, provide important information about subsurface thermal structure. T-D logs are essential in heat flow determinations. Together with thermal conductivity, thermal logging data has also critical importance on lithology characterization of Earth's thermal field (Förster et al., 1997). Geothermal gradient measurements are widely used in geoscience studies particularly in logging geophysics. It is a useful indicator for subsurface temperature distribution. Geothermal gradient is the fundamental parameter which is used in estimation of geothermal resource potentials of an area and in the understanding of regional tectonics. In mineral exploration, borehole temperature measurements are used in the detection of massive minerals. Temperature variations can be a key element in understanding the groundwater flow. The differential temperature curve is used to emphasize the occurrences of changes in fluid movement. Geothermal gradient is a basic parameter used to describe characteristics of the geothermal field of sedimentary basins. In basin analysis, geothermal gradients can provide useful information for studying the development and evolution of sedimentary basins (Mussett & Khan, 2000).

Unfortunately, our knowledge about the temperature of the earth is limited due to the fact that temperature has only been measured at shallow depths. We try to estimate and understand indirectly how it transports and varies in deeper part of the Earth. Generally, temperature increases with the depth and the rate of this increase is related with the local tectonic activity. Continental areas away from tectonically

active zones have average geothermal gradients which are typically 25 to 30 °C per kilometer ($^{\circ}\text{Ckm}^{-1}$). Linear extrapolation of this value would give us an unrealistic result which is about 2500 °C for the Earth's core. Therefore, rate of the increase must decrease with depth (Mussett & Khan, 2000; Lowrie, 2007).

Heat transfer processes must be known to determine the temperature distribution within the earth. As we know that the Earth's crust and mantle are solid so conduction is the dominant process for heat transfer. Convection is only possible in a fluid thus it can take place locally where there is a ground-fluid or magma within crust and mantle. When heat transfers in a homogenous medium conductively and there is no heat generation, the T-D curve becomes straight line with little to no change. In, Figure 5.1 there is only one rock layer cause to a steady gradient. If the subsurface consists of more than one layer, temperature gradient varies corresponding to each lithology. An example of lithology effect is given in Figure 5.2 (Blackwell & Steele, 1989). The geothermal gradient in the upper part of the curve is about $50^{\circ}\text{Ckm}^{-1}$ whereas the temperature gradient in limestone is about $18^{\circ}\text{Ckm}^{-1}$. An increase/decrease in thermal conductivity causes deviation from straight temperature line, giving a constant heat flow along the borehole.

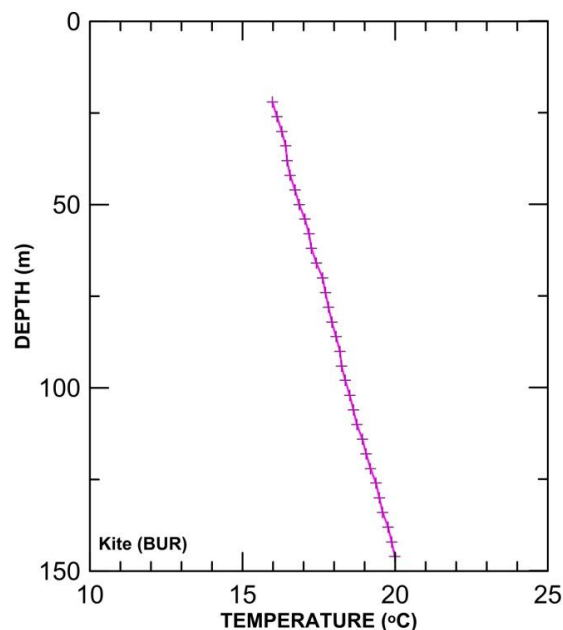


Figure 5.1 Linear Temperature-depth log of Kite from Bursa (data obtained from İlkışık et al., 1996a; 1996b)

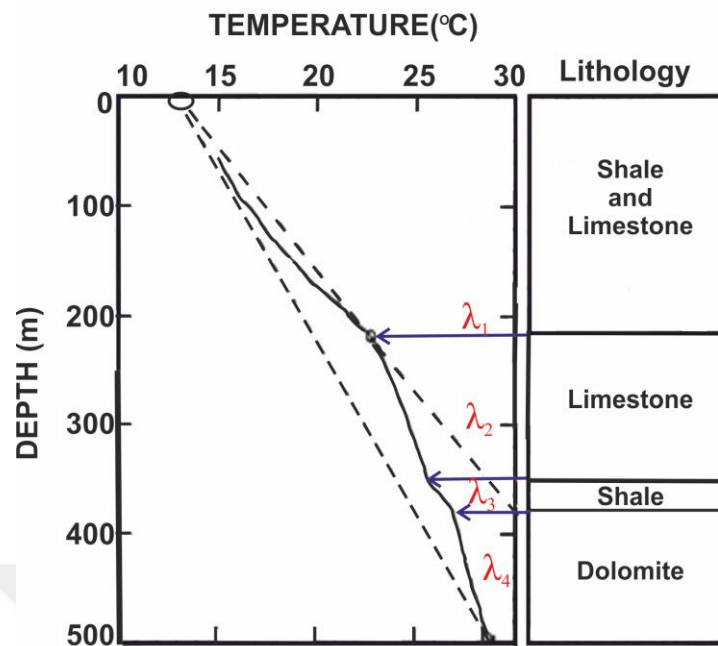


Figure 5.2 T-D curve from eastern Kansas and generalized stratigraphy encountered in the hole. Dashed lines show the results that would be obtained by calculating an average gradient for the well using the mean annual surface temperature and a BHT from 220 m depth or from 500 m depth (Blackwell & Steele, 1989).

T-D curves can be disturbed by intra-borehole fluids flow (IBF), lateral flow of ground water, lithology and microclimate effects. IBF occurs in open boreholes (not cased or grouted) (Figure 5.3a and b). Pressure variations between different aquifers (fracture zones) cause to the water to flow from the area of high pressure to lower pressure. The water may circulate in the borehole which leads to sharp changes in temperature depth curves (SMU Geothermal Lab., 2016).

Daily and seasonal temperature changes on the earth surface affect the shallow geothermal gradient. These climatic effects are generally observed at the first 30 m depth of the T-D curves. Deeper part of the temperatures measurements has constants gradient that, by extrapolation, suggests a surface temperature lower than the present mean. These shallow signals can also be used as an indicator of climatic change records of the past 100-150 years (SMU Geothermal Lab., 2016).

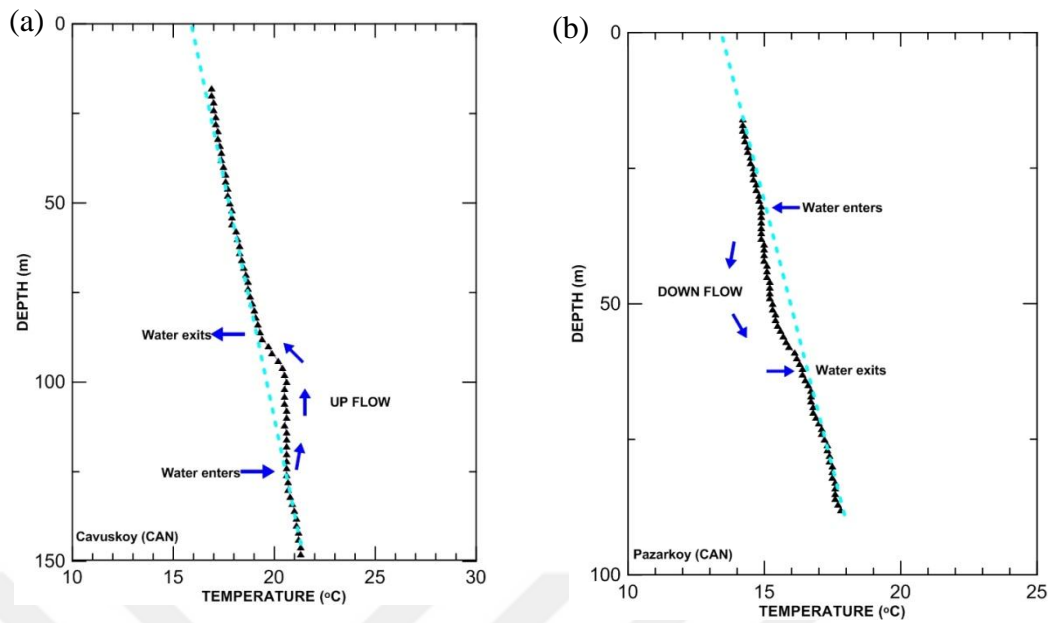


Figure 5.3 Intra-borehole effects a) up flow and b) down flow on temperature-depth curves (data obtained from İlkışık et al., 1996a; 1996b).

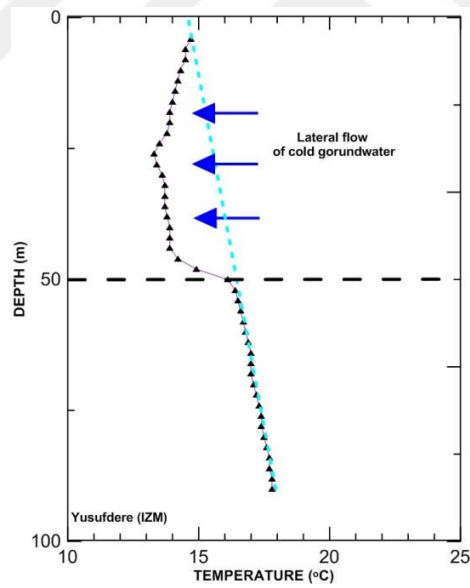


Figure 5.4 Effect of lateral flow on T-D curve (data obtained from İlkışık et al., 1996a; 1996b).

5.1 Geothermal Gradient Data Set

The data set used in this thesis is collected from Aydin, Balıkesir, Çanakkale, İzmir, Kütahya and Manisa as a part of the TUBİTAK project with number of 113R019. Field measuring campaigns between the years of 2013-2016 yield us valuable temperature data from 30 shallow water wells. The wells are partly provided by the State Hydrological Works (DSİ) regional directorates, and partly by private owners. These wells were drilled for water supply or monitoring ground water. Measurements are conducted in unused (not producing) or abandoned wells. Location, depth, static water level, lithologic etc., information are obtained from the personnel of the state offices or from the drillers. T-D measurements are collected by two different tools, one is a custom designed thermistor probe four-wire measurement portable tool, and other is, also custom designed, ADT7420 digital tool. The ADT7420 tool has a negligible temperature drift which eliminates any calibration in the sensor. Both devices work in surface-readout mode. T-D data are collected for each meters of depth below the water table. Totally, 30 T-D data are gathered in this project.

In addition to the new data set, 26 geothermal gradient data from Pfister et al. (1998) are reclassified according to the criteria explained in the next section. 55 geothermal gradient data from Erkan (2015) are also used together to evaluate the conductive geothermal gradient distribution in western Turkey.

5.2 Data Analysis

5.2.1 Data Quality Classification

The new T-D data set consists of temperature measurements at generally shallow wells and some of them disturbed by the local hydrological effects. Unfortunately, intensively disturbed data is not suitable for conductive heat flow calculations. In order to eliminate these wells, the T-D curves are divided into quality classes according to their general characteristics. Classification criteria under the theory of 1D conductive heat flow and estimated relative errors are defined in Table 5.1 (Erkan, 2015).

Table 5.1 Definitions of the data quality classes (Erkan, 2015)

<i>Class</i>	<i>Criteria</i>	<i>Relative error in Geothermal gradient</i>
A	Greater than 100m conductive (linear) T–D section	5 %
B	Greater than 50m conductive (linear) T–D section	10%
C	Disturbed T–D curve due to intra-borehole fluid activity Intermittent conductive sections	25%
D	Intense intra-borehole fluid activity; conductive section too shallow	-
G	Dominated regional geothermal activity on T-D curve	not suitable for heat flow determination
X	Dominated groundwater activity on T-D curve	not suitable for heat flow determination

According to Erkan (2015) classification, T-D curves must be linear with depth as long as the thermal conductivity of related geological section is constant in a well. Class A and B data correspond to the solution of 1-D heat transfer along a borehole (Jaeger, 1965). This kind of data consists of linearly increasing temperature with depth and should extrapolate to the mean annual surface temperature (MAST) at the measurement point. Another evidence of a conductive section is that a change in rock thermal conductivity causes change in the temperature gradient, giving a constant heat flow along the borehole (Roy et al., 1972; Erkan, 2015).

Groundwater movements and fluid flows in the some sections of boreholes cause to disturbed T-D curves. Such kinds of data are classified as C class in this thesis. If water movement affects the large part of the T-D curves, we rated them as D class. In these boreholes, gradients are either constrained from a few control points, or calculated at very shallow (< 50 m) depths (Erkan, 2015).

If the T-D curves are completely under the influence of ground water movement, they are not used for heat flow determination and rated class X. T–D curves for these wells were generally show isothermal behavior, implying dominant vertical groundwater flow. Other types of hydrologically active sites are found near geothermal systems. These sites show the effect of local geothermal activity, which shows distinctly higher temperatures. These types of data are rated class G, and are also not suitable for conductive heat flow determinations (Erkan, 2015).

In this thesis, out of the 30 new sites, 9 gradients fall into class X and they are not taken in consideration in geothermal gradient calculations. 4 sites rated as G class and 4 sites fall into class D. The remaining 13 sites fall into classes A/B/C. (Table 5.2). Distribution of the measurement points is given in Figure 5.5.

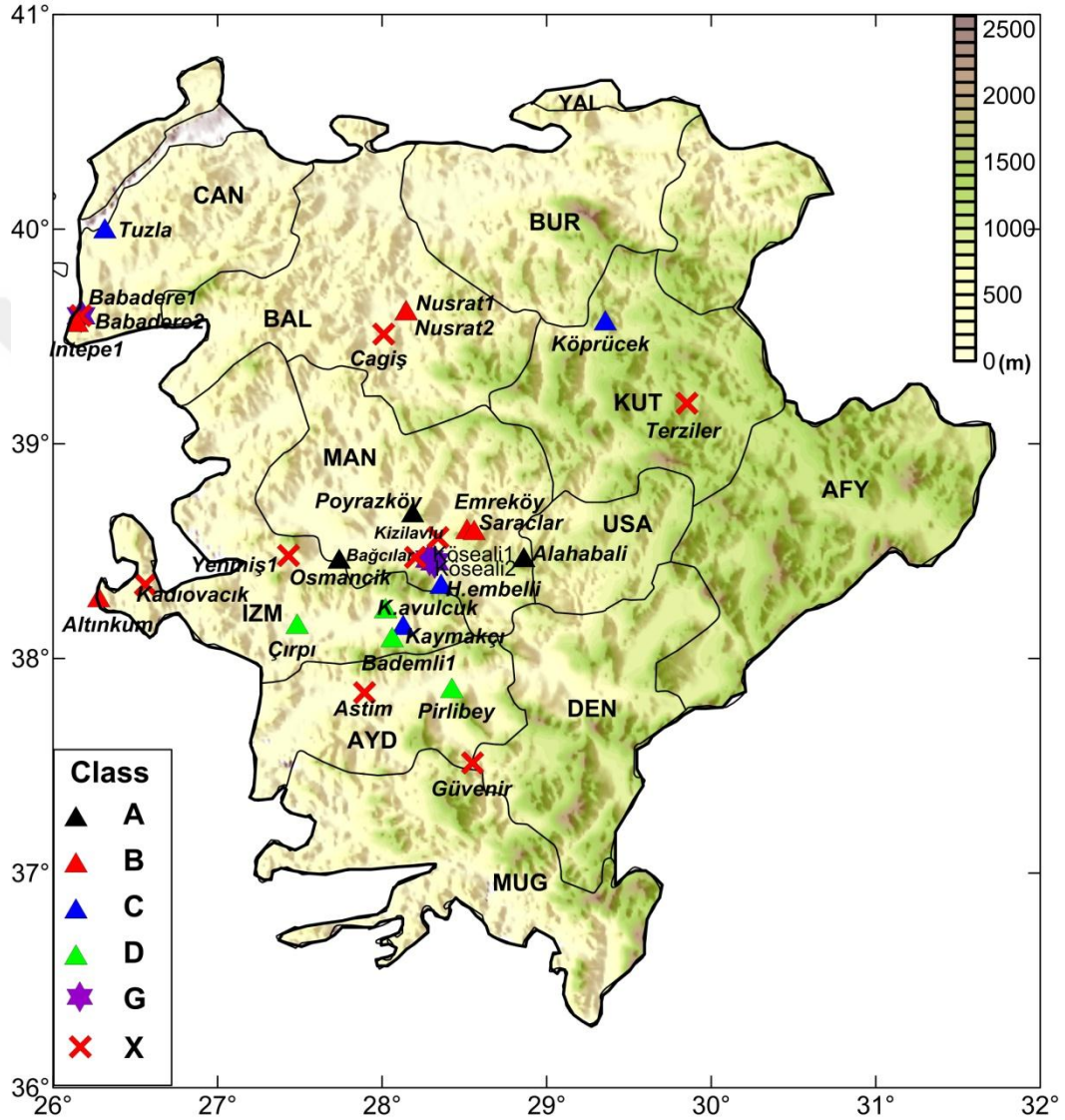


Figure 5.5 Data locations with the corresponding quality classes. Elevations are in meters. AYD:Aydın; AFY: Afyon; BAL: Balıkesir; BUR: Bursa; CAN: Çanakkale; DEN:Denizli; IZM: İzmir; KUT: Kütahya; MAN: Manisa; MUG:Muğla; USA:Uşak.

In addition to our new data 55 T-D from Erkan (2015) are also used. Erkan (2015) analyzed and classified so they do not need any further analyses (Table 5.3).

Table 5.2 Geothermal gradients evaluated in this study

Location	Latitude (°N)	Longitude (°E)	Prov.	Meas Year	Class	Meas.Depth (m)	Elev. (m)	Interval (m)	G	Corr.G (°Ckm ⁻¹)	σG
Pirlibey	37.8633	28.4236	AYD	2015	D	25	67	10-25	58.0	58.0	
Astim	37.8409	27.8928	AYD	2015	X	15	40				
Güvenir	37.5129	28.5500	AYD	2015	X	5	40				
Nusrat1	39.6220	28.1455	BAL	2016	B	110	119	65-115	15.0	15.0	1.5
Nusrat2	39.6223	28.1464	BAL	2016	B	125	120	80-125	13.1	13.1	1.3
Cağış	39.5108	28.0102	BAL	2016	X	100	257				
Babadere1	39.5955	26.1704	CAN	2016	G	130	78	70-125	99.6	99.6	10.0
Babadere2	39.5965	26.1682	CAN	2016	X	124	63				
İntepe1	40.0041	26.3150	CAN	2016	C	136	83	0-136	46.5	46.5	11.6
Tuzla1	39.5682	26.1460	CAN	2016	B	50	11	10-50	48.8	48.8	4.9
Çırpı	38.1620	27.4840	IZM	2015	D	45	20	0-38	61.8	61.8	
Kaymakçı	38.1569	28.1279	IZM	2015	C	110	147	60-93	33.3	40.2	10.1
Altinkum	38.2863	26.2771	IZM	2016	B	111	25	42-108	37.4	37.4	3.7
Bademli1	38.0992	28.0607	IZM	2015	D	78	230	25-74	38.0	38.0	
K.avulcuk	38.2345	28.0202	IZM	2015	D	82	147	25-45	35.5	35.5	
Kadiovacik	38.3446	26.5608	IZM	2014	X	204	220				
Yenmis1	38.4798	27.4303	IZM	2014	X	77	262				
Terziler	39.1888	29.8536	KUT	2015	X	285	1041				
Koprücek1	39.5754	29.3564	KUT	2015	C	61	1087	37-50	44.1	44.1	11.0
Göbekli	38.4496	28.3194	MAN	2013	G	69	144	25-61	72.2	72.2	
H.embelli	38.3484	28.3588	MAN	2015	C	200	846	0-80	27.38	32.80	8.2
Emreköy	38.6033	28.5158	MAN	2015	B	180	687	100-155	20.7	20.7	2.1
Saraçlar	38.5987	28.5598	MAN	2015	B	165	694	110-160	25.0	25.0	2.5
Köseali	38.4655	28.2858	MAN	2015	G	116	160	0-116	113.0	113.0	28.3
Köseali2	38.4623	28.2881	MAN	2015	G	113	121	80-108	104.3	104.3	26.1
Osmancik	38.4655	27.7385	MAN	2014	A	294	298	139-284	24.3	28.2	1.4
Poyrazköy	38.6817	28.1856	MAN	2014	A	167	636	60-167	24.5	24.5	1.2
Bağcılar	38.4714	28.2030	MAN	2013	X	150	170				
Kızılavlu	38.5630	28.3400	MAN	2014	X	95	287				
Alahabali	38.4725	28.8614	USA	2016	A	195	734	65-195	33.5	33.5	1.7

Prov: Province; AYD:Aydın; BAL:Balıkesir; CAN:Çanakkale; IZM:İzmir; KUT: Kütahya; MAN: Manisa; USK:Uşak; Meas. Depth: Measurement depth; Elev: Elevation; G:Geothermal Gradient; Corr.G: Corrected Geothermal Gradient; σ:Standart deviation of G/Corr.G; Corrected Geothermal Gradient; σ:Standart deviation of G/Corr.G. Depth intervals starting with 0 (m) refer that the temperature gradient is calculated based on a hypothetic line using the projected mean annual surface temperature (MAST).

Table 5.3 Geothermal gradient data reported in Erkan (2015).

Location	Latitude (°N)	Longitude (°E)	Prov	Class	G	σ_G (°Ckm ⁻¹)
Kadikoy	38.6365	30.9175	AFY	D	49.1	
Agzikara	38.5900	30.5600	AFY	D	36.4	
Calislar	38.8100	30.0400	AFY	D	36.4	
Derbent	38.9400	31.0000	AFY	D	31.9	
Tekeler	37.5406	27.7799	AYD	D	21.3	
Ortakci	37.9700	28.7200	AYD	D	28.3	
Kargili	37.5877	27.9921	AYD	D	26.5	
Balat	37.4978	27.2848	AYD	D	40.0	
Pursunler	39.2270	28.2017	BAL	B	28.5	2.9
Alacaatli	39.2534	28.0488	BAL	D	24.5	
Akcal	39.6038	27.5416	BAL	D	37.1	
Bulutlucemesme	39.2851	26.8492	BAL	D	42.0	
Kite	40.1972	28.8763	BUR	A	32.5	1.6
Eyerce	40.3375	29.8281	BUR	B	19.8	2.0
Kursunlu	40.4014	29.1105	BUR	C	30.0	7.5
Linyit	40.2512	28.9616	BUR	D	22.6	
Cakirca	40.4762	29.6630	BUR	D	29.0	
As.Vet.	40.3980	29.0986	BUR	D	47.5	
Gurle	40.4313	29.2987	BUR	D	87.5	
Intepe	40.0279	26.3434	CAN	A	43.6	2.2
Pazarkoy	39.8647	27.3855	CAN	B	50.7	5.1
Terzialan	39.9565	27.0234	CAN	B	41.4	4.1
Cavuskoy	40.2480	27.2407	CAN	B	32.4	3.2
Yapildak	40.2005	26.5561	CAN	C	85.3	21.3
Ortuluce	40.3780	27.2111	CAN	C	23.1	5.8
Ciftlikkoy	38.2879	26.2796	IZM	B	50.0	5.0
Ovaciki	38.2898	26.7599	IZM	B	49.0	4.9
Yenmis	38.4597	27.4172	IZM	B	35.3	3.5
Bademli	38.0500	28.0792	IZM	B	25.7	2.1
Yusufdere	38.2172	27.8396	IZM	C	33.6	8.4
Haliller	38.1883	28.2960	IZM	D	28.6	
Y.Kiriklar	39.2315	27.2549	IZM	D	48.9	
Seyrek	38.5500	26.9173	IZM	D	51.8	
Zeytineli	38.1917	26.5250	IZM	D	33.3	
Gumuskoy	39.4882	29.7627	KUT	B	34.5	3.5
Sapcidede	39.5884	29.3348	KUT	B	40.3	4.0
Darica	39.6380	29.8707	KUT	B	50.3	5.0
Kopruccek	39.3660	29.3349	KUT	C	27.7	6.9
Esatlar	39.3439	29.6016	KUT	D	47.0	
Tepekoy	39.2100	30.3300	KUT	D	30.9	
Cataloluk	38.8943	28.4907	MAN	A	25.0	1.3
Kizilavlu	38.5649	28.3404	MAN	B	52.5	5.3
Alahidir	38.5000	27.8974	MAN	B	36.8	3.7
Boyali	38.8338	28.1418	MAN	B	40.5	4.1
Azimli	38.7774	27.6073	MAN	B	33.3	3.3
Ibrahimaga	38.6284	28.6784	MAN	C	55.6	13.9
K.Belen	38.7500	27.2583	MAN	C	57.6	14.4
Bayir	36.7347	28.1509	MUG	B	20.9	2.1
Kuyucakm	37.1119	28.2496	MUG	C	32.3	8.1
Gumuskol	38.4627	29.1657	USA	A	52.1	2.6
Karlik	38.7001	29.5954	USA	A	42.3	2.1
Balabanci	38.3618	28.9149	USA	B	38.0	3.0
Karakuyu	38.7680	29.1116	USA	D	56.1	
Salmanlar	38.5600	29.5700	USA	D	52.0	
Armutlu	40.5158	28.8264	YAL	D	27.8	

Prov: Province; AFY:Afyon; AYD:Aydın; BAL:Balıkesir; BUR:Bursa; CAN:Çanakkale; IZM:İzmir; KUT: Kütahya; MAN: Manisa; MUG:Muğla; USK:Uşak; YAL:Yalova; G:Geothermal Gradient; σ :Standart deviation of G.

Pfister et al. (1998) published geothermal gradient data from shallow boreholes located in northwestern Anatolia. In this study, 26 of their results (Table 5.4) are reclassified according to the criteria given in Erkan (2015) and included in geothermal gradient distribution map of western Turkey (Figure 5.12).

Table 5.4 Geothermal gradient data reported in Pfister et al. (1998)

Location	Latitude (°N)	Longitude (°E)	Prov	Class	G (°Ckm ⁻¹)
Besiktepe	39.2500	26.8692	BAL	C	41.7
Gonen	40.1802	27.6559	BAL	B	65.0
K.Koseler	39.6700	27.9700	BAL	A	32.0
Kurse	39.7703	28.0698	BAL	B	30.0
Selimiye	39.4730	27.9015	BAL	G	97.6
Turfallar	39.4820	28.2971	BAL	A	44.0
An.Lisesi	39.6802	27.9324	BAL	C	35.0
Balci	40.0541	27.5926	BAL	X	24.0
Bandirma	40.3029	27.9441	BAL	X	25.5
Carik	40.2613	27.8309	BAL	X	44.3
Cayirhisar	39.6239	27.9060	BAL	X	40.0
Dogruca	40.3000	28.0400	BAL	G	107.3
Kayapa	39.4910	27.4448	BAL	C	30.0
Cumali	40.2860	29.9294	BIL	D	22.4
Kazikli	40.2579	29.1588	BUR	C	30.0
Ertugrul	40.2000	28.9200	BUR	C	45.0
Inegol	40.1059	29.4382	BUR	X	44.5
Kite	40.1982	28.8765	BUR	D	26.0
Linyitleri	40.2522	28.9618	BUR	X	25.1
M.K.Pasa	40.0495	28.4706	BUR	C	32.0
Soguksu	40.2027	29.4447	BUR	D	21.5
Ssk	40.2200	29.0000	BUR	D	60.0
Biga	40.2455	27.1588	CAN	D	27.0
Geyikli	39.8100	26.2000	CAN	C	54.0
Yolagzi	40.3190	26.3350	CAN	X	36.5
Armutlu	40.5205	28.8235	YAL	C	26.8

Prov: Province; BAL:Balıkesir; BIL:Bilecik; BUR:Bursa; CAN:Çanakkale; YAL:Yalova; G:Geothermal Gradient; σ :Standart deviation of G. Standard deviation of G is assigned based on the criteria from Erkan (2015).

5.2.2 Topography Correction

The topography differences induce the surface temperature distribution within the mountainous terrain. The heat has further to flow to reach the surface beneath a peak compared with in a valley. This suggests that surface temperatures are compressed below valleys and depressed beneath hills. It is crucial to be aware of the topography effect when studying in mountainous regions. Lees (1910) suggested a correction in two dimensions to eliminate the distortion in the geothermal field beneath idealized mountain ranges (Figure 5.6). In his model, the mountains are composed of long and straight ranges with uniform height, H , lying on a horizontal plain. The ranges and the rocks under the plain consist of same composition with the thermal conductivity, λ , and radiogenic heat production, A (Lees, 1910; Powell et al., 1988; Beardsmore & Cull, 2001).

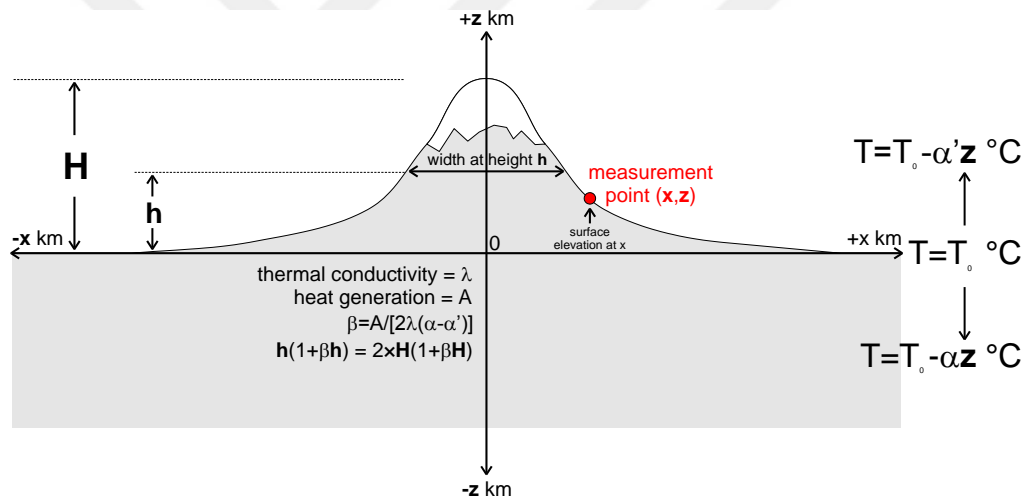


Figure 5.6 Topography correction model (Lees, 1910)

Determining the height, h , is the first step of the correction procedure as follow;

$$\frac{[h(1 + \beta h)]}{[H(1 + \beta H)]} = 0.5 \quad (5.1)$$

$$\text{where } \beta = A / [2\lambda(\alpha - \alpha')] \quad (5.2)$$

and α is the thermal gradient beneath the plain away from mountain range, α' is the decrease in the air temperature with altitude (adiabatic lapse rate).

The mountain range is defined as that its summit is at $x = 0$, $z = -H$, and its elevation varies along a perpendicular section according to

$$z(1 - \beta z) + Hd(1 + \beta H) \frac{z + H + d}{x^2 + (z + H + d)^2} = 0 \quad (5.3)$$

where x is the horizontal and z is the vertical axis. d is the length of the straight line from the summit to a point at height h on the mountainside (d must be greater than H for the correction to be valid). The equation describing the temperature field beneath the mountain range and plain is then

$$T = T_0 + \alpha z - \frac{A}{\lambda} \frac{z^2}{2} + (\alpha - \alpha') Hd(1 + \beta H) \frac{z + H + d}{x^2 + (z + H + d)^2} \quad (5.4)$$

T_0 is the temperature at the surface of the plain and T is the temperature at point (x, z) . The thermal gradient at the summit of the range is given by

$$\frac{\partial T}{\partial z} = \alpha + \frac{A}{\lambda} H - (\alpha - \alpha') Hd(1 + \beta H) / d \quad (5.5)$$

Terrain correction is made on the T-D data where there are steep topographic changes near the measuring point. All topographic corrections applied to the gradients in this thesis are less than $15 \text{ }^\circ\text{Ckm}^{-1}$ and given in Table 5.2

5.2.3 Temperature Depth (T-D) Curves

T-D data were collected from seven different provinces located in western Anatolia. Each T-D data is analyzed and compared with the others collected from the same or adjacent provinces. This enables us to match and compare the surface temperatures of each measurement. T-D curves are also checked with the previous T-D logs (Erkan, 2015) for those were collected from same province.

Three T-D measurements are conducted in Aydın but two of them are rated as X class. Pirlibey is the only one, and has the shallowest new T-D data (Figure 5.7). Depth of 15 m conductive layer is used for geothermal gradient calculation. Köprücek1 in Kütahya shows conductive behavior, and effect of IBF is minimal. High temperatures are recorded at the first 50m depth of Alahabali, this may be results from long term changes in mean annual surface temperature (MAST). The rest of the curve of Alahabali is linearly conductive and classed as A.

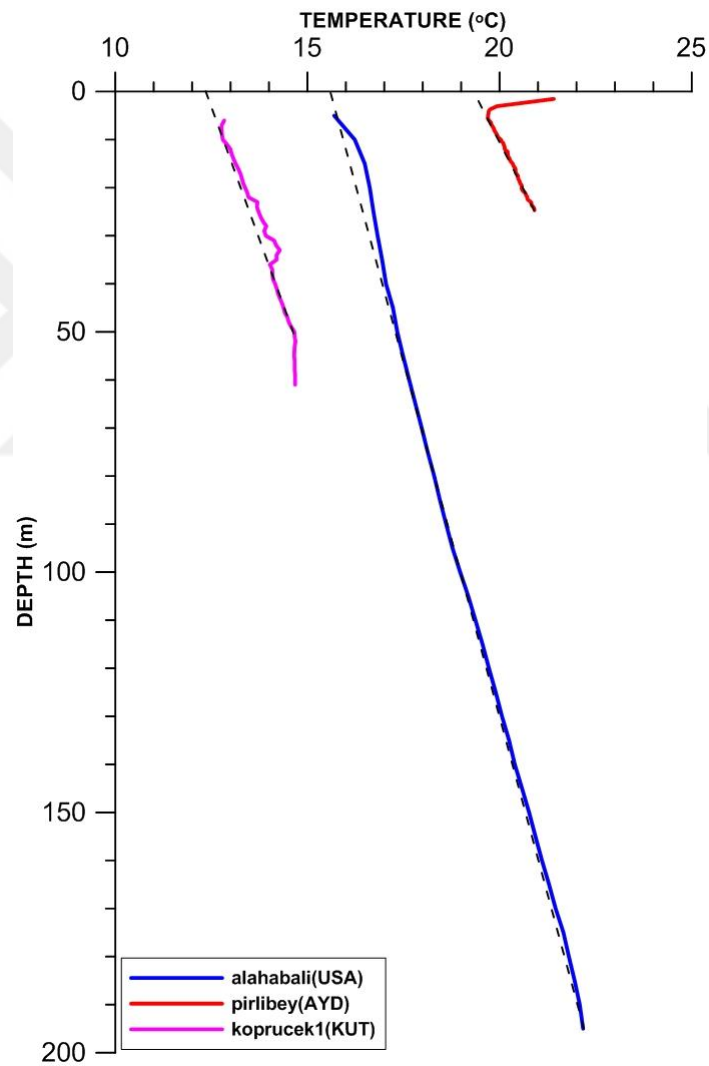


Figure 5.7 Temperature–depth (T–D) curves for Aydın, Kütahya and Uşak

T-D curves of Balıkesir are given in Figure 5.8. Nusrat1 and Nusrat2 wells are about 500m apart from each other, and characterized by conductive thermal regime for almost their entire depths. The projected surface temperatures for them match the MAST.

Four T-D data are recorded in Çanakkale. Babadere1 well is rated as G class with the elevated geothermal gradient. Babadere2 well is logged one day after drilling process so it rated as X due to the non-equilibrium conditions. Intepe1 and Tuzla1 wells are suitable for conductive geothermal gradient calculation. Intepe1 well is under the effect of down flow so geothermal gradient is calculated using bottom hole temperature with projected surface temperature. The effect of IBF is minimal on Tuzla1 well (Figure 5.8).

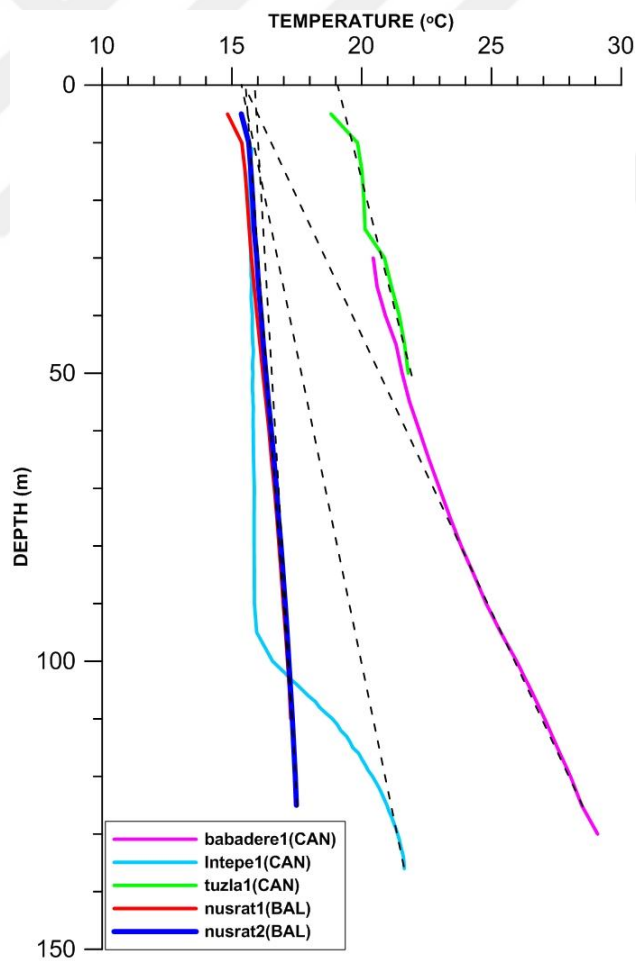


Figure 5.8 Temperature–depth (T–D) curves for Balıkesir and Çanakkale.

T-D curves for İzmir are shown in Figure 5.9. A strong IBF inferred on Bademli1 well. Below 50m, a down flow disturbed the Bademli1 curve. T-D curve is recorded within air through the K.avulcuk well which may explain distortion out of the linear line. Conductive section is apparent for both Kaymakçı and Çırpı well below the water table. For Altinkum, higher temperatures near the surface (~ at first 50 m) may be related with the recent changes in the MAST but the rest of the curve is suitable for conductive geothermal gradient calculation.

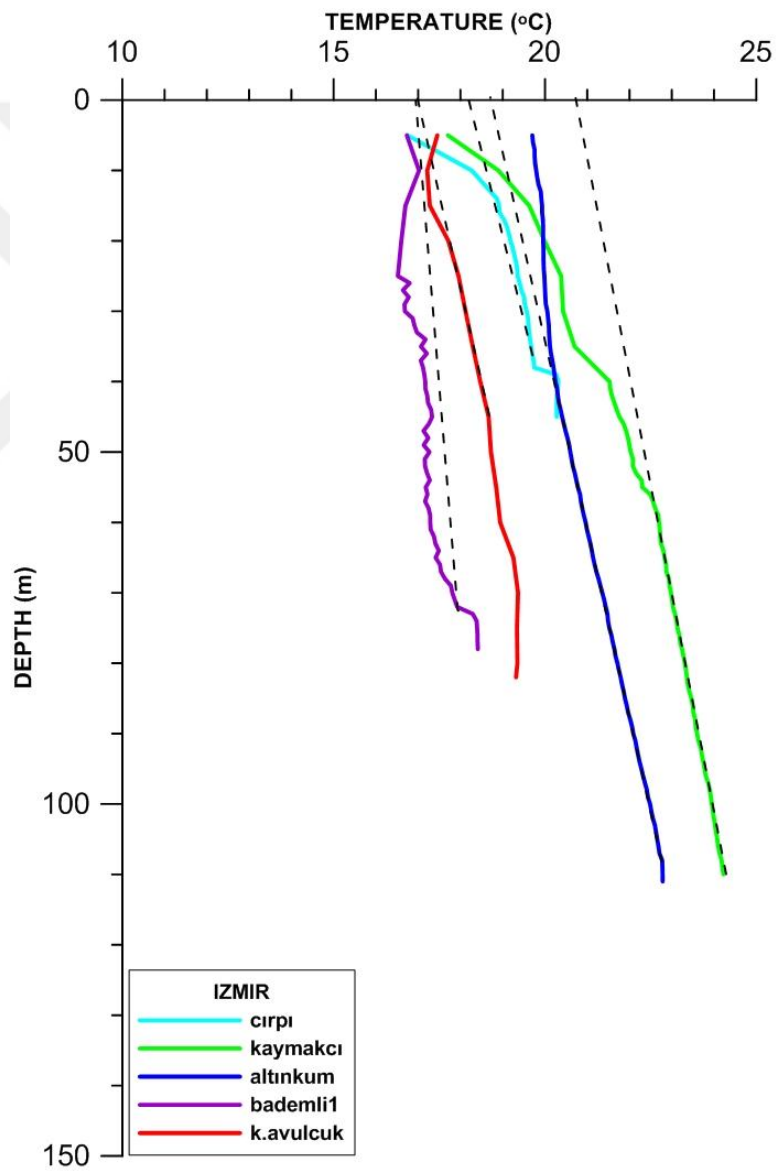


Figure 5.9 Temperature–depth (T–D) curves for İzmir.

Göbekli, Köseali and Köseali2 wells are rated as G class in Manisa (Figure 5.10) with elevated geothermal gradients ($72^{\circ}\text{Ckm}^{-1}$, $113^{\circ}\text{Ckm}^{-1}$ and $104^{\circ}\text{Ckm}^{-1}$ respectively). Interestingly lateral cold water movement perturbs the Göbekli curve at the shallow depths. The effect of down flow is noticed below the 80m in H.embelli. Local hydrological effects disturb at the first 100 m in both of Emreköy and Saraçlar wells. In Osmancik, effect of lateral flow reaches down to 130 m and this level acts like apparent surface of the well. Below 130 m, T-D curve linearly increases with depth. Poyrazköy is an A class T-D curve with the length of 107m linear conductive section.

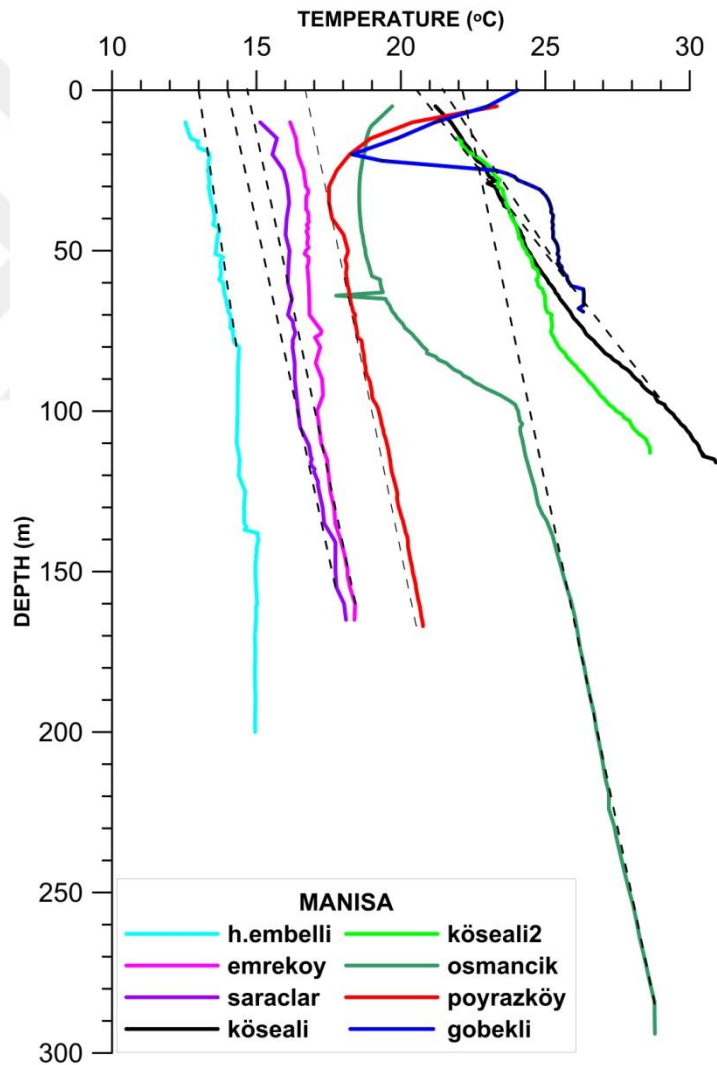


Figure 5.10 Temperature–depth (T–D) curves for Manisa.

5.3 Results

New geothermal gradient data set are given in Table 5.2, together with some detail information. Standard deviations of gradients are assigned according to the criteria given in Table 5.1. Totally 21 new geothermal gradients are calculated for the seven provinces located in western Anatolia. 17 of them are rated as A/B/C/D class and used for geothermal gradient distribution map. Generally for the D class data, geothermal gradients are calculated by drawing a linear line between bottom of the hole and surface (Table 5.2).

Topographic correction is applied to Kaymakçı, H.embelli, Osmancık and Poyrazköy wells. These wells are located on the mountainous terrain and elevation differences cause to a decrease on their gradients. This decrease is eliminated by using Lees' topographic correction model (Lees, 1910).

Together with the previously published data, totally 95 A/B/C/D/G class geothermal gradients are evaluated for western Anatolia. A frequency distribution of them is shown in Figure 5.11. Most of the data lie between 30-50°Ckm⁻¹. A Gaussian curve of the distribution fits on the peak of 41.9°Ckm⁻¹. High gradients around the 100 °Ckm⁻¹ represent the convective transfer of heat. Disregarding these high values, mean conductive geothermal gradient is evaluated as 38°Ckm⁻¹ for the entire study area.

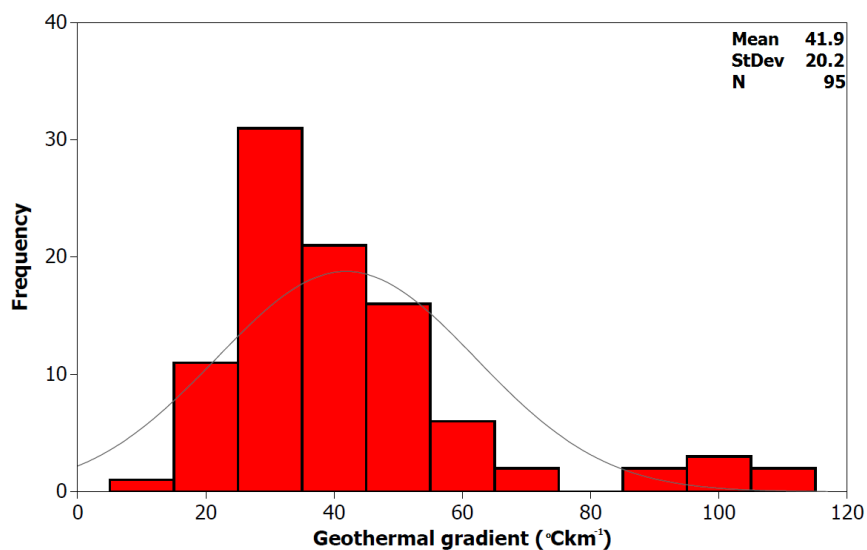


Figure 5.11 Histogram of geothermal gradients in the western Turkey.

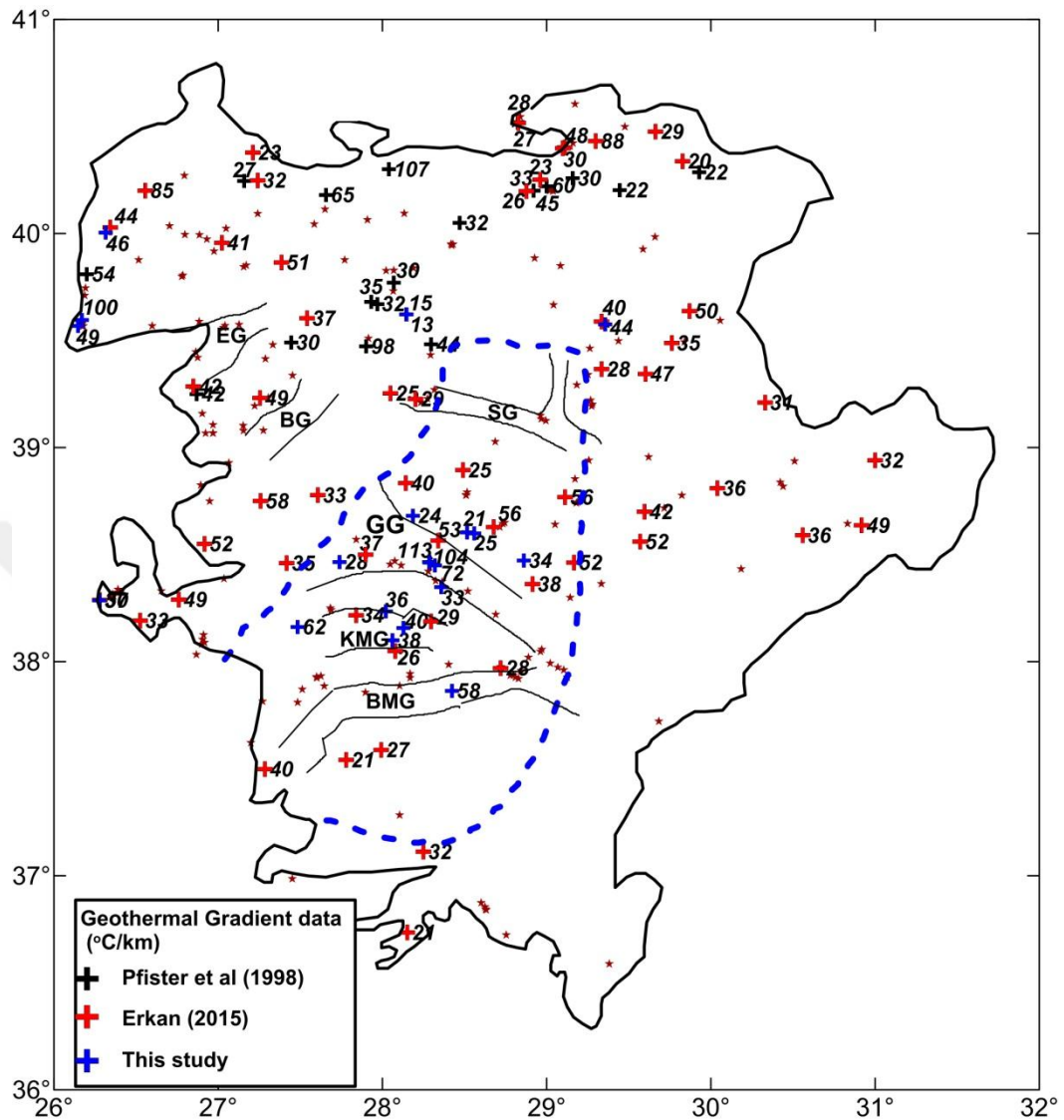


Figure 5.12 Distribution of the geothermal gradients in western Anatolia. Red star symbols show locations of hot springs. Black lines indicate boundaries of horst–graben structures, GG: Gediz Graben; BMG: Büyük Menderes Graben; KMG: Küçük Menderes Graben; EG: Edremit Graben; BG: Bakırçay Graben; SG: Simav Graben.

Figure 5.12 represents the geothermal gradients distribution in the western Anatolia. A/B/C/D/G class data is used in preparation of this distribution. Generally elevated geothermal gradients are recorded on the alluvium units which have lower thermal conductivity than basement rocks. Data points, located on horsts, show low or moderate geothermal gradient values. The maximum gradients are calculated around the hot springs which are signals of the geothermal fields.

5.4 Discussion

Geothermal gradient contour map is generated by combining data in Table 5.2, and previously reported data from Pfister et al. (1998) and Erkan (2015). Totally 56 class of A/B/C data are used for geothermal gradient contour map (Figure 5.13). Unfortunately, wells do not homogeneously distributed because most of the wells were drilled for water supply and locations of them were defined according to the local hydrology.

Geothermal contour map represents regions with elevated ($60-95\text{ }^{\circ}\text{Ckm}^{-1}$) and moderate ($25-45\text{ }^{\circ}\text{Ckm}^{-1}$) geothermal gradient values. Elevated gradients values are calculated in the northwest parts (in Çanakkale and northern part of Balıkesir) of the study area. Elevated gradients in Çanakkale are in accordance with the results of Tezcan & Turgay (1991) and Mihçakan et al. (2006). They pointed out the high gradients around the Çanakkale in their studies. These high values are probably related Miocene volcanism which is responsible for the form of the Biga peninsula. Menderes massif is described with moderate gradients. Geothermal gradients change between $21-58\text{ }^{\circ}\text{Ckm}^{-1}$ within the Gediz graben, $26-62\text{ }^{\circ}\text{Ckm}^{-1}$ in Küçük Menderes graben, and $22-58\text{ }^{\circ}\text{Ckm}^{-1}$ in Büyük Menderes graben. Variation in temperature is directly related with the thermal conductivity. Measurement points located on grabens (e.g. Pirlibey and Çırpı) have higher gradient values than those of located on horsts (e.g. Emreköy and Saraçlar). Thermal conductivity of rocks in basins is lower than basement forming units which causes to elevated gradient on sediments under the constant heat flow case. In Çırpı well, geothermal gradient was calculated as $61.8\text{ }^{\circ}\text{Ckm}^{-1}$ (Erkan, 2015). Lithologic record of this well was assigned as quaternary alluvium which has a quite low thermal conductivity leading to high geothermal gradient although this well does not rated G class. Northeastern (Yalova) and southern end (Muğla) of the study area are characterized with low gradient values. Decrease of the gradient towards to southern end is also mentioned in Tezcan & Turgay (1991) but limited number of the data makes it difficult to discuss reason of the low gradients.

Prevalent extension tectonics in the study area causes to some perturbations on the near surface temperatures due to the sedimentation (Blackwell, 1983). Sedimentation process within a basin results in lower than normal temperature gradient (Beardmore & Cull, 2001). In new data set, measurement points located on quaternary alluvium fans (e.g. Bademli1, K.avulcuk and Osmancik) are expected to experience a considerable effect of sedimentation.

Study area encloses many important geothermal areas and hot springs that are apparent signs of these subsurface hot reservoirs. Due to the tectonic activity around the geothermal areas, relatively high gradients are observed near the hot springs.

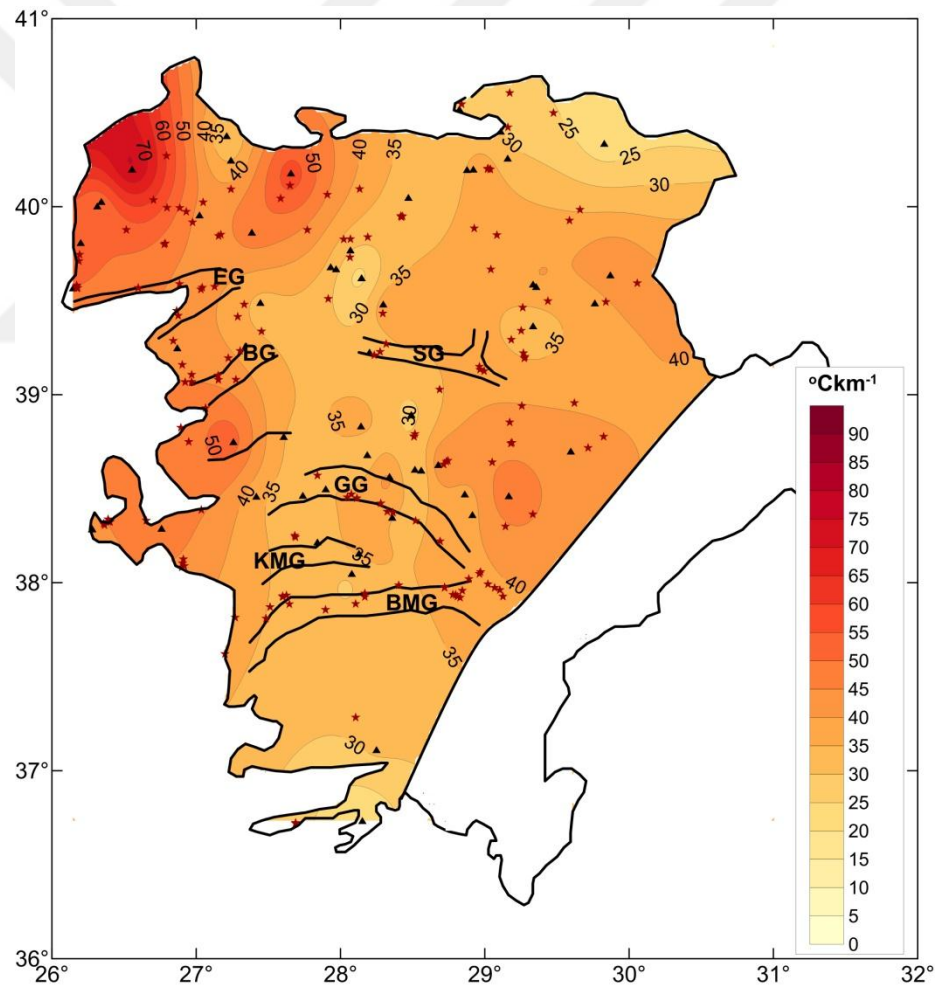


Figure 5.13 Contour map of geothermal gradient. Black triangles are the location of the well rated as A/B/C. Red star symbols show locations of hot springs. Black lines indicate boundaries of horst-graben structures. GG: Gediz Graben; BMG: Büyük Menderes Graben; KMG: Küçük Menderes Graben; EG: Edremit Graben; BG: Bakırçay Graben; SG: Simav Graben.

5.5 Conclusions

30 new T-D data are collected from the seven different provinces in western Anatolia. 9 of them are rated as X class and the remaining 21 data are found to be useful for geothermal gradient calculations. Topographic correction is applied to calculated gradients if necessary. Thus 13 new class A/B/C data with their errors are reported for western Anatolia.

Combining with the previously reported data, distribution of the geothermal gradient (Figure 5.12) and the geothermal gradient contour map are prepared (Figure 5.13). The average conductive geothermal gradient is calculated to be $38 \pm 12^\circ \text{C km}^{-1}$ in the region. The elevated geothermal gradients are observed generally within the alluvium units. Strong effect of sedimentation are experienced the wells located on alluvium fans. This effect will be eliminated before heat flow calculations.

Due to the heterogeneity of the well distribution geothermal contour map includes some uncertainties. New T-D data is required for the interpretation the southern part of study area.

Together with thermal conductivity results given in Chapter 4, geothermal gradient data set will be used as an input for the heat flow determination and thermal modeling studies in the next chapter.

CHAPTER SIX

HEAT FLOW

Heat of the Earth is responsible for its geological evolution, controls the plate tectonics, igneous activity, metamorphism, the evolution of the core, and hence the Earth's magnetic field. Heat transfer in the earth is related to the temperature of the region. Thermal energy of a body increases with increasing temperature. If there is a temperature difference, heat transports from the region with the higher temperature to the region with lower temperature. The interior of the Earth is considerably hotter than its surface thus the heat flow can be defined as the outward flow of the thermal energy from the interior of the Earth through its surface. In practice, measurement of the heat arriving at the Earth's surface requires temperature measurement below the surface with thermal conductivity of related region. In geothermics, heat flow is closely related with temperature which is a fundamental controlling physical property of the Earth forming materials.

6.1 Energy Sources of the Earth

The seismological studies suggested that crust of the Earth is in motion. All geodynamic processes are controlled by heat energy stored within the Earth. Origin of this energy requirement and how this energy is transferred to the Earth surface are some fundamental questions in earth science. Radioactive decay, global cooling and gravitational contraction are the main internal energy sources for the Earth. Although very high amount of energy comes from sun to the Earth, it makes no significant contribution to the internal heat flow. Most of the heat is reflected and radiated back into space.

Earth has cooled since it formed very slowly and at the same time it also produces own internal heat. Radioactive decay of the certain isotopes of elements such as uranium, thorium and potassium in mantle and crust releases energy in the form of heat within the Earth. Gravitational process inside the Earth is the other possibility

for the energy source but rate of the release of gravitational energy has not been estimated yet. The total heat flow through the Earth surface is estimated about 44.2 ± 1.0 TW (Gando et al., 2011). 20 TW of it is generated by radioactive decay (Gando et al., 2011) and this rate was measured based on the bulk silicate Earth model (BSE) (McDonoug & Sun, 1995). Whether the remaining is primordial heat or connected with some other sources is still under debate.

6.2 Heat Transfer Mechanisms in the Earth

Heat can be transferred in Earth by conduction, convection, radiation and advection. In *conduction*, heat flows through a material by atomic and molecular interactions without any motion of the material. Conduction is more effective in solids because the atoms in solids are close each other and unable to move together. Heat is carried with the movement of the warmed fluids via *convective* heat transfer. Convection occurs spontaneously when density changes with increasing temperature. This type of convection is known as free convection. The radiation is the third mechanism in heat transfer which is related to light, radio waves, and other types of electromagnetic radiation (Mussett & Khan, 2000).

Seismological studies show that nearly all crust is in solid form so it might seem that conduction is the dominant mechanism except the regions where there is local groundwater movement. The solid inner core is also available for the conductive heat transfer within the Earth. In the mantle, although the asthenosphere is extremely viscous and heat is transferred mainly by convection within it, the whole of mantle is rigid enough to transmit the S waves. The heat, coming from the deeper part of the Earth, rises up by mainly convection until it reaches the lithosphere where is brittle and cannot convect so heat travels through it by conduction (Lowrie, 2007; Morgan, 2014). Convective heat transfer is also efficient in oceanic crust where the heat energy is transmitted by convection as it forms at mid-ocean ridges, into this lithosphere (Mussett & Khan, 2000). The term of advection is used for the forced convection. When a hot region is uplifted by tectonic events or by erosion and isostatic rebound, heat (called advected heat) is physically lifted up with the rocks.

Radiation can travel in space which is how sun warms the Earth but it is not dominant within the Earth. It is only prevalent in the hottest parts of the core and lower mantle. In the mantle, very little radioactive heat transfer occurs above a temperature of about 500 °C due to the existence of olivine based rocks (Lowrie, 2007).

6.3 Conductive Heat Flow

6.3.1 Heat Conduction Equation

As mention above, heat flows from a hot region to the cold region within the Earth. The rate at which heat conducted through a solid layer is proportional to temperature gradient. If there is a large temperature gradient heat is transferred faster than if there is a small temperature difference (Fowler, 1990). Imagine an infinitely long solid layer with the thickness of d , with its upper surface kept at temperature T_1 and its lower surface at temperature T_2 . The rate of heat flow down through the plate, Q , is therefore

$$Q = -\lambda \frac{T_2 - T_1}{d} \quad (6.1)$$

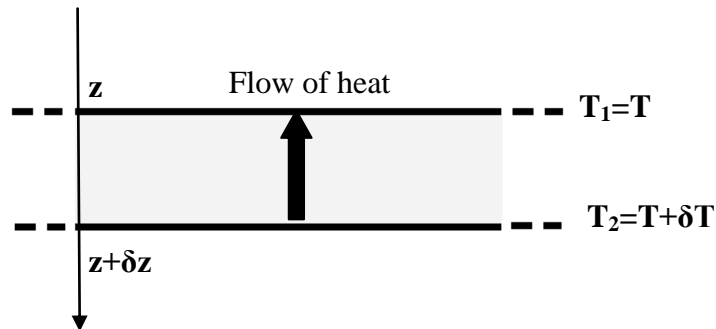


Figure 6.1 Conductive transfer of heat through an infinitely long layer.

We can rewrite equation (6.1) in a differential equation form assuming the temperature of upper surface (at z) is T and the temperature of lower surface (at $z + \delta z$) is $T + \delta T$ (Figure 6.1) as;

$$Q(z) = -\lambda \frac{T + \delta T - T}{z + \delta z - z} \quad (6.2)$$

In the limit as $\delta z \rightarrow 0$,

$$Q(z) = -\lambda \frac{\partial T}{\partial z} \quad (6.3)$$

The minus (-) sign in equation (6.3) indicates that heat flows from high to low temperatures (transfers in the direction the decreasing temperature).

Consider a control volume with height of δz and cross-sectional area of α (Figure 6.2). Any change in temperature δT of this small volume in time δt depends on

- the flow of heat across the volume's surface (net flow is in or out),
- the heat generated in the volume and
- the thermal capacity (specific heat) of the material.

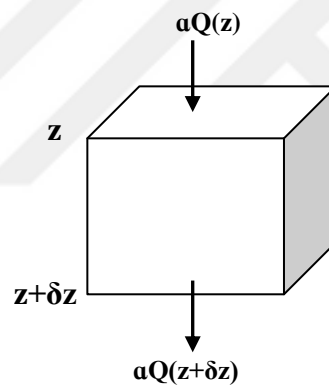


Figure 6.2 Control volume for one-dimensional conduction

The heat per unit time entering the volume across its face at z is $\alpha Q(z)$ whereas the heat per unit time leaving the element across its face at $z + \delta z$ is $\alpha Q(z + \delta z)$

Expanding $Q(z + \delta z)$ in Taylor series gives

$$Q(z + \delta z) = Q(z) + \delta z \frac{\partial Q}{\partial z} + \frac{(\delta z)^2}{2} \frac{\partial^2 Q}{\partial z^2} + \dots \quad (6.4)$$

In equation 6.4, the term $(\delta z)^2$ and those of higher order are very small and can be neglected. From equation (6.4) the net net gain of heat per unit time is

Heat entering across z – heat leaving across the $z + \delta z$

$$\begin{aligned}
&= aQ(z) - aQ(z + \delta z) \\
&= -a\delta z \frac{\partial Q}{\partial z}
\end{aligned} \tag{6.5}$$

If there is a radiogenic heat generation with rate of A in this volume, it denoted as

$$Aa\delta z \tag{6.6}$$

Radioactive heat is the main internal heat source for the Earth as a whole so it must take in consideration for calculation total energy gain per unit time

$$Aa\delta z - a\delta z \frac{\partial Q}{\partial z} \tag{6.7}$$

The specific heat c_p of the material of which the volume is made determines the rise in temperature due to this gain in heat since specific heat is defined as the amount of heat necessary to raise the temperature of 1 kg of the material by 1°C. If the material has density ρ and specific heat c_p , and undergoes a temperature increase δT in time δt , the rate at which heat is gained is

$$c_p a\delta z \rho \frac{\delta T}{\delta t} \tag{6.8}$$

Thus equating the expressions (6.7) and (6.8) for the rate at which heat is gained by the volume element gives

$$c_p a\delta z \rho \frac{\delta T}{\delta t} = Aa\delta z - a\delta z \frac{\partial Q}{\partial z} \text{ or } c_p \rho \frac{\delta T}{\delta t} = A - \frac{\partial Q}{\partial z} \tag{6.9}$$

In the limiting case when $\delta z, \delta t \rightarrow 0$, equation (6.9) becomes

$$c_p \rho \frac{\partial T}{\partial t} = A - \frac{\partial Q}{\partial z} \tag{6.10}$$

Using equation. (6.3) for Q (heat flow per unit area), we can write

$$c_p \rho \frac{\partial T}{\partial t} = A + \lambda \frac{\partial^2 T}{\partial z^2} \quad (6.11)$$

$$\frac{\partial T}{\partial t} = \frac{\lambda}{\rho c_p} \frac{\partial^2 T}{\partial z^2} - \frac{A}{\rho c_p} \quad (6.12)$$

This is the one-dimensional heat-conduction equation. In the derivation of this equation, temperature was assumed to be a function solely of time t and depth z . It was assumed not to vary in the x and y directions (Fowler, 1990).

Using differential-operator notation we can obtain

$$\frac{\partial T}{\partial t} = \frac{\lambda}{\rho c_p} \nabla^2 T - \frac{A}{\rho c_p} \quad (6.13)$$

The equations 6.12 and 6.13 are known as heat conduction equation. For steady state condition which means there is no temperature change with time, equation 6.13 becomes

$$\nabla^2 T = -\frac{A}{\lambda} \quad (6.14)$$

and if there is no radiogenic heat production equation (6.14) returns to

$$\nabla^2 T = 0 \quad (6.15)$$

which forms the basis for thermal modeling studies. Temperature distribution within the Earth can be calculated by integrating with respect to z 6.15 twice;

$$T = C_1 z + C_2 \quad (6.16)$$

where C_1 and C_2 are the integration constants that have to be determined from geological boundary conditions. Let us consider two pairs of boundary condition as;

i) $T_0=0$ is the surface temperature $z=0$

ii) T_1 is the temperature at depth of z_1

Applying boundary conditions to the equation (6.16)

$$T = T_1 \frac{z}{z_1} \quad (6.17)$$

Thus we can calculate temperature distribution with depth using equation 6.17 for given T_1 and z (Fowler, 1990).

6.3.2 Radioactive Heat Production

A considerable part of the heat of the Earth is yielded by the decay of the radioactive elements (Uranium, Thorium and Potassium). Therefore, determining the temperature distribution within the Earth requires the understanding of radiogenic heat production. During the radioactive decay the mass is converted into energy and significant rate of this energy is converted into heat. Equation for the amount of the radiogenic energy was given by (Rybach, 1988) as;

$$A = \rho(9.52_{C_U} + 2.56_{C_{Th}} + 3.48_{C_K})10^{-5} \quad (6.18)$$

where A is in μWm^{-3} , ρ is the density of the rock in kgm^{-3} , C is the concentration of uranium, thorium and potassium, in ppm (or mgkg^{-1}) for uranium and thorium, in % for potassium. Almost half of the radiogenic heat energy comes from Potassium-40 which encountered primarily in the mantle together with thorium-232 while Uranium-238 is only common elements in crusts.

Studies show that there is a linear relationship between surface heat flow and near surface heat production as given in Figure 6.3. The intercept of the straight line with the heat flow axis corresponds to q value for study area. If there is no radiogenic heat production in observation province q would be the surface heat flow. Three common models for the distribution of the radioactive heat sources in lithosphere are built as; Step model, linear model and exponential model. Each model has own consistency but linear and the exponential models are commonly used in heat flow studies. It is assumed that radioactive heat generation decreases with depth for all three models (Morgan et al., 1987).

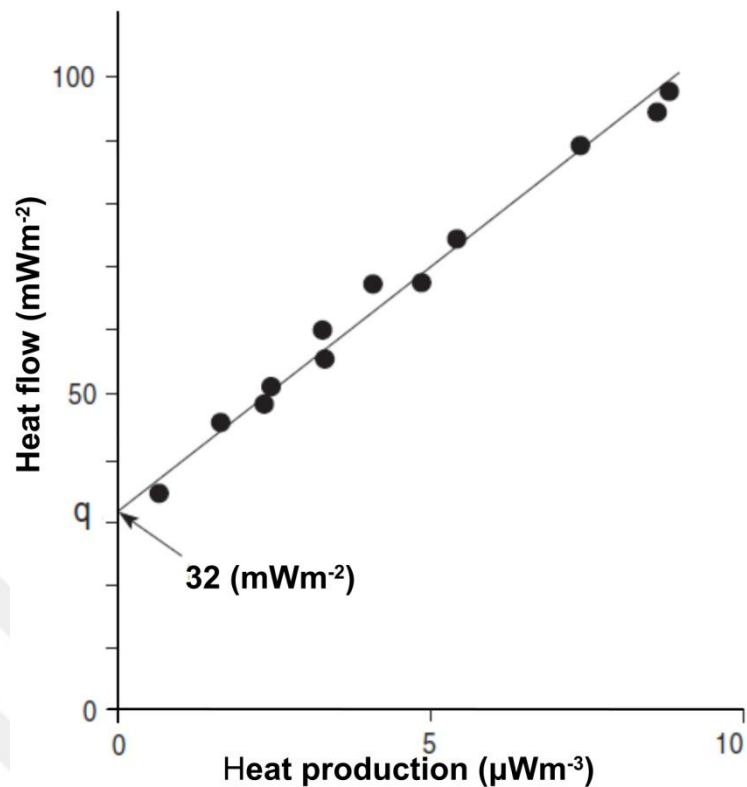


Figure 6.3 Heat flow versus heat production (Mussett & Khan, 2000).

6.4 Continental Heat Flow

The measuring of heat flow on land requires two measurements. Thermal conductivities of the rocks represent the study area are determined in laboratory. Vertical temperature gradient carried out in a borehole located in investigation site. Temperature within the hole can be disturbed during the drilling processes so the hole should be left to return its original condition before geothermal gradient measurements. From the temperature log, the mean geothermal gradient is determined for a geological unit or selected depth as mentioned in Chapter 5. The geothermal gradient is then multiplied by the mean thermal conductivity of related geological unit (Lowrie, 2007).

Heat flow distribution over the Earth's surface varies from place to place. Although continental crust is rich in radioactive isotopes, the amount of the heat flow in ocean basins is greater than in continents. The cooling and creation processes of the oceanic lithosphere as it diverges from the mid-ocean ridges are responsible for elevated heat flow values. The higher heat flow values are generally observed over the young oceanic crusts while lower values are observed over the deep oceans basins with older age (Fowler, 1990). It is also same for continental crust, heat flow values decrease with increasing age.

6.5 Heat Flow Data Set

Theoretically, heat flow should be calculated by multiplying the geothermal gradient by in situ thermal conductivity of related geological unit. Actually, in situ thermal conductivities were not available for study area as mentioned in Chapter 4. Thermal conductivity value is assigned according to the geological description for the depths interval where the geothermal gradient is calculated. The average thermal conductivity values given in Chapter 4 are taken for heat flow calculations except for the quaternary alluvium unit which is obtained from Erkan (2015).

Total heat flow data consist of new 31 measurements as given Table 6.1. 19 of them are computed from the new geothermal data set collected as a part of the TÜBİTAK project with number of 113R019. The remaining 12 measurements are obtained from the data set of Erkan (2015). Heat flow of some data points were not calculated in Erkan (2015), due the lack of lithology information. In this thesis, heat flow of these data points are computed and evaluated together with new data set.

Table 6.1 Class (A/B/C/D/G)-type data used in this study, along with gradients, thermal conductivities, heat flow values, and their respective errors

Location	Latitude (°N)	Longitude (°E)	Prov.	M.Y.	Class	G (°Ckm ⁻¹)	σG	λ (Wm ⁻¹ K ⁻¹)	σλ	q (mWm ⁻²)	σq	Lithology
Kadikoy	38.6365	30.9175	AFY	1996	D	49.1		1.5(L)	0.3	74		Q. Alluvium
Agzikara	38.5900	30.5600	AFY	1996	D	36.4		1.4	0.2	51		Andesite
Derbent	38.9400	31.0000	AFY	1996	D	31.9		1.3	0.6	41		Tuff
Ortakci	37.9700	28.7200	AYD	1995	C	38.1	9.5	3.5	0.2	132	41	Schist
Pirlibey	37.8633	28.4236	AYD	2015	D	58.0		1.5(L)	0.3	87		Q. Alluvium
Nusrat1	39.6220	28.1455	BAL	2016	B	15.0	1.5	1.3(L)	0.6	20	11	Tuff
Nusrat2	39.6223	28.1464	BAL	2016	B	13.1	1.3	1.3(L)	0.6	17	10	Tuff
Babadere1	39.5955	26.1704	CAN	2016	G	99.6		1.0(L)	0.4	102		Claystone
Tuzla1	39.5682	26.1460	CAN	2016	B	48.8	4.9	1.5(L)	0.3	73	22	Q. Alluvium
Çırıpı	38.1620	27.4840	IZM	2015	D	61.8		1.5(L)	0.3	93		Q. Alluvium
Kaymakçı	38.1569	28.1279	IZM	2015	C	40.2	10.1	1.5(L)	0.3	60	27	Q. Alluvium
Altinkum	38.2863	26.2771	IZM	2016	B	37.4	3.7	2.3	0.1	85	12	Marl
Bademli1	38.0992	28.0607	IZM	2015	D	38.0		1.5(L)	0.3	57*		Q. Alluvium fan
K.avulcuk	38.2345	28.0202	IZM	2015	D	35.5		1.5(L)	0.3	53*		Q. Alluvium fan
Gumuskoy	39.4882	29.7627	KUT	1996	B	34.5	3.5	3.5(L)	1.4	120	60	C. Limestone
Darica	39.6380	29.8707	KUT	1996	B	50.3	5.0	0.7	0.2	35	14	Tuff
Koprucuk	39.3660	29.3349	KUT	1996	C	27.7	6.9	1.3(L)	0.6	36	26	Tuff
Tepekoy	39.2100	30.3300	KUT	1996	D	30.9		0.9	0.2	28		Tuff
Göbekli	38.4496	28.3194	MAN	2013	G	72.2		1.5(L)	0.3	108	22	Q. Alluvium
H.embelli	38.3484	28.3588	MAN	2015	C	32.80	8.2	3.2(L)	0.9	105	56	Schist
Emreköy	38.6033	28.5158	MAN	2015	B	20.7	2.1	3.1	0.4	64	14	Schist
Saraçlar	38.5987	28.5598	MAN	2015	B	25.0	2.5	1.2	0.1	30	5	Basalt
Köseali	38.4655	28.2858	MAN	2015	G	113.0		1.5(L)	0.3	170		Q. Alluvium
Köseali2	38.4623	28.2881	MAN	2015	G	104.3		1.5(L)	0.3	156		Q. Alluvium
Osmançik	38.4655	27.7385	MAN	2014	A	28.2	1.4	1.5(L)	0.3	42*	11	Q. Alluvium fan
Poyrazköy	38.6817	28.1856	MAN	2014	A	24.5	1.2	3.2(L)	0.9	78	26	Schist
Gumuskol	38.4627	29.1657	USA	1996	A	52.1	2.6	1.3(L)	0.2	68	14	Tuff
Balabanci	38.3618	28.9149	USA	1996	B	38.0	3.8	1.5(L)	0.3	57	17	Q. Alluvium
Karakuyu	38.7680	29.1116	USA	1996	D	56.1		2.8	0.2	156		Limestone
Karlık	38.7001	29.5954	USA	1996	A	42.3	2.1	1.5(L)	0.5	64	24	Marl
Alahabali	38.4725	28.8614	USA	2016	A	33.5	1.7	3.2(L)	0.9	107	36	Schist

Prov: Province; AFY:Afyon; AYD:Aydın; BAL:Balıkesir; BUR:Bursa; CAN:Çanakkale; IZM:İzmir; KUT: Kütahya; MAN: Manisa; MUG:Muğla; USK:Uşak; YAL:Yalova; M.Y.: measurement year; G:geothermal gradient; σG: Standard deviation of G; λ:thermal conductivity; σλ: standard deviation of λ; q:heat flow; σq: standard deviation of q. Literature thermal conductivities are indicated by (L) next to the value, and are obtained from Erkan (2015) and Balkan et al. (2017).

Four data are rated as G class due to the extremely high geothermal gradients so reminder 27 data are classified as A-B-C or D type. Heat flow values together with their standard deviations are given Table 6.1. The data measured in 1995 and 1996 indicates that they are imported from Erkan (2015). A-B-C class data is used together with the previously published data from Pfister et al (1998) and Erkan (2015) to create new heat flow map of western Anatolia.

6.6 Results

Erkan (2015) reported the first detailed heat flow data set for western Anatolia. In this study this data set is updated with the new heat flow data collected from Aydin, Balıkesir, Çanakkale, İzmir, Kütahya and Manisa as a part of the TUBİTAK project with number of 113R019. Histogram of heat flow data set shows that the mean heat flow is calculated to be $77 \pm 32 \text{ mWm}^{-2}$ based on A/B/C/D/G type data in Figure (6.4). Parts of high heat flows in the distribution present the convective heat transfer and they are excluded from heat flow contour map.

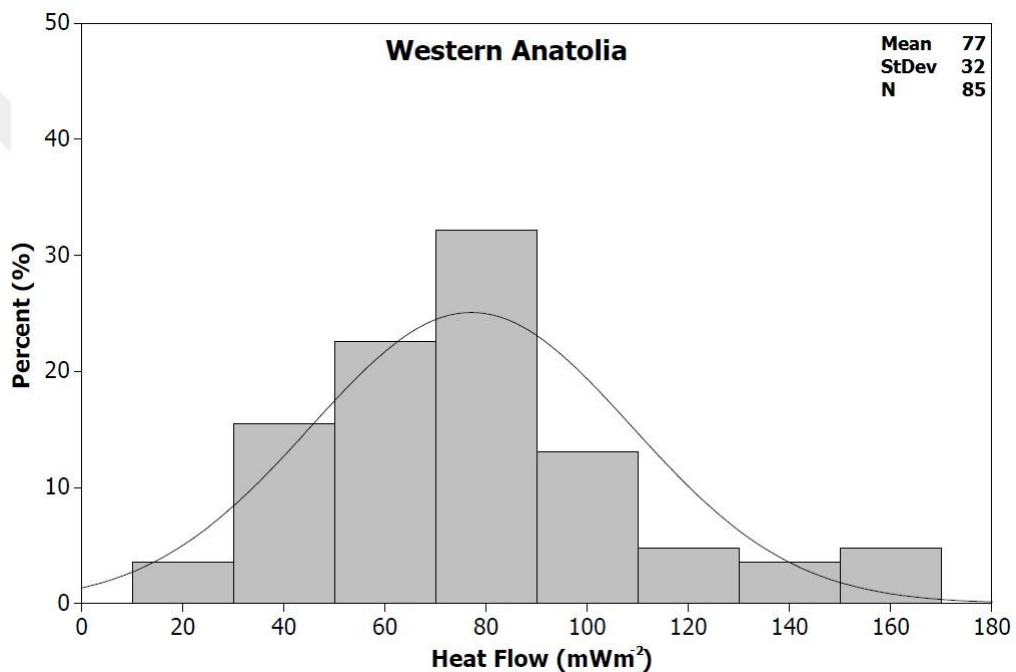


Figure 6.4 Histogram of heat flow data located in study area.

Figure 6.5 shows the regional heat flow distribution in the western Anatolia. A/B/C/D/G class data is used in preparation of this distribution. Increasing number of the data enables us to make more realistic determination about the region, particularly in Menderes Massif and in eastern part of the region. New measurements close to the previous ones also provide us a chance of comparison for their accuracy. Generally, it is concluded that new measurements are in good agreement with the previous ones.

As it seen in Figure 6.5 the heat flow values, greater than the average value, are generally founded within the basins located in Menderes Massif and in the vicinity of hot springs. Babadere1 (102 mWm^{-2}) in Çanakkale, Göbekli (108 mWm^{-2}) Köseali (170 mWm^{-2}) and Köseali2 (156 mWm^{-2}) in Manisa are rated as G class and the last three of them are located southern edge of Gediz graben. Heat flow distribution in Küçük Menderes is comparatively lower than Gediz graben. It is clearly seen from the Figure 6.5 that data points located within the basins have higher heat flow than those of located at the horsts in Menderes Massif.

Northern part of the study (Balıkesir and Çanakkale) area is generally characterized with moderate heat flow values with some exceptions. Crustal heat flow is locally under the effect of groundwater activity. The low heat flow values in centre of Balıkesir are probably results from the prevalent karstic activity in the region. Movement of the groundwater within the karstic regions disturbs the both geothermal gradient and heat flow. However, in Çanakkale whose groundwater activity is lower than Balıkesir, higher heat flow values are observed. Local high values in the Çanakkale are situated near the Çam geothermal site.

Middle-eastern part (Kütahya, Afyon and Uşak) of the study area is represented with low-moderate values. Moderate to high heat flows are located in Izmir, around Ilıca hot spring in Çeşme peninsula and Küçük Menderes graben. However, at southern end of the map, heat flow gets moderate values.

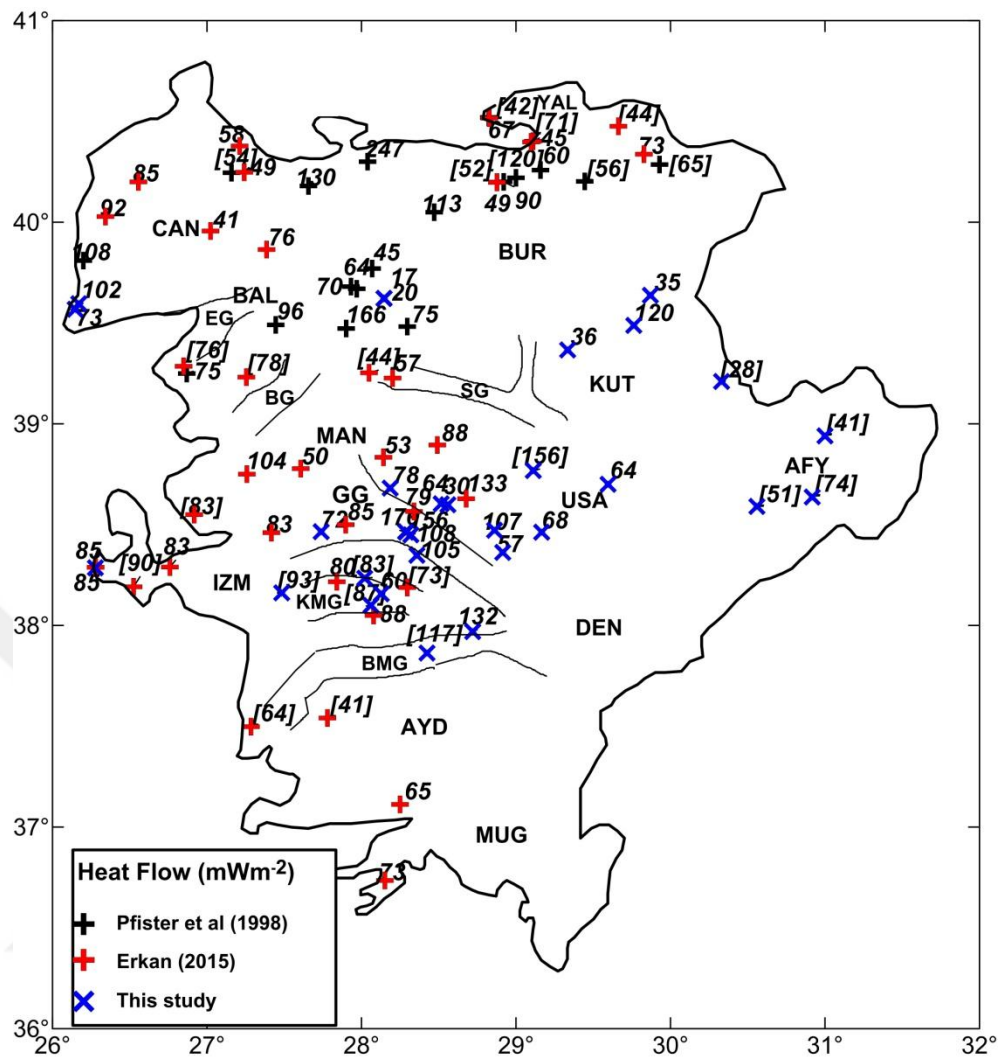


Figure 6.5 Regional distribution of new heat flow data together with the previous heat flow data from Pfister et al. (1998) and Erkan (2015). Black lines indicate boundaries of horst–graben structures. The D-type data is indicated within the parenthesis [].

6.7 Correction of Sedimentation and Thermal Refraction Effect

Steady state heat flow determinations in the extension dominated regions may be perturbed by transient/long term effects such as erosion/sedimentation and thermal refraction (Blackwell, 1983). The horst-graben systems located in the Menderes Massif have suitable condition for occurrence these effects. Sedimentation in grabens results in a reduction in the observed surface heat flow depending on the sedimentation rates. In opposite, the erosion process makes an increase on surface heat flow (Beardsmore & Cull, 2001) near the mountainous regions. Thermal

conductivity contrast between horst and graben fills causes refraction at their boundaries. Basin fill units with low thermal conductivity acts as thermal blanket refracting the heat through the surface. Thus, false elevated heat flow values are observed at the boundaries of these structures (Thakur et al., 2012).

Erkan (2015) suggested a model using Beardsmore's module (Beardsmore & Cull, 2001) for Menderes Massif (Figure 6.6). According to his model the surface heat flow changes about 10-15 mWm^{-2} with the increasing sedimentation rates in the region. Erosion effect gets the surface heat flow up to the 130 mWm^{-2} even if it normally is 85 mWm^{-2} .

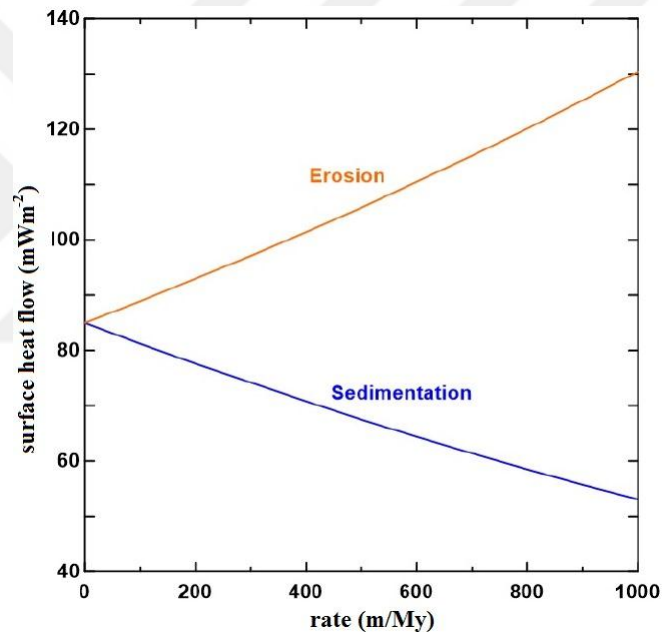


Figure 6.6 Changes in the surface heat flow in Menderes Massif with increasing rate of sedimentation and erosion (Erkan, 2015).

In the present data set, Bademli1, K.avulcuk and Osmancık points are located on the alluvial fans within the grabens. These points are expected to be under the effect of both sedimentation and thermal refraction. So their values corrected to the normal surface heat flow values before using in heat flow contour map.

6.8 Discussion and Conclusion

The heat flow contour map of study area is generated using only A/B/C class data as given in Figure 6.7. The heat flow values, outside the range of 40-140 mWm⁻² are excluded. The gridding is applied using the minimum curvature method and grid space is determined as 0.01 °C in both directions.

The study area is presented with two types of heat flow anomalies; moderate and moderate to high. Crustal extension and subduction related volcanism control thermal condition of the western Turkey. Generally moderate to high values are observed around the Menderes Massif due to the intense tectonic activity. The highest heat flow values are recorded around the geological structures which are formed as a result of these activities. For example, heat flow at the intersection of E-W trending grabens within the Menderes massif is extremely high (Figure 6.7). The high radioactive content within Menderes metamorphics may be source for required heat. The area around the Kula volcano is presented by high values. This anomaly is also mentioned in previous studies (Tezcan & Tugay, 1991; Erkan, 2015). Rapid uplift of the mantle causes to high temperature around the Kula basalts. On the other hand, northeastern part of Çanakkale and central of Balıkesir and Yalova regions are characterized with moderate heat flow values. In Balıkesir, local hydrological effects are thought to be reason for relatively low heat flow values but it is not clear for Çanakkale. Coastal site of Çanakkale is denoted with higher heat flow values and host many hot spring associated with geothermal systems while it is opposite in central part. Therefore, temperature measurements in deep borehole are suggested for detailed interpretations for Çanakkale region.

Seismological studies describe the study region with lower velocities than average continental values (Akyol et al., 2006) emphasizing high heat flow values. Interpretation of heat flow distribution with b-values in a region reveals the deep structural features. b-values are associated with directly tectonic and thermal characteristics and high b-values corresponds to high thermal gradients (Warren & Latham, 1970; Katsumata, 2006; Kalyoncuoğlu et al., 2013). Sayil & Osmanşahin (2008) and Bayrak & Bayrak (2012) reported b-values for the sub regions of western

Anatolia in their studies. The highest b-values are obtained around the Gediz graben in both studies which are in coincidence with high heat flow values in this study. In addition, high heat flow of Simav and Bergama graben are corresponding to the high b-values.

Excluding the D/G type data, the mean value of heat flow for the western Turkey is $74 \pm 26 \text{ mWm}^{-2}$. This value is obviously lower than heat flow values reported in (Tezcan & Turgay, 1991; Karlı et al., 2006) while in accordance with Erkan (2015). Using the constant thermal conductivity value of $2.1 \text{ Wm}^{-1}\text{K}^{-1}$ gives rise to questionable results in Tezcan & Turgay (1991). Their heat flow map also does not include measurement points which make it hard to interpret with our results. Unfortunately, any correction and analysis were not applied the data set used in Karlı et al. (2006)'s study. Thus their map may only represent unrealistic results for the study area. Finally we can conclude that heat flow contours in the coastal line of the study area are comparable with the values measured in Aegean Sea (Jongsma, 1974; Erickson et al., 1977, Fytikas, 1980).

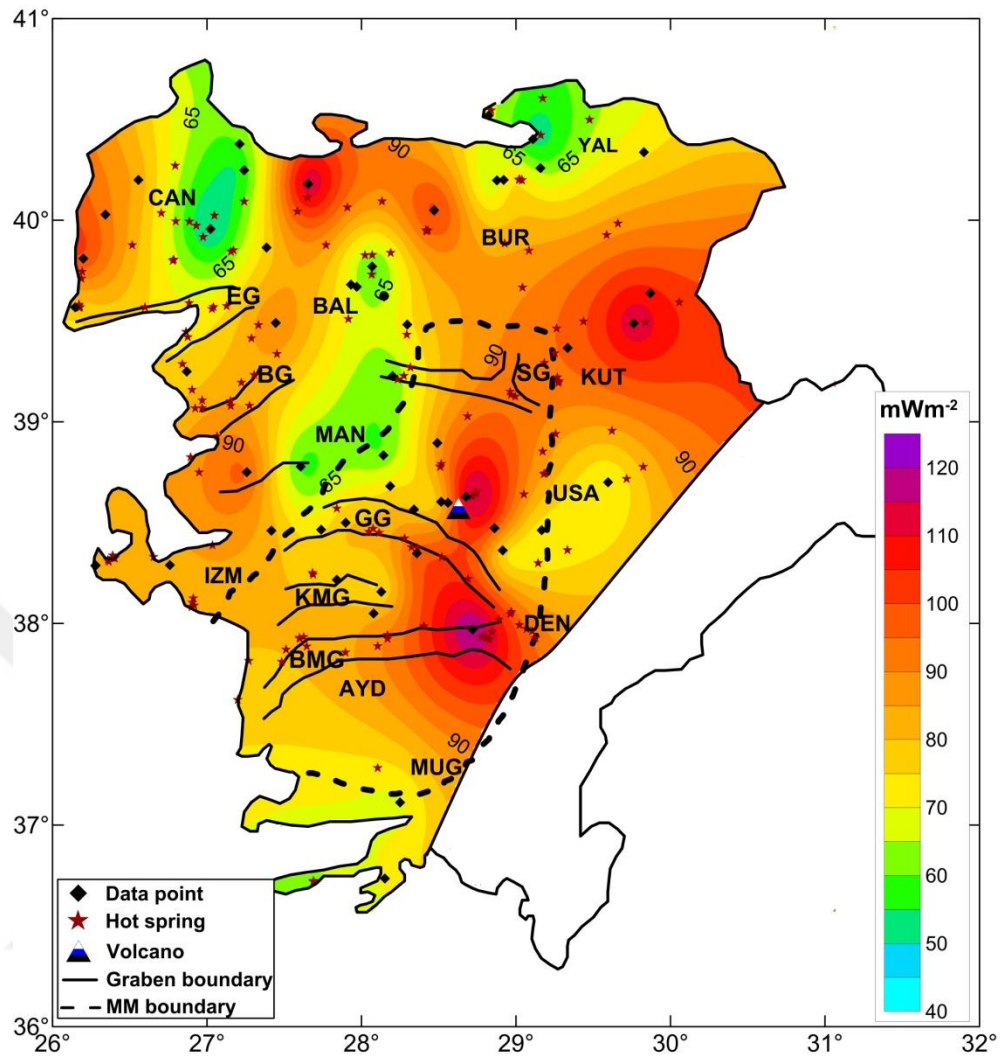


Figure 6.7 Heat flow map of study area using the results of this study (class A/B/C data in Table 6.3) with those of Erkan (2015) and of Pfister et al. (1998). Black lines indicate the boundary of Menderes Massif.

CHAPTER SEVEN

THERMAL MODELING

Determination of temperature distribution within the depths of the Earth, where it is not possible to measurement temperature, is the main objective of thermal modeling. Conduction is the most dominant mechanism in the Earth's crust as mentioned before. Resulting from this, we assume conduction is the main heat-driving process, and steady-state solution depends only on rock thermal conductivity and radiogenic heat production, for the given boundary conditions. Modeling the conductive heat transfer requires to apply thermodynamics of energy conservation along with Fourier's law. Mathematical description of heat conduction process is expressed by differential equations which are susceptible to analytic solutions. Several researchers dealt with the exact solution to heat conduction problem. However, the analytic approach to problem is limited to relatively simple geometric shapes. In practice heat conduction includes complex geometries and boundaries, or non-linear components. In such cases, approximate solutions can be obtained by numerical and computational methods (Kreith et al., 2012).

Solution of heat conduction equation given in Chapter 6 can be solved for a certain point in space and time using analytic methods. In contrast, numerical solutions are derived from the approximate solution only at discrete points within the given boundaries. Discretization is the first step of any numerical approach which transforms the differential equations to a system of algebraic equations. Dealing with the solution of discrete points instead of complex differential equations decreases the time required to find the solution. Discretization of initial and boundary conditions that have been specified for the problem is also crucial in the solving process. Every approximation approach introduces errors in to solution so we also need to minimize them. Finally, under some conditions, the numerical methods may give a solution that oscillates in time or space. We need to know how to avoid these *stability* problems (Kreith et al., 2012).

There are several ways for discretizing the differential equations of heat conduction. The finite elements, finite difference and boundary elements methods are the commonly used methods. Each method has its own advantages and disadvantages.

The aim of this chapter is to estimate temperature distribution in western Anatolia. To achieve this, thermal models of Gediz and Büyük Menderes grabens are investigated using the *finite element method (FEM)* under the assumption of conductive heat transfer. The previously published geophysical and geological studies are used to evaluate geological geometry of models for both Gediz and Büyük Menderes grabens.

7.1 Finite Elements Approximation to Heat Conduction Equation

The finite element approximation is one of the most used numerical methods in thermo-mechanical modeling. The finite elements method was originally developed to study the stress analysis in complex air-frame structures (Clough, 1960) and it has extended and applied to the general field of continuum mechanics (Zienkiewicz & Cheung, 1965). The main advantage of the method over other numerical approximations is its ability to solve problems in irregular and complex geometries with unusual boundary conditions (Mitsoulis & Vlachopoulos, 1984).

The basic principle in FEM is the subdivision of the study domain of the mathematical model into discrete, interconnected sub-regions or elements of simple geometry called finite elements. In this way, the problem is represented by simpler components. The physical laws of the related problem are applied to each element using interpolation functions. Approximating functions in finite elements are determined as nodal values of a physical field. A continuous physical problem is turned into a discretized finite element problem with unknown nodal values. For a linear problem a system of linear algebraic equations should be solved. Values inside finite elements can be recovered using nodal values.

A basic steady state heat conduction equation were derived in Chapter 6

$$\frac{d}{dz} \left(\lambda \frac{dT}{dz} \right) + A = 0 \quad (7.1)$$

where A refers to heat generation and λ indicates thermal conductivity. Equation (7.1) can be solved with appropriate boundary conditions. It is assumed that the *boundary conditions* can be of the following types:

- Specified temperature ($T_{z=0} = T_0$)
- Specified heat flow (or insulated) ($q_{z=d} = q_d$)
- Convection

Various type of boundary conditions can be considered.

One-dimensional element is used in one dimensional heat conduction. The two-mode element with linear shape functions is taken to discrete in z dimension as given in

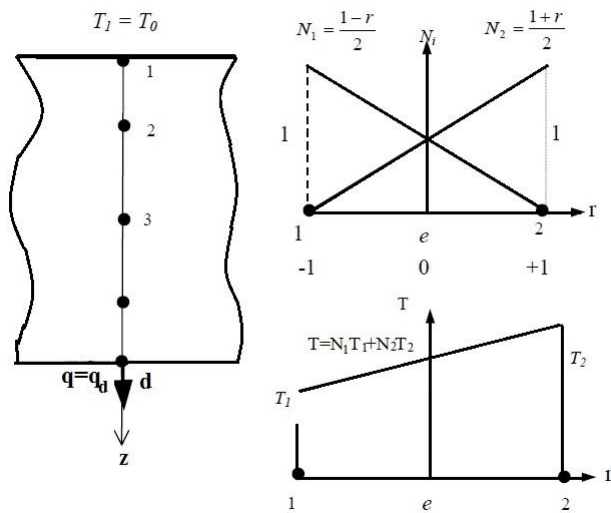


Figure 7.1 Finite element modeling and shape functions for linear interpolation of the temperature field.

$$T(\zeta) = N_1T_1 + N_2T_2 = NT^e \quad (7.2)$$

where $N_1 = (1-\xi)/2$, $N_2 = (1+\xi)/2$, ξ varies -1 to +1 $N = [N_1, N_2]$ and $T^e = [T_1, T_2]^T$.

Noting the relations

$$\zeta = \frac{2}{z_2 - z_1}(z_2 - z_1) \quad (7.3)$$

$$d\xi = \frac{2}{z_2 - z_1} dz \quad (7.4)$$

we have

$$\frac{dT}{dz} = \frac{dT}{d\xi} \frac{d\xi}{dz} \quad (7.5)$$

$$= \frac{2}{z_2 - z_1} \frac{dN}{d\xi} \bullet T^e \quad (7.6)$$

$$= \frac{1}{z_2 - z_1} [-1 \quad 1] T^e \text{ or } \frac{dT}{dz} = B_T T^e \quad (7.7)$$

Using the Galerkin method, we can rewrite the heat conduction equation in the following form:

$$\int_0^d \phi \left[\frac{d}{dz} \left(\lambda \frac{dT}{dz} \right) + Q \right] dz = 0 \quad (7.8)$$

For every ϕ constructed from the same basis functions as those of T , with $\phi(0)=0$. $\phi(d)=0$ where T is specified. Integrating the first term by parts we have

$$\phi \lambda \frac{dT}{dz} \Big|_0^d - \int_0^d \lambda \frac{d\phi}{dz} \frac{dT}{dz} dz + \int_0^d \phi Q dz = 0 \quad (7.9)$$

Now,

$$\phi \lambda \frac{dT}{dz} \Big|_0^d = \phi(d) \lambda(d) \frac{dT}{dz}(d) - \phi(0) \lambda(0) \frac{dT}{dz}(0) \quad (7.10)$$

Since $\phi(0)=0$ and $q=-\lambda(L)(dT(L)/dz)$

Thus

$$\int_0^d \phi Q dz = \int_0^d \lambda \frac{d\phi}{dz} \frac{dT}{dz} dz \quad (7.11)$$

Using isoparametric relations $T=NT^c$. Further, a global virtual-temperature vector is denoted as $\psi=[\psi_1, \psi_2, \dots, \psi_d]$ and the test function within each element is interpolated as

$$\phi = N\psi \quad (7.12)$$

Analogous to $dT/dz=B_T T^c$ in equation (7.7) we have

$$\frac{d\phi}{dz} = B_T \psi \quad (7.13)$$

Hence (7.11) becomes

$$\sum_e \psi^T \frac{Q_e d_e}{2} \int_{-1}^1 N^T d\xi = \sum_e \psi^T \left(\frac{\lambda_e d_e}{2} \int_{-1}^1 B_T^T B_T d\xi \right) T \quad (7.14)$$

$$\psi^T R = \psi^T K_T T \quad (7.15)$$

This should be satisfied for all ψ . The global matrices K_T and R are assembled from element matrices k_T and r_Q as given

$$k_T = \frac{k_e}{d_e} \begin{bmatrix} 1 & -1 \\ -1 & 1 \end{bmatrix} \quad (7.16)$$

$$r_Q = \frac{Q_e d_e}{2} \begin{Bmatrix} 1 \\ 1 \end{Bmatrix} \quad (7.17)$$

When each ψ is chosen in turn as $[0,1,0 \dots,0]^T, \dots, [0,0,1,0, \dots]^T$ and since $T_1=T_0$ then equation 7.14 (7.15) yields

$$\begin{bmatrix} K_{22} & K_{23} & \cdots & K_{2d} \\ K_{32} & K_{33} & \cdots & K_{3d} \\ \vdots & & & \vdots \\ K_{d2} & K_{d3} & \cdots & K_{dd} \end{bmatrix} \begin{Bmatrix} T_2 \\ T_3 \\ \vdots \\ T_d \end{Bmatrix} = \begin{Bmatrix} R_2 \\ R_3 \\ \vdots \\ q_d \end{Bmatrix} - \begin{Bmatrix} K_{21}T_0 \\ K_{31}T_0 \\ \vdots \\ K_{d1}T_0 \end{Bmatrix} \quad (7.18)$$

Obtained equation can be solved for T_2, T_3, \dots, T_d . So the Galerkin approach naturally leads to the elimination approach for handling nonzero specified temperature $T=T_0$ at node 1. However it is also possible to develop Galerkin's method with a penalty approach to handle $T_1=T^0$. In this case, the equations are given by

$$\begin{bmatrix} K_{12} + C & K_{12} & \cdots & K_{1d} \\ K_{21} & K_{22} & \cdots & K_{2d} \\ \vdots & & & \vdots \\ K_{d1} & K_{d2} & \cdots & K_{dd} \end{bmatrix} \begin{bmatrix} T_1 \\ T_2 \\ \vdots \\ T_d \end{bmatrix} = \begin{bmatrix} R_1 + CT_0 \\ R_2 \\ \vdots \\ q_d \end{bmatrix} \quad (7.19)$$

7.2 Applications

The Gediz and Büyük Menderes graben are the most prominent features of Menderes Massif and they are the largest grabens compared with others basins in western Anatolia. However, thermal modeling studies were very limited in the region due to the lack of a comprehensive and systematic data set. In this chapter, forward modeling is used to evaluate 2D steady state subsurface temperatures of the Gediz and Büyük Menderes grabens using Comsol MultiphysicsTM software. Model results are validated against measured temperatures in deep wells if available.

The two-dimensional steady-state heat conduction equation is given as;

$$\frac{\partial}{\partial x} \left(\lambda \frac{\partial T}{\partial x} \right) + \frac{\partial}{\partial z} \left(\lambda \frac{\partial T}{\partial z} \right) + A = 0 \quad (7.20)$$

Here, $\lambda(x, z)$ is thermal conductivity, $T(x, z)$ is temperature field and $A(x, z)$ is heat production (Cermak et al., 1991).

Modeling the temperature distribution within the Earth requires the knowledge about the geometry and thermal properties of the subsurface geology and some boundary conditions.

Simplified structural models of each grabens are evaluated using previously published geological cross sections based up on seismic reflection data (Çiftçi & Bozkurt, 2009a; Çiftçi et al., 2010; Çiftçi et al., 2011).

The subsurface geometry for each graben is presented by simple layers with constant thermal properties and boundary conditions under the assumption of thermal properties of each layer do not change significantly laterally on a local or regional scale. Temperature dependence of thermal conductivity is taken in to account during using the equation (7.21) developed by Kukkonen & Jöeleht (1996).

$$\lambda(T) = \frac{\lambda_0}{(1+bT)} + c(T+273.15K)^3 \quad (7.21)$$

In this equation, λ_0 is the thermal conductivity at surface conduction (20 °C), T is temperature (°C), b (K^{-1}) and c ($Wm^{-1}K^{-4}$) are the experimental constants. For b the value of 0.0015 is assigned which represent the lattice conductivity of rocks (Zoth & Haenel, 1988) for the temperatures lower than 1000 °C. The value of 1.10^{-10} is assumed for c parameters (Schatz & Simmons, 1972).

Thermal conductivity of each layer is assigned using results of Chapter 4 according to the stratigraphic definition given in previously published studies (Çiftçi & Bozkurt, 2009a; Çiftçi et al., 2011). Previously published thermal conductivity values are used for the rocks types which are not reported in Chapter 4.

For heat production, a constant (step) model is assumed within the grabens. The knowledge of heat production distribution of the common rocks types of the study area is not available so radiogenic heat production rate is also obtained from literature. Vilà et al., (2010) reported radiogenic heat production (RHP) distribution of different worldwide rocks obtained from 102 published studies. They pointed out the high variability in (RHP) values from a petrogenetic viewpoint suggesting reasonable effects on crustal geotherms in thermal modeling. Due to the variability in RHP for similar or same lithological unit, scenario analysis is applied to demonstrate thermal structure of the grabens in Menderes Massif.

Graben models in this study consist of sedimentary rocks which fill the metamorphic basement rock. Three cases (minimum, mean and maximum) of RHP distribution in sedimentary and metamorphic rocks are considered as possible scenarios during the numerical thermal modeling. Developed scenarios are given Table 7.1

Table 7.1 Scenarios for RHP distribution (Vila et al., 2010)

<i>Scenario</i>	<i>RHP (μWm^{-3})</i>	
	<i>sedimentary rocks</i>	<i>metamorphic rocks</i>
A (minimum)	0.318	0.215
B (mean)	1.055	1.288
C (maximum)	1.806	3.206

Solution of the equation 7.20 is objected under the certain initial and boundary conditions. Temperature at the graben's surface $T(x, z=0) = 18 \text{ }^{\circ}\text{C}$ is considered as the mean annual surface temperature (Şensoy et al., 2008).

No temperature differences boundary conditions are applied to the vertical boundaries of the models $\left(\frac{\partial T}{\partial x} = 0\right)$ at $x=0$ and $x=L$ where L is the length of the graben model.

A constant vertical heat flow is assigned at the bottom the models. A percent distribution of heat flow in Menderes Massif is given Figure 7.2. A Gaussian curve fit to the distributions showed a peak at 80 mWm^{-2} . This value is used as the vertical heat flow value at the bottom of the grabens.

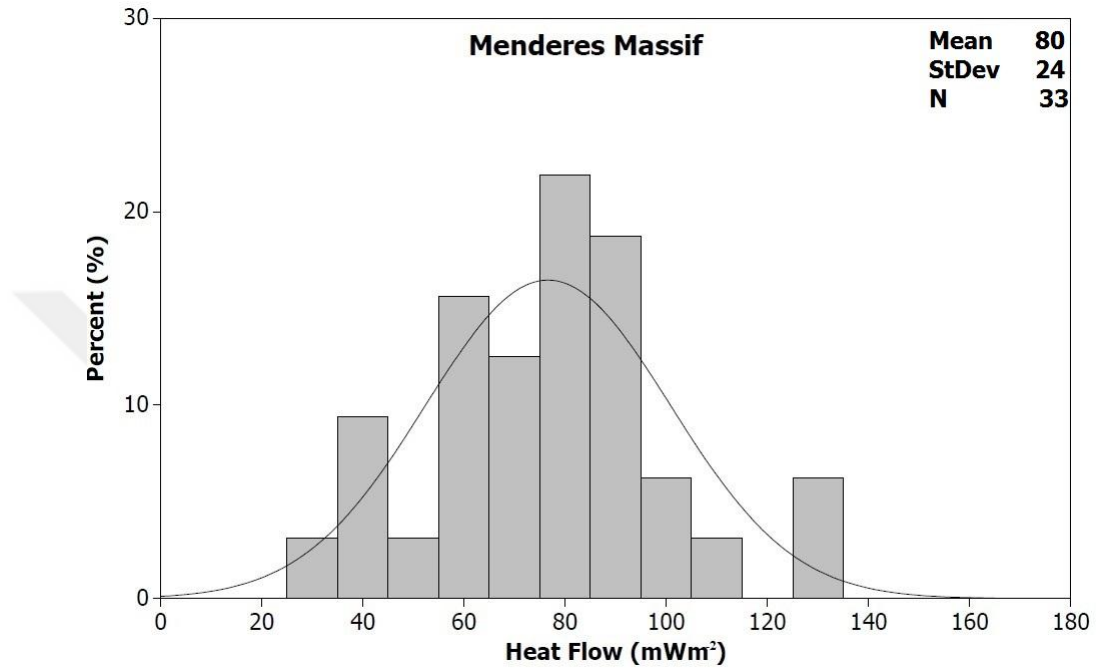


Figure 7.2 Histogram of heat flow in Menderes Massif.

7.2.1 Thermal Model of Gediz Graben

As mentioned in chapter 2 transverse geological cross section of Gediz graben was published by Çiftçi et al. (2010) as given in Figure 7.3. To obtain this cross section they used totally 270 km length 2D seismic reflection data interpreted with logs from three boreholes (Figure 7.4). There is a good match between the lithostratigraphic formations and the seismic stratigraphic units (SSU) identified by Çiftçi & Bozkurt (2009a). Location of the seismic profiles and boreholes are given in Figure 2.5.

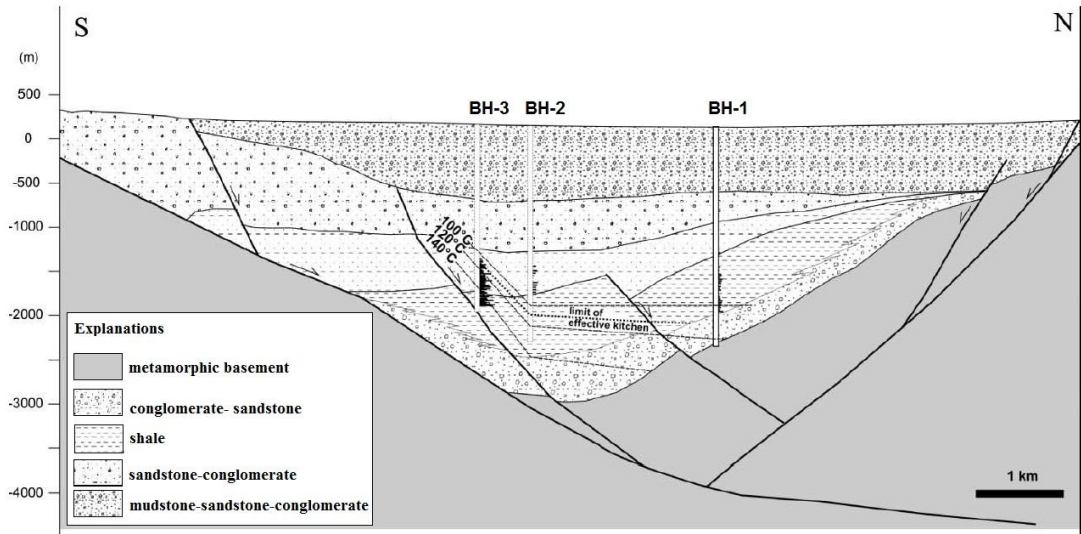


Figure 7.3 Transverse geological cross section of Gediz graben. BH: Borehole (Çiftçi et al., 2010).

In Figure 7.5, interpreted seismic reflection data is given with the extended geological cross section (Çiftçi & Bozkurt, 2010). We benefited from all these previously published data and integrated them by simplifying in to our thermal model as given in Figure 7.6.

The Gediz graben model consists of basement rock and sedimentary fill which is divided into four sub-sections in the vertical direction based on thermal conductivity and each layer has constant thermal conductivity. Thermal conductivity of each layer is assigned according to the formation type given by Çiftçi & Bozkurt (2009a) in Figure 7.4 and as tabulated in Table 7.2. The basement units represented the metamorphic rocks which are generally composed schist, marble and quartzite. The basin fill that is covering the basement rocks consist of four layers in the vertical direction. Alaşehir formation is located above the basement. SSU-I mainly composed of shale, conglomerate units. Above the Alaşehir formation, there is Çaltılık formation (SSU-2) which has higher thermal conductivity due to the limestone content. Gediz, Kaltepe and Bintepeler formations comprise the SSU-III unit. In seismic section, SSU-III contains also Quaternary alluvium but in this thesis Quaternary alluvium is considered as separate layer due to significant difference of thermal conductivity between other units.

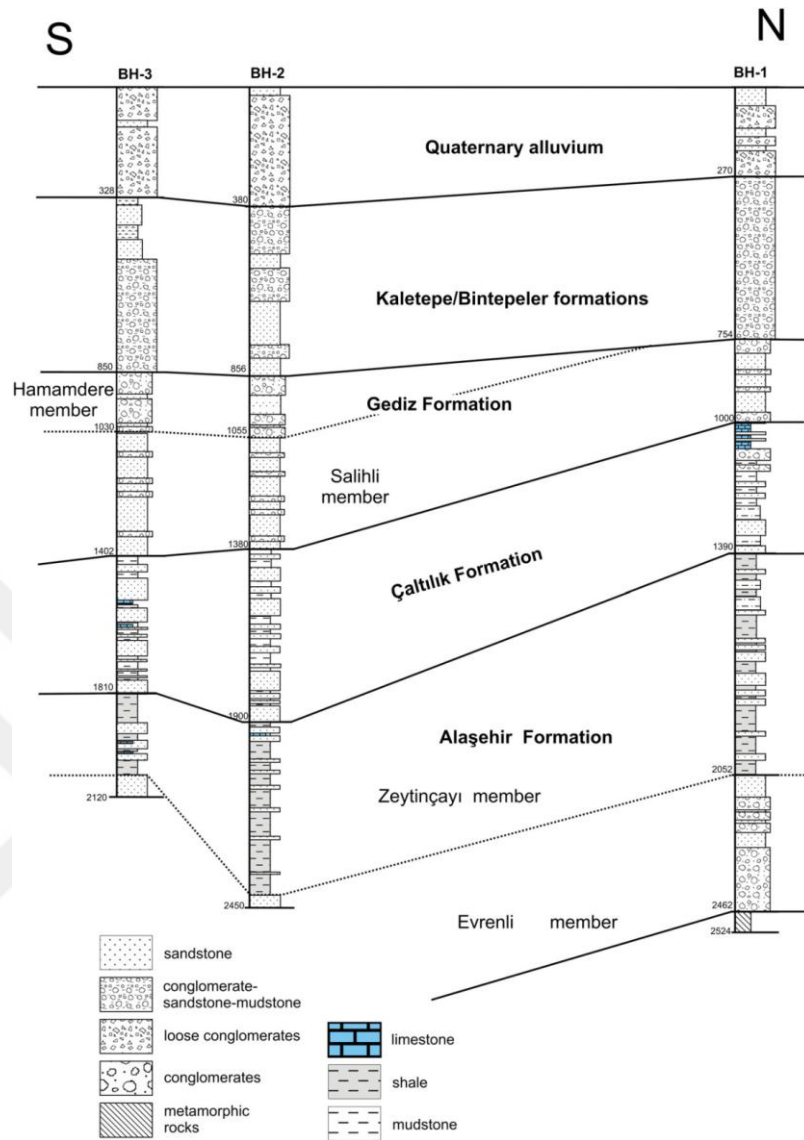


Figure 7.4 The boreholes drilled in Gediz graben. See Figure 2.5 for their locations. (Çiftçi & Bozkurt, 2009a).

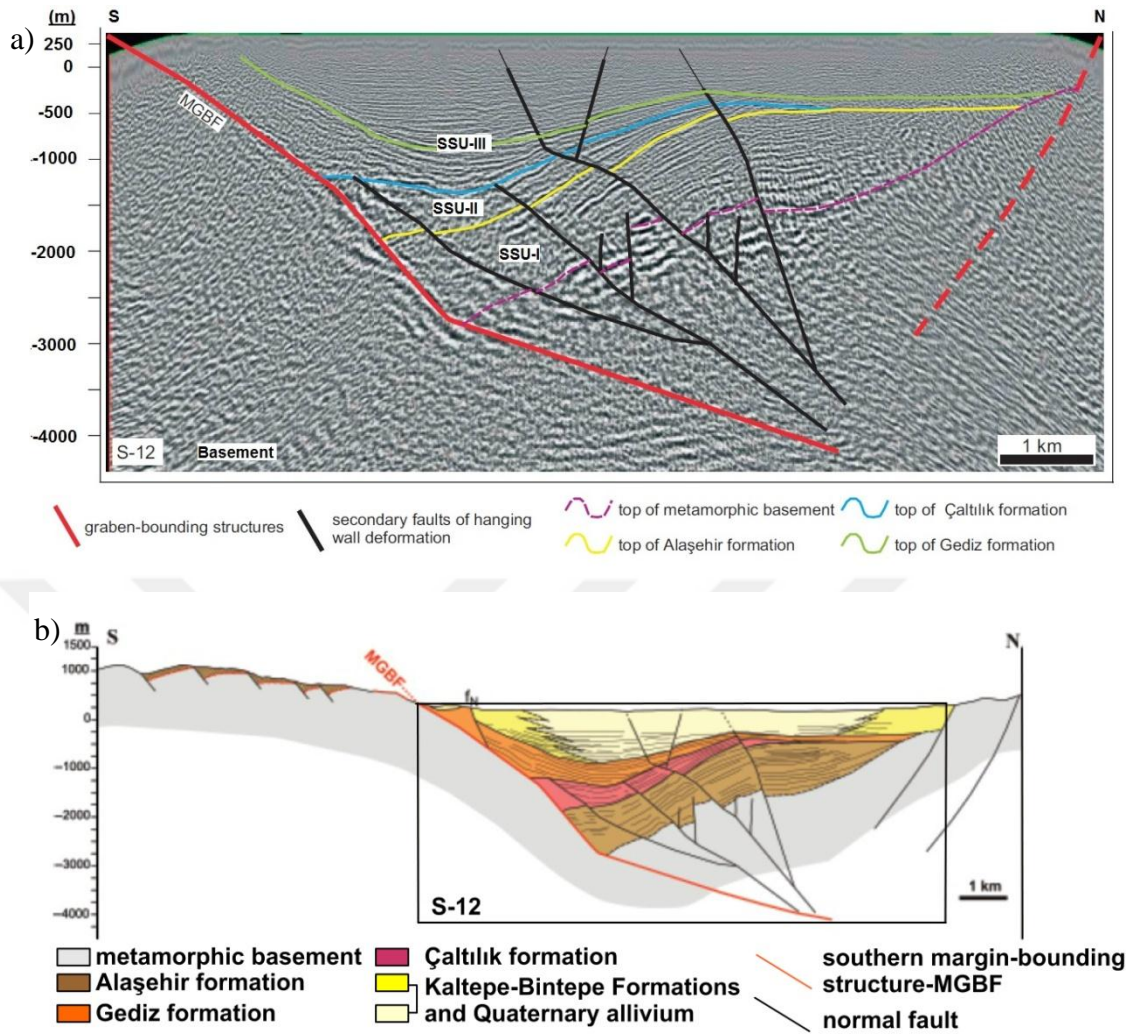


Figure 7.5 a) Interpreted seismic reflection profile S-12 b) geological cross section of Gediz graben (see Figure 2.5 for location of the section) (Çiftçi & Bozkurt, 2010)

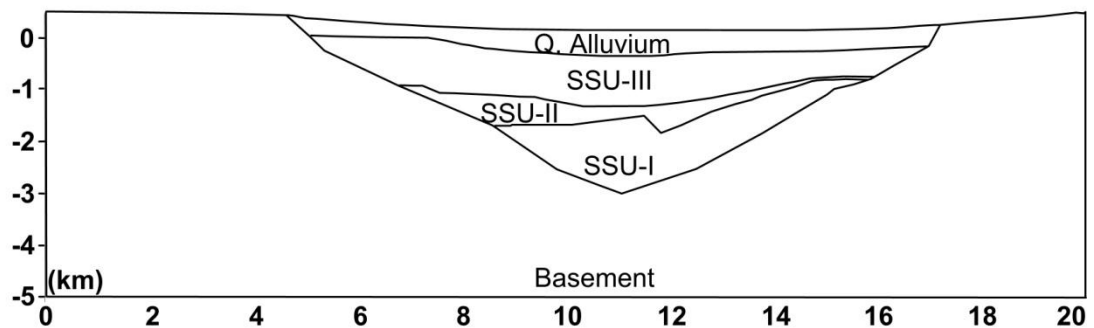


Figure 7.6 Simplified thermal model of Gediz Graben.

Table 7.2 Thermal conductivity values used in Gediz Graben model

<i>Dominant Lithology</i>	<i>Stratigraphic Unit</i>	λ (W/m/K)
Loose conglomerate-clastic rocks	Quaternary alluvium	1.50
Conglomerate-Sandstone-Mudstone	SSU-III (Gediz, Kaltepe ve Bintepe formations)	2.56
Sandstone-Mudstone-Conglomerate-Limestone	SSU-II (Çaltılık formation)	2.24
Shale-Conglomerate-Sandstone-Mudstone	SSU-I (Alaşehir formation)	1.93
Schist-Marble-Quartzite	Basement (Menderes Massif Metamorphics)	3.10

Grid interval is selected as 0.01 km both in vertical and horizontal direction. On the surface of the model, temperature is fixed at 18 °C, which is the annual mean temperature for the region. Reduced heat flow at the bottom of model is determined as 80 mWm⁻² derived from Figure 7.2. This reduced heat flow does not include radiogenic heat production rate. To examine effect of the RHP input on the temperature fit, different RHP parameters scenarios (minimum, mean and maximum) are applied. The applied scenarios are given in Table 7.1. It is assumed that the sides of the model are insulated which means there is no lateral heat flow at the sides of the model.

7.2.1.1 Thermal Modeling Results of Gediz Graben

Finite elements method is used to solve two-dimensional steady state heat conduction equation. The differences between measured and calculated temperatures for three different scenarios are given in Figure 7.7, Figure 7.8 and Figure 7.9. To minimize differences between calculated and measured temperature, initial model parameters are calibrated within the reasonable range. Table 7.3 shows calibrated values for each scenario. Differences in RHP values results to changes in heat flow value at the bottom of the model. Consequently, very good agreement between measured and calculated temperatures is obtained for all scenarios.

Table 7.3 Calibrated model parameters for Gediz Graben

Scenario	q_b (mW/m^2)	λ_c ($W/m/K$)	λ_i	T_b (°C)	q_s (mW/m^2)		RMS(%)		
					range	valley	BH-1	BH-2	
A (minimum) $A_s=0.318$ $A_m=0.215$	85	Q.Alluvium	1.50	1.50	214	90	77	1.98	1.72
		SSU-IIIa	2.60	2.56					
		SSU-II	2.15	2.24					
		SSU-I	1.93	1.93					
Basement	3.10	3.10							
B (mean) $A_s=1.055$ $A_m=1.288$	80	Q.Alluvium	1.50	1.50	209	91	77.4	1.61	1.27
		SSU-IIIa	2.45	2.56					
		SSU-II	2.15	2.24					
		SSU-I	2.00	1.93					
Basement	3.10	3.10							
C (maximum) $A_s=1.806$ $A_m=3.206$	75	Q.Alluvium	1.50	1.50	208	96	79.5	1.80	1.54
		SSU-IIIa	2.60	2.56					
		SSU-II	2.15	2.24					
		SSU-I	1.93	1.93					
Basement	3.10	3.10							

A_s : Heat production of sedimentary rocks (μWm^{-3}), A_m : heat production of metamorphic rock (μWm^{-3}), q_b : calibrated heat flow for the bottom of the model; λ_c : calibrated thermal conductivity; λ_i : initial thermal conductivity T_b : The maximum temperature at the bottom of the graben; q_s : heat flow at the surface of the graben.

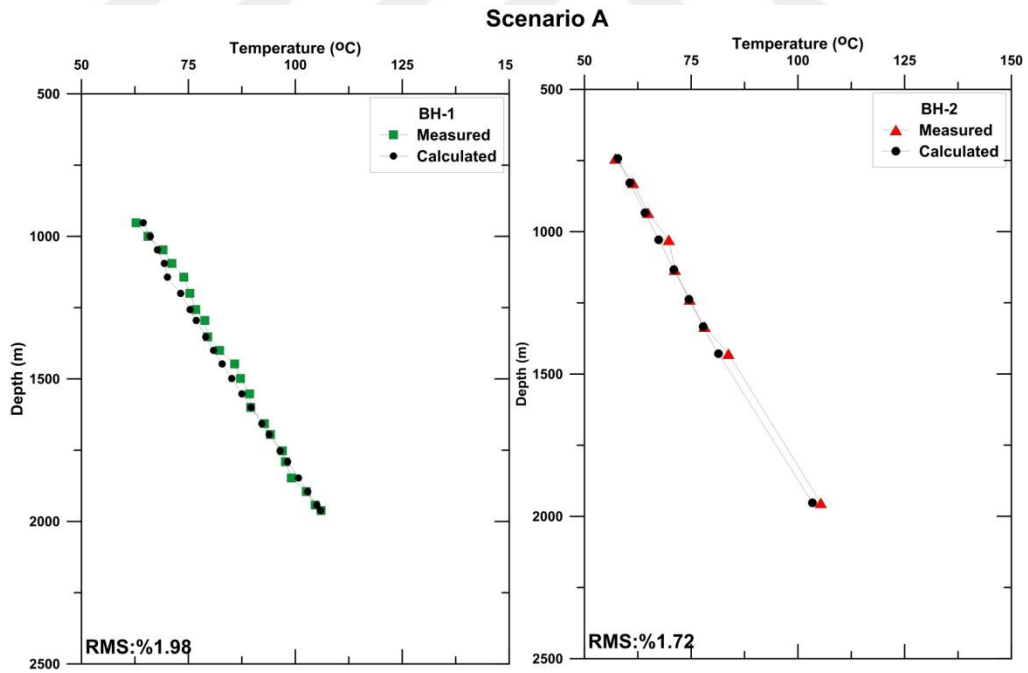


Figure 7.7 Measured and modeled temperatures for BH-1 and BH-2 with RMS values for the scenario A.

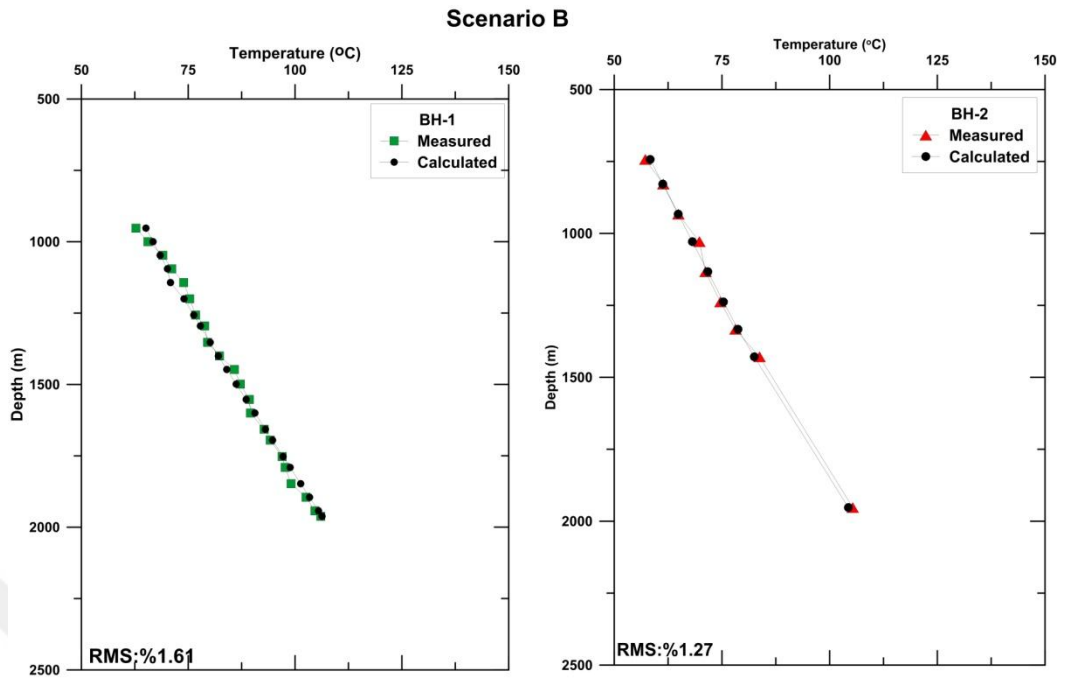


Figure 7.8 Measured and modeled temperatures for BH-1 and BH-2 with RMS values for the scenario B.

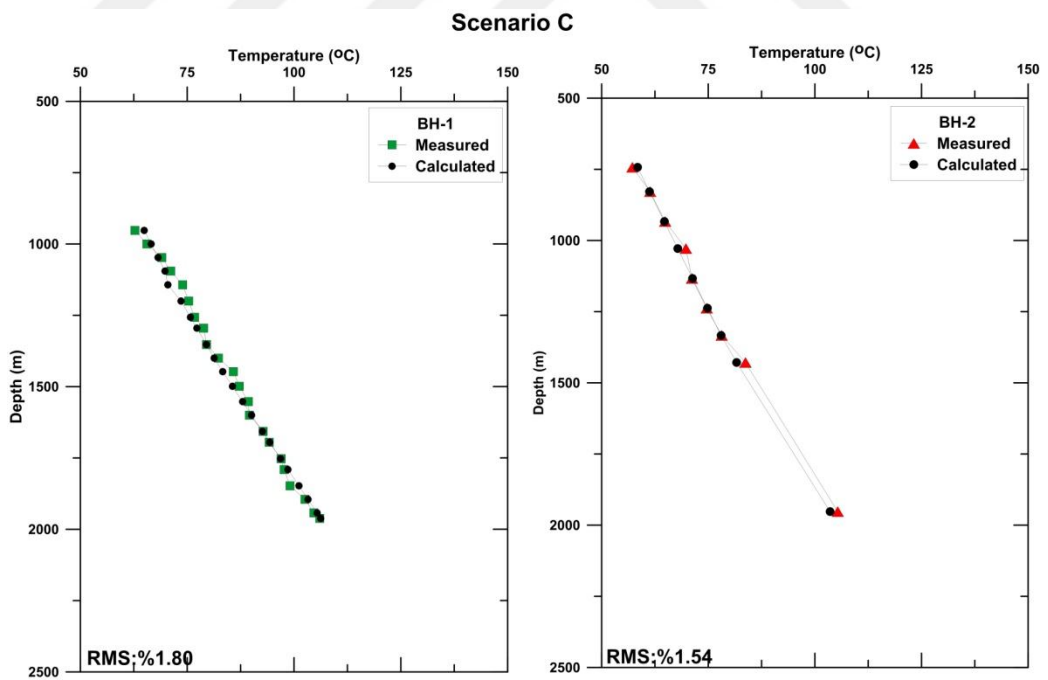


Figure 7.9 Measured and modeled temperatures for BH-1 and BH-2 with RMS values for the scenario C.

Although all scenarios give good matches, the minimum RMS errors are obtained in Scenario B. In this scenario the vertical heat flow at the bottom of the graben is 80 mWm^{-2} . This value is also in accordance with the regional heat flow value calculated in Menderes Massif (Figure 7.2). The highest temperature for the bottom of the graben is calculated in scenario A. In each case, calculated temperatures exceed the $140 \text{ }^\circ\text{C}$ at the bottom of the sedimentary fill at the depth of 3 km.

Vertical distribution of temperature within basin and range is given in Figure 7.10 for each scenario. As expected calculated temperatures increasing with depth. While slope is unique at the range, slope in the basin changes according to the thermal conductivity value of each layer.

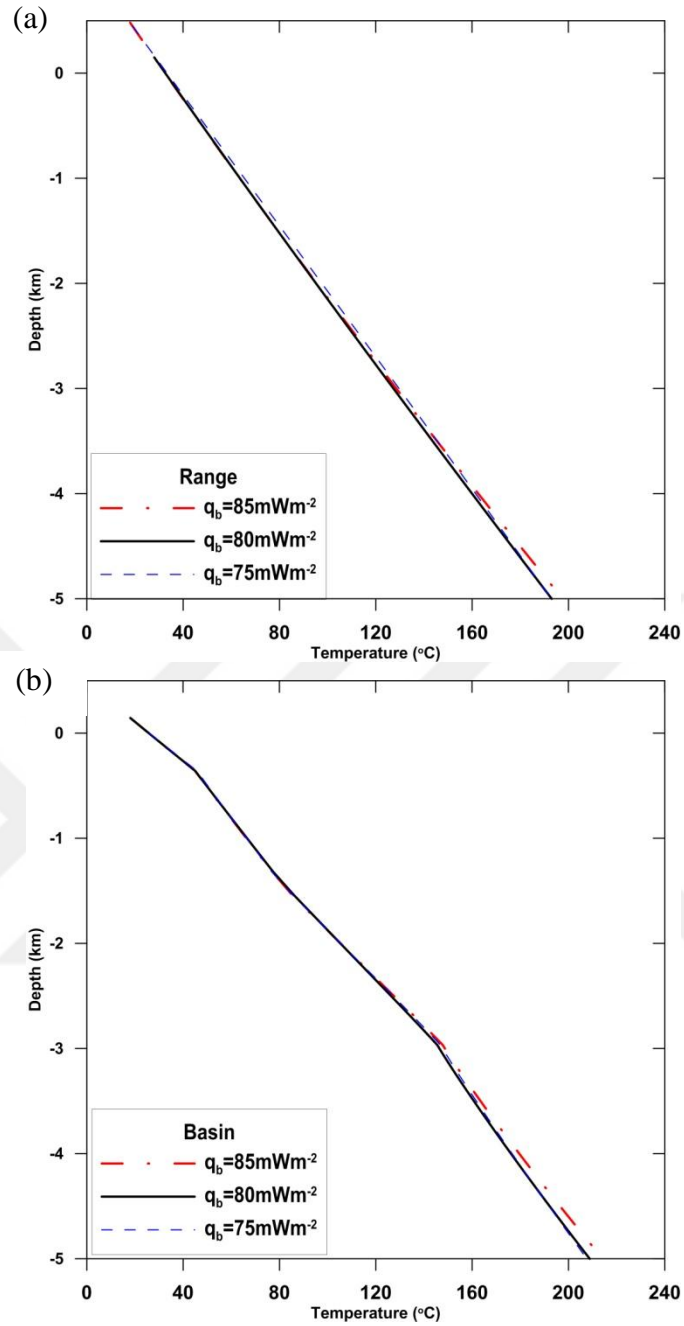


Figure 7.10 a) Vertical distributions of temperatures obtained the horizontal distance of 2 km b) Vertical distributions of temperatures obtained the horizontal distance of 11 km for each scenario.

Calculated surface heat flow of Gediz graben ranges between 70-180 mWm^{-2} in each scenario. Differences between calibrated thermal conductivity of each scenario cause to change heat flow differences within the basin. The geometry of 3km thick of basin fill results in heat refraction at the surface due to the thermal conductivity contrast between basin fill and basement rock types. Even though the heat flow at the bottom of the graben is lower than 90 mWm^{-2} , the calculated heat flow varies from 60-170 mWm^{-2} within and around the graben. The heat coming from the bottom of the graben transfers through the basement rocks with high thermal conductivity causes to high temperature at the edge of the sedimentary fill. Due to the low thermal conductivity of graben fill rocks heat cannot transfer in to the basin (Figure 11b).

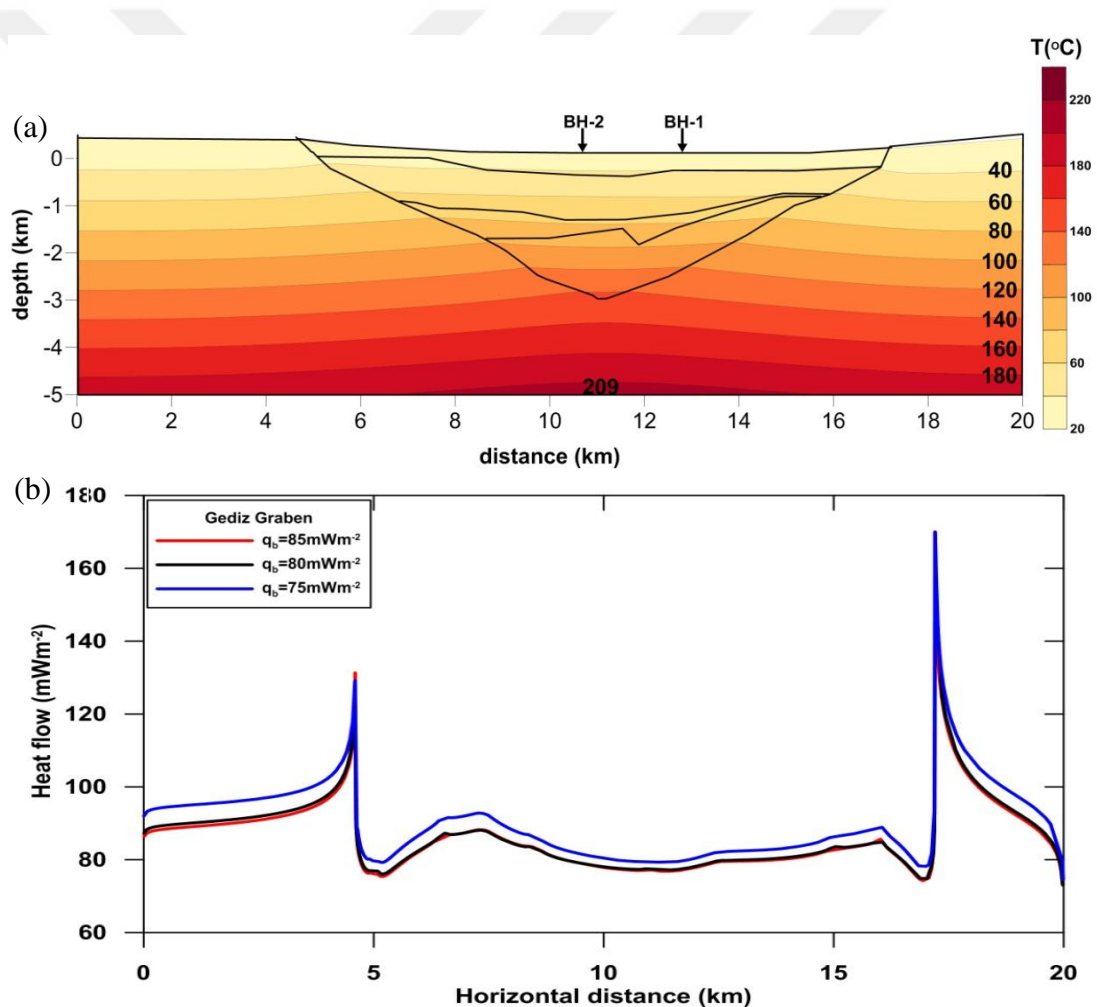


Figure 7.11 a) The calculated 2D subsurface temperature distribution for scenario (B) and b) surface heat flow variation for each scenario.

7.2.2 Thermal Model of Büyük Menderes Graben

In contrast to Gediz graben, seismic reflection data together with borehole information is limited in Büyük Menderes graben. Geological cross section based on a seismic reflection data was published by Çifçi et al. (2011). In geological cross section, Büyük Menderes graben consists of basement rock and sedimentary fill which is divided into four sub-sections in the vertical direction (Figure 7.12). According to the stratigraphic information given by Çifçi et al., (2011) sedimentary sequences I-II and III are considered as a unique unit based on thermal conductivity. For details about the geology, see the information given in Chapter 2. Thus simplified geometric model for Büyük Menderes graben is obtained as given in Figure 7.13. The concerned graben model with the 5km depth and 12 km length composes of three layers and each layer has constant thermal conductivity. Thermal conductivity of each layer is assigned according to the formation type as tabulated in Table 7.4. On the surface of the model, temperature is fixed at 18 °C, which is the annual mean temperature for the region. For the lower boundary condition, vertical heat flow at the basement of the model is assumed as 80 mWm⁻². This value is the mean heat flow value of Menderes Massif (Figure 7.2) and does not include radiogenic heat production rate. In the thermal modeling of the Büyük Menderes graben only scenario B (mean) is applied for heat production rate.

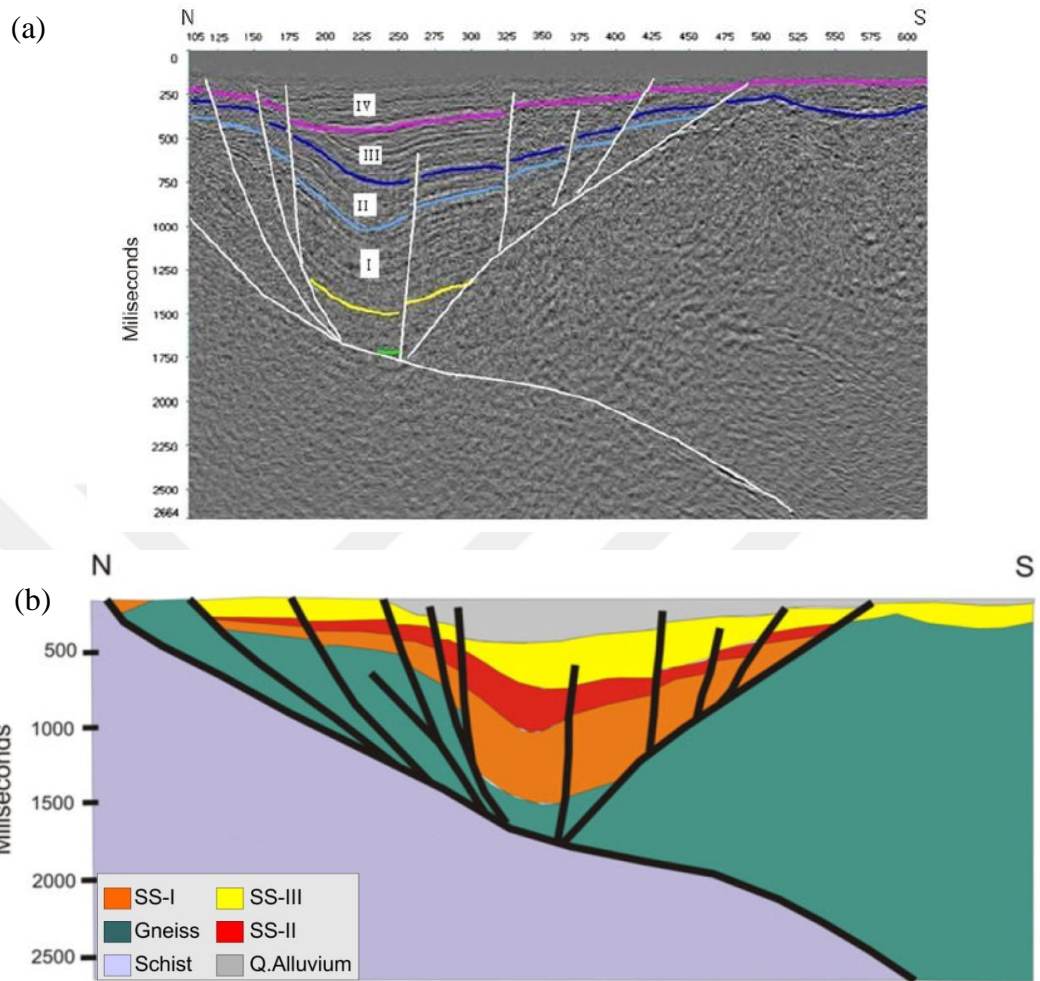


Figure 7.12 a) Interpreted seismic reflection profile b) geological cross section of Büyük Menderes (see Figure 2.11 for location of the seismic section).

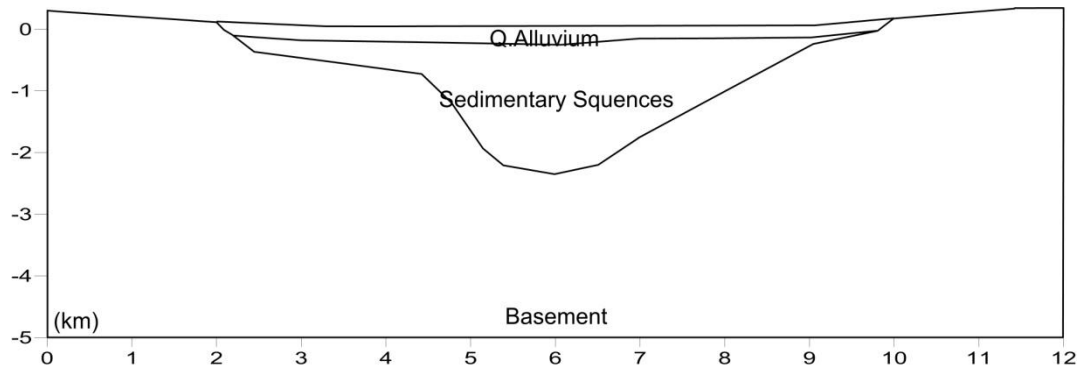


Figure 7.13 Simplified thermal model for Büyük Menderes graben.

Table 7.4 Thermal conductivity values used in Büyük Menderes graben model

<i>Dominant Lithology</i>	<i>Stratigraphic Unit</i>	λ (W/m/K)
Unconsolidated clastic rocks	Quaternary alluvium	1.50
Conglomerate-Sandstone-Mudstone	SSU-III	2.16
Sandstone-Mudstone-Conglomerate	SSU-II	2.16
Shale-Conglomerate-Sandstone-Mudstone	SSU-I	2.16
Schist-Marble-Quartzite	Basement Menderes Massif Metamorphic	3.10

7.2.2.1 Thermal Modeling Results of Büyük Menderes Graben

The 2-D subsurface temperature distribution of the Büyük Menderes graben is evaluated as given in Figure 7.14a. Unfortunately, there is no available temperature-depth log in the area. Thus accuracy of the result cannot be validated. The maximum temperature of 188 °C is calculated at the bottom of the graben. Although the heat flow at the bottom of the graben is 80 mWm⁻², it ranges between 60-180 mWm⁻² within the graben. Thermal refraction at the edges of the graben is results from the thermal conductivity contrast between sediments and basement rocks.

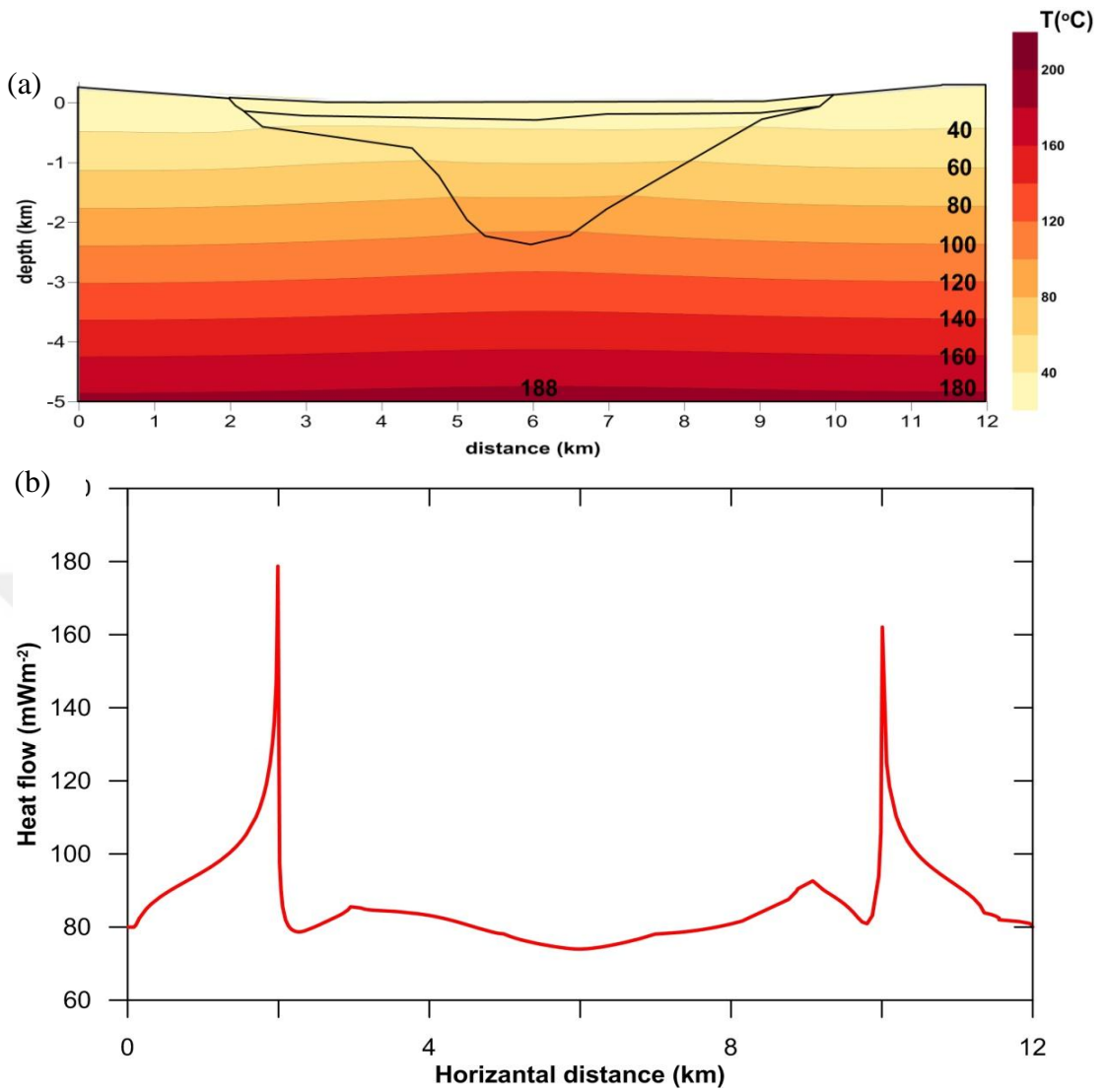


Figure 7.14 a) Calculated 2D subsurface temperature for Büyük Menderes Graben b) surface heat flow variation.

7.3 Discussion and Conclusion

Understanding thermal regime of the basins is benefited from the construction of the valuable data set using seismic and well data. In recent years, investigation of sedimentary basins has been new targets for geothermal researches (McKenna & Blackwell, 2004). Gediz and Büyük Menderes grabens have already been suggested as potential geothermal fields including reservoirs with high temperatures (Baba, 2012). However, the direct temperature measurements are rare and shallow and must therefore be extrapolated carefully. With the thermal modeling results in this thesis, high precision temperature measurements and thermal conductivity data are now available to find out temperature distribution of the study areas, which uses previously published seismic and deep-well temperature data.

Two-dimensional forward modeling technique is applied to obtain subsurface temperature and heat flow distribution of the Gediz and Büyük Menderes grabens located in western Anatolia. Scenario based analysis is used to thermal model of Gediz graben to examine different possibilities which cause the same or approximate temperature distribution. . Our results shows that high heat flow values around Gediz garben can be explained 2D steady-state conductive thermal model. The scenario B with the minimum rms errors is the best scenario that represents the present thermal statue of the Gediz graben.

Modeling results show that recent sediments in basins are regarded as thermally insulating and interpreted to warm regions. In Western Anatolia, grabens are filled with continental sediment with minor carbonates in lacustrine alluvial and fluvial environments and they are characterized with low thermal conductivity. Volcanic rocks are also important part of these sequences.. Thickness of the graben fills reaches to 3000 m meters in the middle of the basins where the temperatures of 110°C and 140 °C are calculated for Büyük Menderes and Gediz grabens respectively.

Temperature dependence of thermal conductivity may cause to remarkable thermal anomalies in sedimentary basins (Clauser & Huenges, 1995). Elevated temperatures at the bottom of the basins fill are the results of the low thermal conductivity of sediments which are already low at the surface temperature. Thermal conductivity contrast between the basement and sedimentary fill rocks is the responsible for the calculated high heat flow pattern. It is clearly seen that temperature distribution within the graben is controlled by thermal conductivity of rocks in conjunction with the RHP values and geometry of the grabens.

Some mismatches found between modeling results and measurements are to be attributed to additional heat transport by groundwater flow in the subsurface which is not taken into account in the present model. Hydro-geological effect, heterogeneities in the sedimentary sequences within the graben and locally groundwater flow existed from fault zone may disturb the temperature-depth curves. The modeling results and the comparative study with the available measurements provide us some quantitative about the surface heat flow in sedimentary basins. Therefore our findings have importance for the future modeling studies.

CHAPTER EIGHT

CONCLUSION

Thermal state of the western Turkey has been investigated in this dissertation. The lack of the systematically collected data was the main reason for limited conventional heat flow studies in the region until this thesis. Reported results in this study will provide valuable data base for future geothermic studies.

In the previous studies a constant thermal conductivity value was used in heat flow calculations because thermal conductivity values were not available for the rock types located in the study area. In this thesis thermal conductivity of ten different major rock types statistically analyzed and reported. Limestone was found the most common lithologic unit and it is analyzed together with its subunits. Statistical analyses reveals that the range of the thermal conductivity values observed for sedimentary rocks is too wide to assign a constant thermal conductivity values for heat flow and thermal modeling studies. Thermal conductivity values given in this thesis can be widely used in not only geothermic studies but also in geophysical exploration investigations.

Beside the thermal conductivity, accurate geothermal gradient determinations are vital in heat flow studies. Numerous investigations were carried to explore geothermal fields located around the western graben system. Temperature depth measurements, conducted in geothermal wells, were generally under the effect of thermal water circulation. Therefore most of them are not suitable for conductive heat flow calculations. The new geothermal gradient data set reported in this thesis yields us more detail knowledge about temperature distribution in the study area. The mean conductive geothermal gradient is evaluated as $38^{\circ}\text{Ckm}^{-1}$ for the entire study area. Additionally, the mean geothermal gradient around the Menderes Massif is computed as 40 Ckm^{-1} . The geothermal gradient distribution and contour maps are generated for the first time. The elevated geothermal gradients are observed generally within the alluvium units near the graben systems.

The preliminary heat flow map of western Turkey is updated by adding 31 new heat flow measurements. The new heat flow contour map of western Turkey implies moderate and high heat flow anomalies in the study area. The mean heat flow for the entire study area is calculated as $74 \pm 26 \text{ mWm}^{-2}$. These values are in accordance with the mean heat flow of $80 \pm 22 \text{ mWm}^{-2}$ measured in the Aegean Sea. The new heat flow data have added to our knowledge of geologic regions particularly in Gediz graben. The maximum heat value is evaluated in the intersection point of the Büyük Menderes and Gediz grabens. Regional tectonic and high heat production rate in Menderes Massif is probably the main reason for this high value but for more realistic interpretation new data points are required. The second high heat flow anomaly around the Kula is observed in more than one data point supporting each others. Rapid uplift of the mantle causes to high temperature around the Kula basalts. Moderate values are observed in the central part of Manisa Balıkesir and Çanakkale. In Manisa, absence of any hot spring in the area supports these moderate values. Regional hydrologic effects explain the moderate values of in Balıkesir. But in Çanakkale, although there are many hot springs in the area and the western part is represented with high values, central part of the province shows moderate heat flow anomaly. T-D measurements from deep wells can provide us to make more detail interpretation for the region.

2D numerical temperature models have been developed for Gediz and Büyük Menderes grabens. The forward modeling approach is novel as it is performed for the first time a comprehensive investigation of high precision T-D data. Our results shows that relatively high heat flow values around Gediz graben may be explained by 2D steady-state conductive thermal modeling. According to the results, temperature distribution within the graben is mainly controlled by sedimentary fill with low thermal conductivity. The insulating effects of the entire sediment fill results in a long-wavelength variation of temperatures in response to heat refraction effects caused by the contrast between insulating sedimentary rocks and highly conductive basement metamorphics. We concluded the maximum temperature at the

base of the sedimentary fills reaches to 140 °C in Gediz graben and to 110 °C in Büyük Menderes graben.

In addition, the silica heat flow map of western Turkey is updated by adding new chemical data obtained from Inventory of Turkey Geothermal Resources (Akkuş et al., 2005). The new map includes more detailed anomalies which suggest that highest heat flow value of 301 mWm⁻² is calculated in Kızıldere geothermal field. Additionally, in Gediz graben the value of 265 mWm⁻² is calculated for the Kurşunlu. These values extremely higher than world average heat flow value calculated by conventional method. Geothermometers are the empiric equations and they are the indicators of the possible geothermal fields where the heat mainly transport by convection.

8.1 Future Research Recommendations

This study may be extended in the following ways:

- New thermal conductivity measurement of the rock types which are not reported in this dissertation may increase the thermal conductivity data set for the study area. Thermal conductivity measurements of rocks collected from drill core instead of outcrops may give more realistic heat flow determinations.
- T-D measurements collected from the regions with rare density may increases our understanding of the thermal regime of western Turkey.
- T-D measurements from deep boreholes should be used for validating temperature distribution within the Büyük Menderes graben.

REFERENCES

- Ahlatçı, B. (2005). *Türkiye’de yüzeyden ısı enerji boşalımı ve ısı akısının alansal ve stratigrafik litoloji dağılımına bağlı olarak kestirimi*. Graduation Thesis, Istanbul Technical University, Istanbul.
- Akar, S., Atalay, O., Kuyumcu, Ç., Solaroğlu, D. U., Çolpan, B., & Arzuman, S. (2011). 3D Subsurface modeling of Gümüşköy geothermal area, Aydın, Turkey. *Geothermal Resources Council Transactions*, 35, 669-676.
- Akçığ, Z. (1983). *Batı Anadolu Gravite verilerinin veri işlem yöntemleri ile yorumu*. PhD Thesis, Dokuz Eylül University, İzmir
- Akın, U., & Çiftçi, Y. (2011). Kırşehir masifi'nin ısı akısı ve radyojenik ısı üretiminin jeolojik kaynakları. *MTA Dergisi*, 143, 53-73.
- Akın, U., Ulugergerli, E.U, & Kutlu, S. (2014). The assessment of geothermal potential of Turkey by means of heat flow estimation. *Bulletin of the Mineral Research and Exploration*, 149, 201-210.
- Akkuş, İ., Akıllı, H., Ceyhan, S., Dilemre, A., & Tekin, Z. (2005). *Türkiye jeotermal kaynakları envanteri*. Ankara: Maden Tetkik ve Arama Genel Müdürlüğü.
- Akyol, N., Zhu, L., Mitchell, B. J., Sözbilir, H., & Kekovalı, K. (2006). Crustal structure and local seismicity in western Anatolia. *Geophysical Journal International*, 166(3), 1259-1269.
- Alptekin, Ö., İlkışık, O.,M., Ezen, U., & Ucer, S. B. (1990). Heat flow, seismicity, and the crustal structure of western Anatolia. *International Earth Sciences Congress on Aegean Region: Proceedings, II*, 1-12
- Arnórsson, S. (2000). *Isotopic and chemical techniques in geothermal exploration, development and use: sampling methods, data handling, interpretation*. Vienna:International Atomic Energy Agency.

- Arnórsson, S., Gunnlaugsson, E., & Svavarsson, H. (1983). The chemistry of geothermal waters in Iceland. III. Chemical geothermometry in geothermal investigations. *Geochimica et Cosmochimica Acta*, 47(3), 567-577.
- Ates, A., Bilim, F., & Buyuksarac, A. (2005). Curie point depth investigation of Central Anatolia, Turkey. *Pure and Applied Geophysics*, 162(2), 357-371.
- Aydın, İ., Karat, H.İ., & Koçak, A. (2005). Curie-point depth map of Turkey. *Geophysical Journal International*, 162, 633-460.
- Baba, A. (2012). Present energy status and geothermal utilization in Turkey. The *Congress of the International Association of Hydrogeologists*, 401.
- Baba, A., Bundschuh, J., & Chandrasekaram, D. (Ed.). (2014). *Geothermal systems and energy resources: Turkey and Greece*. London: CRC Press.
- Baeyens, B., & Bradbury, M. H. (1994). *Physico-chemical characterisation and calculated in situ porewater chemistries for a low permeability Palfris marl sample from Wellenberg*. Retrieved October 10, 2015 from [http://www.nagra.ch/data/documents/database/dokumente/\\$default/Default%20Folder/Publikationen/NTBs%201994-2000/e_ntb94-22.pdf](http://www.nagra.ch/data/documents/database/dokumente/$default/Default%20Folder/Publikationen/NTBs%201994-2000/e_ntb94-22.pdf)
- Balkan, E., Erkan, K., & Salk, M., (2017). Thermal conductivity of major rock types in western and central Anatolia regions, Turkey. *Journal of Geophysics and Engineering*, (in Press).
- Balkan, E., & Salk, M., (2014). 2D Refraction of heat flow in Gediz graben Turkey. *European Geosciences Union General Assembly Conference*, 16, 765.
- Başel, E. D. K., Serpen, U., & Satman, A. (2008). Geothermal potentials of the fields utilized for district heating systems in Turkey. *New Zealand Geothermal Workshop & New Zealand Geothermal Association Seminar*, 11-13.

- Başel, E. D. K., Serpen, U. & Satman, A. (2010). Turkey's geothermal energy potential: updated results. *Proceedings Thirty-Fifth Workshop on Geothermal Reservoir Engineering*, 1-3.
- Bayrak, Y., & Bayrak, E. (2012). Regional variations and correlations of Gutenberg–Richter parameters and fractal dimension for the different seismogenic zones in Western Anatolia. *Journal of Asian Earth Sciences*, 58, 98-107.
- Beardsmore, G. R., & Cull, J. P. (2001). *Crustal heat flow: a guide to measurement and modeling*. New York: Cambridge University Press.
- Bektaş, Ö., Ravat, D., Büyüksaraç, A., Bilim, F., & Ateş, A. (2007). Regional geothermal characterisation of East Anatolia from aeromagnetic, heat flow and gravity data. *Pure and Applied Geophysics*, 164(5), 975-998.
- Blackwell, D. D. (1983). Heat flow in the northern Basin and Range province. *Geothermal Resources Council Special Report*, 13, 81-92.
- Bhattacharyya, B. K. (1965). Two-dimensional harmonic analysis as a tool for magnetic interpretation. *Geophysics*, 30(5), 829-857.
- Bhattacharyya, B. K. (1966). Continuous spectrum of the total-magnetic-field anomaly due to a rectangular prismatic body. *Geophysics*, 31(1), 97-121.
- Birch, A. F., & Clark, H. (1940). The thermal conductivity of rocks and its dependence upon temperature and composition. *American Journal of Science*, 238(8), 529-558.
- Birch, F., Roy, R. F., & Decker, E. R. (1968). Heat flow and thermal history in New England and New York. *Studies of Appalachian Geology*, 437-451.
- Blackwell, D. D., Bowen, R. G., Hull, D. A., Riccio, J., & Steele, J. L. (1982). Heat flow, arc volcanism, and subduction in northern Oregon. *Journal of Geophysical Research: Solid Earth*, 87, 8735-8754.

- Blackwell, D. D., & Priest, G. R. (1996). Comment [on “Rates and patterns of groundwater flow in the Cascade Range volcanic arc and the effect on subsurface temperatures” by SE Ingebritsen, DR Sherrod, and RH Mariner]. *Journal of Geophysical Research: Solid Earth*, 101(B8), 17561-17568.
- Blackwell, D. D., & Steele, J. L. (1989). Thermal conductivity of sedimentary rocks: measurement and significance. In *Thermal history of sedimentary basins* (13-36). New York: Springer.
- Bozkurt, E. (2000). Timing of extension on the Büyük Menderes Graben, Western Turkey and its tectonic implications. In: Bozkurt, E. Winchester, J.A. & Piper J.A.D. (eds), tectonics and magmatism in Turkey and the surrounding area. *Journal of Geological Society of London*, 173, 385–403.
- Bozkurt, E. (2001). Neotectonics of Turkey—a synthesis. *Geodinamica Acta*, 14, 3–30.
- Bozkurt, E. (2003). Origin of NE-trending basins in western Turkey. *Geodinamica Acta*, 16, 61–81.
- Bozkurt, E., & Sözbilir, H. (2004). Tectonic evolution of the Gediz Graben: Field evidence for an episodic, two stage extension in western Turkey. *Geological Magazine*, 141, 63–79.
- Bozkurt, E., & Park, R.G. (1994). Southern Menderes Massif-an incipient Metamorphic Core Complex in Western Anatolia, Turkey. *Journal of Geological Society of London*, 151, 213–216.
- Bridgman, P. W. (1922). The effect of pressure on the thermal conductivity of metals. *Proceedings of the American Academy of Arts and Sciences*, 57(5), 77-127.
- Brigaud, F., Chapman, D. S., & Le Douaran, S. (1990). Estimating thermal conductivity in sedimentary basins using lithologic data and geophysical well Logs (1). *American Association of Petroleum Geologists Bulletin*, 74(9), 1459-1477.

- Brigaud, F., & Vasseur, G. (1989). Mineralogy, porosity and fluid control on thermal conductivity of sedimentary rocks. *Geophysical Journal International*, 98(3), 525-542.
- Brigaud, F., Vasseur, G., & Caillet, G. (1992). Thermal state in the north Viking Graben (North Sea) determined from oil exploration well data. *Geophysics*, 57(1), 69-88.
- Can, I., (2002). A new improved Na/K geothermometers by artificial neural networks. *Geothermics*, 31(6), 751–760.
- Catlos, E.J., & Çemen, İ. (2005). Monazite ages and rapid exhumation of the Menderes Massif, western Turkey. *International Journal of Earth Sciences*, 94, 204–217.
- Cermak, V., Hurting E., Kutas, R.L., Lodo, M., Lubimova, E.A., Mongelli, F., Morgan, P., Smimov, Ya.B., & Tezcan, A.K. (1977). Heat flow map of Southern Europe and Mediterranean Region. *Proceeding International Congress On Thermal Waters, Geothermal Energy and Volcanism of Mediterranean Area*, 149-168.
- Cermak, V., & Rybach, L. (1979). *Terrestrial heat flow in Europe*. Berlin: Springer Verlag.
- Cermak, V., & Rybach, L. (1982). Thermal conductivity and specific heat of minerals and rocks. *Landolt-Bornstein; Zahlenwerte und Funktionen aus Naturwissenschaften und Technik*, 305-343.
- Chapman, D. S., Keho, T. H., Bauer, M. S., & Picard, M. D. (1984). Heat flow in the Uinta Basin determined from bottom hole temperature (BHT) data. *Geophysics*, 49(4), 453-466.
- Clark, S. P. (1966). Section 21: thermal conductivity. *Geological Society of America Memoirs*, 97, 459-482.

- Clauser, C., & Huenges, E. (1995). Thermal conductivity of rocks and minerals. In *Rock physics & phase relations: a handbook of physical constants* (105-126). Chicago: American Geophysical Union.
- Clauser, C. (2006). Geothermal energy. *Landolt-Börnstein, group VIII: advanced materials and technologies*, 3, 493-604.
- Clough, R. W. (1960). The finite element analysis in plane stress analysis. *Proceeding American Society of Civil Engineers Conference on Electronic Computation*.
- Cohen, H. A., Dart, C. J., Akyüz, H. S., & Barka, A. (1995). Syn-rift sedimentation and structural development of the Gediz and Büyük Menderes graben, western Turkey. *Journal of the Geological Society*, 152(4), 629-638.
- Çağlar, K. Ö. (1961). *Türkiye maden suları ve kaplıcaları*. Maden Tetkik ve Arama Enstitüsü Yayınları, Seri B, (no:11), Ankara.
- Çağlar, M. (1965). Chiropterenfauna der Türkei. *İstanbul Üniversitesi Fen Fakültesi Mecmuaları Seri B*, 30, 125-134.
- Çanakcı, H., Demirboğa, R., Karakoç, M. B., & Şirin, O. (2007). Thermal conductivity of limestone from Gaziantep (Turkey). *Building and Environment*, 42(4), 1777-1782.
- Çemen, İ., Catlos, E.J., Göğüş, O., & Özerdem, C. (2006). Postcollisional extensional tectonics and exhumation of the Menderes Massif in Western Anatolia extended terrane, Turkey. *Geological Society of America Special Publication*, 409, 353-379.
- Çemen, İ., Göncüoğlu, C., & Dirik, K. (1999). Structural evolution of the Tuzgölü Basin in Central Anatolia, Turkey. *Journal of Geology*, 107, 693-706.
- Çemen, I., Helvacı, C., & Ersoy, E. Y. (2014). Cenozoic extensional tectonics in western and central Anatolia, Turkey: Introduction. *Tectonophysics*, 635, 1-5.

- Çiftçi, G., Pamukçu, O., Çoruh, C., Çopur, S., & Sözbilir, H. (2011). Shallow and deep structure of a supradetachment basin based on geological, conventional deep seismic reflection sections and gravity data in the Büyük Menderes Graben, western Anatolia. *Surveys in Geophysics*, 32(3), 271-290.
- Çiftçi, N. B., & Bozkurt, E. (2009a). Evolution of the Miocene sedimentary fill of the Gediz Graben, SW Turkey. *Sedimentary Geology*, 216(3), 49-79.
- Çiftçi, N. B., & Bozkurt, E. (2009b). Pattern of normal faulting in the Gediz Graben, SW Turkey. *Tectonophysics*, 473(1), 234-260.
- Çiftçi, N. B., & Bozkurt, E. (2010). Structural evolution of the Gediz Graben, SW Turkey: temporal and spatial variation of the graben basin. *Basin Research*, 22(6), 846-873.
- Çiftçi, N. B., Temel, R. O., & İztan, Y. H. (2010). Hydrocarbon occurrences in the western Anatolian (Aegean) grabens, Turkey: Is there a working petroleum system?. *American Association of Petroleum Geologists Bulletin*, 94(12), 1827-1857.
- Çiftçi, N. B., Temel, R. O., & Terzioğlu, N. M. (2004). Neogene stratigraphy and hydrocarbon system of the region surrounding the Gulf of Edremit, NW Anatolia, Turkey. *Bulletin of Turkish Association of Petroleum Geologists*, 16, 81-104.
- D'Amore, F., & Arnórsson, S. (2000). *Geothermometry*. In *Isotopic and chemical techniques in geothermal exploration, development and use* (152-199). Vienna: International Atomic Energy Agency.
- Davies, J. H., & Davies, D. R. (2010). Earth's surface heat flux. *Solid Earth*, 1(1), 5.
- Demirboğa, R. (2003). Influence of mineral admixtures on thermal conductivity and compressive strength of mortar. *Energy and Buildings*, 35(2), 189-192.

- Demirel, Z., & Sentürk, N. (1996). Geology and hydrogeology of deep thermal aquifers in Turkey. *Proceeding of the Regional Seminar on Integration of Information Between Oil Drilling and Hydrogeology of Deep Aquifers*, 38.
- Dewey, J.F., & Şengör, A.M.C. (1979). Aegean and surrounding regions: complex multiple and continuum tectonics in a convergent zone. *Geological Society of America Bulletin* 90, 84–92.
- Díaz-González, L., Santoyo, E., & Reyes-Reyes, J. (2008). Tres nuevos geotermómetros mejorados de Na/K usando herramientas computacionales y geoquimiométricas: aplicación a la predicción de temperaturas de sistemas geotérmicos. *Revista Mexicana de Ciencias Geológicas*, 25(3), 465-482.
- Dolmaz, M.N., Hisarli, Z.M., Ustaömer, T., & Orbay, N. (2005a). Curie point depths based on spectrum analysis of aeromagnetic data, western Anatolian province, Turkey. *Pure and Applied Geophysics*, 162, 571-590.
- Dolmaz, M. N., Ustaömer, T., Hisarli, Z. M., & Orbay, N. (2005b). Curie point depth variations to infer thermal structure of the crust at the African-Eurasian convergence zone, SW Turkey. *Earth, Planets and Space*, 57(5), 373-383.
- Drury, M. J., & Jessop, A. M. (1983). The estimation of rock thermal conductivity from mineral content: an assessment of techniques. *Zentralblatt für Geologie und Palaeontologie*, 1, 35-48.
- Emre, T. (1996). Geology and tectonics of the Gediz graben. *Turkish Journal of Earth Science*, 5, 171–185.
- Emre, T., & Sözbilir, H. (1997). Field evidence for metamorphic core complex, detachment faulting and accommodation faults in the Gediz and Büyük Menderes grabens, western Anatolia. *International Earth Sciences Colloquium on the Aegean Region*, 73-93.
- Eckstein, Y. (1978). Review of heat flow data from the eastern Mediterranean region. *Pure and Applied Geophysics*, 117, 150-159.

- Erickson, A.J. (1970). *The measurement and interpretation of the heat flow in the Mediterranean and Black Seas*. Ph.D. Thesis, Massachusetts Institute of Technology, Boston.
- Erkan, K. (2015). Geothermal investigations in western Anatolia using equilibrium temperatures from shallow boreholes. *Solid Earth*, 6, 103-113.
- Erkan, K., & Blackwell, D. D. (2008). A thermal test of the post-subduction tectonic evolution along the California transform margin. *Geophysical Research Letters*, 35(7).
- Erkan, K., Doğruel, M., Bayat, K., Akkoyunlu, B., Tayanc, M., Balkan, E., & Hamamci, S. (2015). Development of a digital output temperature probe for precision measurements. *Geothermal Resources Council Annual Meeting*, Nevada, USA.
- Ersoy, E. Y., Çemen, İ., Helvacı, C., & Billor, Z. (2014). Tectono-stratigraphy of the Neogene basins in Western Turkey: Implications for tectonic evolution of the Aegean Extended Region. *Tectonophysics*, 635, 33-58.
- Fouillac, C., Michard, G. (1981). Sodium/lithium ratio in water applied to geothermometry of geothermal reservoirs. *Geothermics*, 10, 55–70.
- Fournier, R. O. (1977). Chemical geothermometers and mixing models for geothermal systems. *Geothermics*, 5(1), 41-50.
- Fournier, R. O. (1979). A revised equation for the Na/K geothermometer. *Geothermal Resources Council Transactions*, 3, 221-224.
- Fournier, R. O. (1989). Geochemistry and dynamics of the Yellowstone National Park hydrothermal system. *Annual Review of Earth and Planetary Sciences*, 17(1), 13-53.
- Fournier, R. O. (1991). Water geothermometers applied to geothermal energy. *Application of Geochemistry in Geothermal Reservoir Development*, 37-69.

- Fournier, R. O., & Potter, R. W. (1982). Revised and expanded silica (quartz) geothermometer. *Bulletin of Geothermal Resource Council*, 11(10).
- Fournier, R. O., & Truesdell, A. H. (1973). An empirical Na-K-Ca geothermometer for natural waters. *Geochimica et Cosmochimica Acta*, 37(5), 1255-1275.
- Fowler, C. M. R. (1990). Heat. In *The solid earth: an introduction to global geophysics* (2nd ed.) (269-325). Cambridge:Cambridge University Press.
- Förster, A., Schrötter, J., Merriam, D. F., & Blackwell, D. D. (1997). Application of optical-fiber temperature logging-An example in a sedimentary environment. *Geophysics*, 62(4), 1107-1113.
- Fuchs, S., Schütz, F., Förster, H. J., & Förster, A. (2013). Evaluation of common mixing models for calculating bulk thermal conductivity of sedimentary rocks: correction charts and new conversion equations. *Geothermics*, 47, 40-52.
- Funnell, R., Chapman, D., Allis, R., & Armstrong, P. (1996). Thermal state of the Taranaki basin, New Zealand. *Journal of Geophysical Research: Solid Earth*, 101(B11), 25197-25215.
- Fytikas, M. D. (1980). Geothermal exploitation in Greece. *Proceeding of the second International Seminar on the results of E.C. Geothermal Energy Research*. Strazbourg, France.
- Fytikas, M., Innocenti, F., Manetti, P., Peccerillo, A., Mazzuoli, R., & Villari, L. (1984). Tertiary to Quaternary evolution of volcanism in the Aegean region. *Geological Society, London, Special Publications*, 17(1), 687-699.
- Gessner, K., Gallardo, L.A., Markwitz, V., Ring, U., & Thomson, S.N. (2013). What caused the denudation of the Menderes Massif: Review of crustal evolution, lithosphere structure, and dynamic topography in southwest Turkey. *Gondwana Research*, 24, 243–274.

- Gessner, K., Ring, U., Johnson, C., Hetzel, R., Passchier, C. W., & Güngör, T. (2001). An active bivergent rolling-hinge detachment system: Central Menderes metamorphic core complex in western Turkey. *Geology*, 29(7), 611-614.
- Giggenbach, W. F. (1988). Geothermal solute equilibria. derivation of Na-K-Mg-Ca geoindicators. *Geochimica et Cosmochimica Acta*, 52(12), 2749-2765.
- Göktürkler, G., Sarı, C., & Şalk, M. (2003). Numerical modeling of the conductive heat transfer in western Anatolia. *Journal of Balkan Geophysical Society*, 6, 1-15.
- Görür, N., Şengör, A.M.C., Sakıncı, M., Tüysüz, O., Akkök, R., Yiğitbaş, E., et al. (1995). Rift formation in the Gökova region, southwest Anatolia: implications for the opening of the Aegean Sea. *Geological Magazine*, 132, 637-650.
- Gretener, P. E. (1981). *Geothermics: Using temperature in hydrocarbon exploration: AAPG Education Course Note Series 17*. Tulsa: American Association of Petroleum Geologist.
- Grubbe, K., Haenel, R., & Zoth, G. (1983). Determination of the vertical component of thermal conductivity by line source methods. *Zentralblatt für Geologie und Paläontologie*, 1, 49-56.
- Güngör, T., & Erdoğan, B. (2002). Tectonic significance of mafic volcanic rocks in a Mesozoic sequence of the Menderes Massif, West Turkey. *International Journal of Earth Sciences*, 91, 386-397.
- Gürer, F. Ö., Bozcu, M., Yılmaz, K., & Yılmaz, Y. (2001). Neogene basin development around Söke-Kuşadası (western Anatolia) and its bearing on tectonic development of the Aegean region. *Geodinamica Acta*, 14(1-3), 57-69.
- Gürer, A., Pinçe, A., Gürer, Ö. F., & İlkışık, O. M. (2002). Resistivity distribution in the Gediz Graben and its implications for crustal structure. *Turkish Journal of Earth Sciences*, 11(1), 15-25.

- Gürer, Ö. F., Sarica-Filoreau, N., Özbüran, M., Sangu, E., & Doğan, B. (2009). Progressive development of the Büyük Menderes Graben based on new data, western Turkey. *Geological Magazine*, 146(05), 652-673.
- Hetzl, R., Passchier, C. W., Ring, U., & Dora, Ö. O. (1995a). Bivergent extension in orogenic belts: the Menderes massif (southwestern Turkey). *Geology*, 23(5), 455-458.
- Hetzl, R., Ring, U., Akal, C., & Troesch, M. (1995b). Miocene NNE-directed extensional unroofing in the Menderes Massif, southwestern Turkey. *Journal of the Geological Society*, 152(4), 639-654
- Hisarlı, M. (1995). Edremit-Susurluk bölgesinin Cuire nokta derinliklerinin saptanması. *Jeofizik Dergisi*, 9(1), 117-117.
- Hou, Z., Şen, O., Gou, Y., Eker, A. M., Li, M., Yal, G. P., et al., (2015). Preliminary geological, geochemical and numerical study on the first EGS project in Turkey. *Environmental Earth Sciences*, 73(11), 6747-6767.
- Hurtig, E., Cermak, V., Haenel, R., & Zui, V. (1992). *Geothermal atlas of Europe*. Gotha:Haack.
- Innocenti, F., Agostini, S., Di Vincenzo, G., Doglioni, C., Manetti, P., Savaşçın, M. Y., & Tonarini, S. (2005). Neogene and Quaternary volcanism in Western Anatolia: magma sources and geodynamic evolution. *Marine Geology*, 221(1), 397-421.
- Işık, V., & Tekeli, O. (2001). Late orogenic crustal extension in the northern Menderes Massif (Western Turkey); evidence for metamorphic core complex formation. *International Journal of Earth Science*, 89, 757-765.
- Işık, V., Seyitoğlu, G., & Çemen, İ. (2003). Ductile–brittle transition along the Alaşehir detachment fault and its structural relationship with the Simav detachment fault, Menderes massif, western Turkey. *Tectonophysics*, 374(1), 1-18.

- İlkışık, O.M. (1989). Kuzeybatı Anadolu'da ısı akısı dağılımı. *Jeofizik*, 3, 83-91.
- İlkışık, O. M., Yalçın, M. N., Sari, C., Okay, N., Bayrak, M., Öztürk, S., Sener, Ç., Yenigün, H. M., Yemen, H., Sözen, I., & Karamanderesi, I. H. (1996a). *Ege bölgesi'nde ısı akısı arařtırmaları*, TÜBİTAK Proje No: YDABÇAG-233/G, Ankara.
- İlkışık, O. M., Sari, C., Bayrak, M., Öztürk, S., Sener, Ç., Yenigün, H. M., & Karamanderesi, I. H. (1996b). *Ege bölgesinde jeotermik arařtırmalar*, TÜBİTAK, Proje No: YDABÇAG-430/G, Ankara.
- İlkışık, O.M. (1995). Regional heat flow in western Anatolia using silica temperature from thermal springs. *Tectonophysics*, 244, 175-184.
- İztan, H., & Yazman, M. (1990). Geology and hydrocarbon potential of the Alaşehir (Manisa) area, western Turkey. *Proceedings of International Earth Sciences Congress, Aegean Region*, 327-333.
- İztan, H., & Yazman, M. K., (1991). *Alaşehir (Manisa) Bölgesinin jeolojisi ve hidrokarbon olanakları*. Technical report (unpublished), Türkiye Petrolleri Anonim Ortaklığı.
- Jaeger, J. C. (1965). Application of the theory of heat conduction to geothermal measurements. In *Terrestrial Heat Flow* (7-23). Washington: American Geophysical Union.
- Jaupart, C., Labrosse, S., & Mareschal, J. C. (2007). Temperatures, heat and energy in the mantle of the earth. *Treatise on Geophysics*, 7, 223-270.
- Jaupart, C., & Mareschal, J. C. (2007). Heat flow and thermal structure of the lithosphere. In *Treatise on Geophysics*. (217-251). Holland: Elsevier.
- JICA (1987). *The pre-feasibility study on the Dikili-Bergama geothermal development project*. Final Report, Japan International Cooperation Agency.

- Jolivet, L. & Brun, J. P. (2010). Cenozoic geodynamic evolution of the Aegean. *International Journal of Earth Science*, 99, 109–138.
- Jolivet, L., Faccenna, C., Huet, B., Labrousse, L., Le Pourhiet, L., Lacombe, O., et al. (2013). Aegean tectonics: Strain localization, slab tearing and trench retreat. *Tectonophysics*, 597–598, 1–33.
- Jongsma, D. (1974). Heat flow in the Aegean Sea. *Geophysical Journal of the Royal Astronomical Society*, 37, 337-346.
- Kalyoncuoglu, U. Y., Elitok, Ö., & Dolmaz, M. N. (2013). Tectonic implications of spatial variation of b-values and heat flow in the Aegean region. *Marine Geophysical Research*, 34(1), 59-78.
- KamLAND Collaboration. (2011). Partial radiogenic heat model for Earth revealed by geoneutrino measurements. *Nature Geoscience*, 4(9), 647-651.
- Kappelmeyer, O., & Haenel, R. (1974). *Geothermics with special reference to application*. Berlin:Gebrueder Borntraeger Geoexploration Monographs Series.
- Karakuş, H., & Şimşek, Ş. (2012). Spatial variations of carbon and Helium isotope ratios in geothermal fluids of Buyuk Menderes Graben. *5th Geochemistry Symposium*, 82–83.
- Karakuş, H., (2013). Tracing deep thermal water circulation systems in the E–W trending Büyük Menderes Graben, western Turkey. *Journal of Volcanology and Geothermal Research*, 252, 38-52.
- Karingithi, C. W. (2009). Chemical geothermometers for geothermal exploration. *Short Course IV on Exploration for Geothermal Resources: United Nations University, Geothermal Training Program*, 1-22.
- Karlı R., Öztürk, S. & Destur, M. (2006). *Türkiye ısı akısı haritası projesi raporu*. (Rapor No: 10937) (yayımlanmamış), Maden Tetkik ve Arama Genel Müdürlüğü, Ankara.

- Katsumata, K. (2006). Imaging the high b-value anomalies within the subducting Pacific plate in the Hokkaido corner. *Earth, Planets and Space*, 58(11), 49-52.
- Kharaka, Y. K., Lico, M. S., & Law, L. M. (1982). Chemical geothermometers applied to formation waters, Gulf of Mexico and California Basins: Abstract. *American Association of Petroleum Geologists Bulletin*, 66(5), 588-588.
- Kharaka, Y. K., & Mariner, R. H. (1989). Chemical geothermometers and their application to formation waters from sedimentary basins. In *Thermal history of sedimentary basins* (99-117). New York: Springer.
- Koçyiğit, A., Yusufoglu, H., & Bozkurt, E. (1999). Evidence from the Gediz graben for episodic two-stage extension in Western Turkey. *Journal of Geological Society of London*, 156, 605–616.
- Koçyiğit, A. (2005). The Denizli graben-horst system and the eastern limit of western Anatolian continental extension: basin fill, structure, deformational mode, throw amount and episodic evolutionary history, SW Turkey. *Geodinamica Acta*, 18(3), 167–208.
- Korkmaz, E. D., Serpen, U., & Satman, A. (2014). Geothermal boom in Turkey: Growth in identified capacities and potentials. *Renewable Energy*, 68, 314-325.
- Kreith, F., Manglik, R. M., & Bohn, M. S. (2012). Heat conduction. In *Principles of heat transfer*. (7th ed.) (70-165). Stanford: Cengage Learning.
- Kreith, F., Manglik, R. M., & Bohn, M. S. (2012). Numerical analysis of heat conduction. In *Principles of heat transfer*. (7th ed.) (70-165). Stanford: Cengage Learning.
- Kukkonen, I. T., & Jöeleht, A. (1996). Geothermal modelling of the lithosphere in the central Baltic Shield and its southern slope. *Tectonophysics*, 255(1), 25-45.

- Kukkonen, I., & Lindberg, A. (1998). *Thermal properties of rocks at the investigation sites: measured and calculated thermal conductivity, specific heat capacity and thermal diffusivity*. Working Report (unpublished), Geological Survey of Finland, Helsinki.
- Lachenbruch, A.H. (1968). Preliminary geothermal model of the Sierra Nevada. *Journal of Geophysical Research*, 73, 6977-89.
- Lees, C. H. (1910). On the shapes of the isotherms under mountain ranges in radio-active districts. *Proceedings of the Royal Society of London. Series A, Containing Papers of a Mathematical and Physical Character*, 83(563), 339-346.
- Lee, W. H., & Uyeda, S. (Ed.) (1965). Review of heat flow data. In *Terrestrial heat flow* (87-190). Washington: American Geophysical Union.
- Lee, Y., & Deming, D. (1998). Evaluation of thermal conductivity temperature corrections applied in terrestrial heat flow studies. *Journal of Geophysical Research*, 103, 2447-2454.
- Le Pichon, X., & Angelier, J. (1979). The Hellenic arc and trench system: A key to the neotectonic evolution of the Eastern Mediterranean area. *Tectonophysics*, 60, 1-42.
- Le Pichon, X., Angelier, J., Osmaston, M. F., & Stegena, L. (1981). The Aegean Sea [and Discussion]. *Philosophical Transactions of the Royal Society of London A: Mathematical, Physical and Engineering Sciences*, 300(1454), 357-372.
- Lips, A.L.W., Cassard, D., Sözbilir, H., Yılmaz, H., & Wijbrans, J.R. (2001). Multistage exhumation of the Menderes Massif, Western Anatolia (Turkey). *International Journal of Earth Science*, 89, 781-792.
- Lowrie, W. (2007). *Fundamentals of geophysics (2nd ed.)*. New York: Cambridge University Press.

- Ma, L., & Daemen, J. J. K. (2006). An experimental study on creep of welded tuff. *International Journal of Rock Mechanics and Mining Sciences*, 43(2), 282-291.
- Maden, N. (2010). Curie-point depth from spectral analysis of magnetic data in Erciyes stratovolcano (Central TURKEY). *Pure and Applied Geophysics*, 167(3), 349-358.
- Maden, N., Aydin, A., & Kadirov, F. (2015). Determination of the crustal and thermal structure of the Erzurum-Horasan-Pasinler Basins (Eastern Türkiye) using gravity and magnetic data. *Pure and Applied Geophysics*, 172(6), 1599-1614.
- Maden, N., & Öztürk, S. (2015). Seismic b-Values, bouguer gravity and heat flow data beneath Eastern Anatolia, Turkey: Tectonic Implications. *Surveys in Geophysics*, 1-22.
- Manger, G. E. (1963). *Porosity and bulk density of sedimentary rocks: contributions to geochemistry*. Washington: United States Government Printing Office.
- Mart, Y., & Woodside, J., (1994). Preface: Tectonics of the Eastern Mediterranean. *Tectonophysics*, 234, 1-3.
- McDonough, W. F., & Sun, S. S. (1995). The composition of the Earth. *Chemical geology*, 120(3-4), 223-253.
- McKenna, J. R., & Blackwell, D. D. (2004). Numerical modeling of transient Basin and Range extensional geothermal systems. *Geothermics*, 33(4), 457-476.
- McKenzie, D. (1978). Active tectonics of the Alpine-Himalayan belt: the Aegean sea and surrounding regions. *Geophysical Journal of the Royal Astronomical Society*, 55, 217-254.
- Melnikov, N. W., Rshewski, W. W., & Prodottjakonov, M. M. (1975). Spravochnik (kadastr.) fiziceskich svoistv gornich porod. *Izdat. Nedra, Moscow*

- Mertoğlu, O., Başarır, N., & Saraçoğlu, B. (2015). Turkey's geothermal potential on EGS - Enhanced Geothermal System. *Proceedings World Geothermal Congress*. Melbourne.
- Mihçakan, M. & Öcal, M., (1998). A Survey on Geothermal Gradient Distribution in Turkey. *12th International Petroleum Congress and Exhibition of Turkey*, 12-15.
- Mihçakan, İ. M., & Öcal, M. (2000). A survey on geothermal gradient distribution in Turkey. *Turkish Journal of Oil and Gas*, 6(3), 41-53.
- Mihçakan, M., Onur, M., Ercelebi, S.G., Okay, A., Yilmazer, M. (2006). Map of subsurface temperature gradient distribution of Turkey Using deep well temperatures and variogram analysis. *TUBİTAK, Report No: YDABCAG-100Y040*, November.
- Mitsoulis, E., & Vlachopoulos, J. (1984). The finite element method for flow and heat transfer analysis. *Advances in Polymer Technology*, 4(2), 107-121.
- Morgan, P., Sawka, W. N., & Furlong, K. P. (1987). Introduction: Background and implications of the linear heat flow-heat production relationship. *Geophysical Research Letters*, 14(3), 248-251.
- Muelenkamp, J.E., Wortel, M.J.R., Van Wamel, W.A., Spakman, W., & Hoogerduyn Straring, E. (1988). On the Hellenic subduction zone and geodynamic evolution of Crete since the late Middle Miocene. *Tectonophysics*, 146, 203-215.
- Muelenkamp, J.E., Van DerZwaan, G.J., & Van Wamel, W.A. (1994). On the Late Miocene to recent vertical motions in the Cretan segment of the Hellenic arc. *Tectonophysics*, 234, 53-272.
- Mussett, A. E., & Khan, M. A. (2000). *Looking into the earth: an introduction to geological geophysics*. Newyork: Cambridge University Press.
- Nicholson, K. (2012). *Geothermal fluids: chemistry and exploration techniques*. Berlin:Springer-Verlag.

- Nieva, D., & Nieva, R. (1987). Developments in geothermal energy in Mexico—part twelve. A cationic geothermometer for prospecting of geothermal resources. *Heat recovery systems and CHP*, 7(3), 243-258.
- Okay, A. I., Satir, M., Maluski, H., Siyako, M., Monie, P., Metzger, R., et al. (1996). Paleo-and Neo-Tethyan events in northwest Turkey Geological and geochronological constraints. In A. Yin, M. Harrison (Ed.). *Tectonic Evolution of Asia*, 420–441, Cambridge: Cambridge University Press.
- Okay, A.İ., & Tüysüz, O. (1999). Tethyan Sutures of northern Turkey. In: Durand, B., Jolivet, L., Hovarth, F., and Séranne, M. (Ed.), *The Mediterranean Basins: 170 Tertiary Extension within the Alpine Orogen*. *Journal of Geological Society of London*, 156, 475–515.
- Özer, S. & Sözbilir, H. (2003). Presence and tectonic significance of Cretaceous rudist species in the so-called Permo-Carboniferous Göktepe Formation, central Menderes Massif, western Turkey. *International Journal of Earth Sciences*, 92, 397–404.
- Özyalın, Ş., Pamukçu, O., Gönenç, T., Yurdakul, A., & Sözbilir, H. (2012). Application of boundary analysis and modeling methods on Bouguer gravity data of the Gediz Graben and surrounding area in Western Anatolia and its tectonic implications. *Journal of the Balkan Geophysical Society*, 15(2), 19-30.
- Paton, S. (1992). Active normal faulting, drainage patterns and sedimentation in southwestern Turkey. *Journal of the Geological Society*, 149(6), 1031-1044.
- Papazachos, B. C., & Comninakis, P. E. (1971). Geophysical and tectonic features of the Aegean arc. *Journal of Geophysical Research*, 76(35), 8517-8533.
- Pfister, M., Ryback, L., & Şimşek, Ş. (1998). Geothermal reconnaissance of the Marmara Sea region (NW Turkey): surface heat flow density in an area of active continental extension. *Tectonophysics*, 291, 77–89.

- Poelchau, H. S., Baker, D. R., Hantschel, T., Horsfield, B., & Wygrala, B. (1997). Basin simulation and the design of the conceptual basin model. In *Petroleum and basin evolution* (3-70). Berlin: Springer.
- Pollack, H. N., & Chapman, D. S. (1977). On the regional variation of heat flow, geotherms, and lithospheric thickness. *Tectonophysics*, 38(3-4), 279-296.
- Popov, Y. A., Pevzner, L. A., Romushkevich, R. A., Korostelev, V. M., & Vorob'yev, M. G. (1995). Thermophysical and geothermal sections obtained from Kolvinskaya well logging data. *Izvestiya Physics of the Solid Earth*, 30(9), 778-789.
- Powell, W. G., Chapman, D. S., Balling, N., & Beck, A. E. (1988). Continental heat-flow density. In *Handbook of terrestrial heat-flow density determination* (167-222). Netherlands: Springer.
- Purvis, M., & Robertson, A. (2005). Sedimentation of the Neogene–Recent Alaşehir (Gediz) continental graben system used to test alternative tectonic models for western (Aegean) Turkey. *Sedimentary Geology*, 173(1), 373-408.
- Rimmelé, G., Oberhänsli, R., Goffé, B., Jolivet, L., Candan, O., & Çetinkaplan, M. (2003). First evidence of high-pressure metamorphism in the 'Cover Series' of the southern Menderes Massif. Tectonic and metamorphic implications for the evolution of SW Turkey. *Lithos*, 71, 19– 46.
- Ring, U., Glodny, J., Will, T., & Thomson, S. (2010). The Hellenic Subduction System: High-Pressure Metamorphism, Exhumation, Normal Faulting, and Large-Scale Extension. *Annual Review of Earth and Planetary Sciences*, 38, 45-76.
- Robertson, E., C. (1988). Thermal conductivity of rocks. Retrieved May 15, 2014, from <https://pubs.usgs.gov/of/1988/0441/report.pdf>.
- Roy, R. F., Blackwell, D. D., & Decker, E. R. (1972). Continental heat flow. In *The nature of the solid earth* (506–543). New York: McGraw Hill.

- Rybach, L. (1988). Determination of heat production rate. In *Handbook of Terrestrial Heat Flow Density Determination*, 125-142. London: Springer Science & Business Media.
- Quiel, F. (1975). Thermal/IR in geology. *Photogrammetric Engineering and Remote Sensing*, 41(3).
- Sari, C., & Şalk, M. (2006). Sediment thicknesses of the western Anatolia graben structures determined by 2D and 3D analysis using gravity data. *Journal of Asian Earth Sciences*, 26(1), 39-48.
- Sarıca N. (2000) The Plio-Pleistocene age of Büyük Menderes and Gediz grabens and their tectonic significance on N-S extensional tectonics in West Anatolia: mammalian evidence from the continental deposits. *Geological Journal*, 35, 1–24.
- Sass, J. H., Lachenbruch, A. H., Moses, T. H., & Morgan, P. (1992). Heat flow from a scientific research well at Cajon Pass, California. *Journal of Geophysical Research: Solid Earth*, 97(B4), 5017-5030.
- Satman, A. (2007). Türkiye'nin jeotermal enerji potansiyeli. *8.Ulusal Tesisat Mühendisliği Kongresi-Teskon*, 3-18.
- Sayıl, N., & Osmanşahin, İ. (2008). An investigation of seismicity for western Anatolia. *Natural Hazards*, 44(1), 51-64.
- Schatz, J. F., & Simmons, G. (1972). Thermal conductivity of earth materials at high temperatures. *Journal of Geophysical Research*, 77(35), 6966-6983.
- Seipold, U. (1998). Temperature dependence of thermal transport properties of crystalline rocks—a general law. *Tectonophysics*, 291(1), 161-171.
- Sekiguchi, K. (1984). A method for determining terrestrial heat flow in oil basinal areas. *Tectonophysics*, 103(1), 67-79.
- Serpen, U., (2006). Status of geothermal energy and its utilization in Turkey. *Geothermal Resources Council Transactions*, 30, 683–688.

- Serpen, U., & Mihcakan, M. (1999). Heat flow and related geothermal potential of Turkey. *Geothermal Resources Council Transactions*, 23, 485-490.
- Serpen, U., Aksoy, N., & Öngür, T. (2010). Present Status of Geothermal Energy in Turkey. *Proceedings, Thirty-Fifth Workshop on Geothermal Reservoir Engineering, Stanford University*.
- Seyitoglu, G. (1997). The Simav graben: an example of young E–W trending structures in the late Cenozoic extensional system of western Turkey. *Turkish Journal of Earth Sciences*, 6, 135-142.
- Seyitoğlu, G., & Scott, B.C. (1992). Late Cenozoic volcanic evolution of the northeastern Aegean region. *Journal of Volcano and Geothermal Research*, 54, 157–176.
- Seyitoğlu, G., Scott, B.C., & Rundle, C.C. (1992). Timing of Cenozoic extensional tectonics in west Turkey. *Journal of the Geological Society*, 149, 533–538.
- Seyitoğlu, G., & Scott, B. C. (1996). Age of the Alaşehir graben (west Turkey) and its tectonic implications. *Geological Journal*, 31(1), 1-11.
- Schön, J. (2011). *Physical properties of rocks: A workbook* (Vol. 8). Netherlands: Elsevier.
- Sclater, J., Jaupart, C., & Galson, D. (1980). The heat flow through oceanic and continental crust and the heat loss of the Earth. *Reviews of Geophysics*, 18(1), 269-311.
- Somerton, W. H. (1992). *Thermal properties and temperature-related behavior of rock/fluid systems* (Vol. 37). Netherlands: Elsevier.
- Sonney, R., & Vuataz, F. D. (2010). Validation of chemical and isotopic geothermometers from low temperature deep fluids of northern Switzerland. *Proceedings World Geothermal Congress*, 14(1423), 1-12.

- Sözbilir, H. (2001). Extensional tectonics and the geometry of related macroscopic structures: field evidence from the Gediz detachment, western Turkey. *Turkish Journal of Earth Sciences*, 10, 51–67.
- Sözbilir, H. (2002). Geometry and origin of folding in the Neogene sediments of the Gediz Graben, western Anatolia, Turkey. *Geodinamica Acta*, 15, 277–288.
- Sözbilir, H., & Emre, T. (1996). Supradetachment basin and rift basin developed during the neotectonic evolution of the Menderes Massif. *49th Geological Congress of Turkey*, 30–31.
- Spakman, W., Wortel, M.J.R., & Vlaar, N.J. (1988). The Hellenic subduction zone: a tomographic image and its geodynamic implications. *Geophysical Research Letters*, 15, 60-63.
- Spector, A., & Bhattacharyya, B. K. (1966). Energy spectrum and auto correlation functions of anomalies due to dikes; the complex gradient method. *Geophysics*, 46, 1572-1578.
- Sümer, Ö., İnci, U., & Sözbilir, H. (2013). Tectonic evolution of the Söke Basin: extension-dominated transtensional basin formation in western part of the Büyük Menderes Graben, Western Anatolia, Turkey. *Journal of Geodynamics*, 65, 148-175.
- Swanberg, C. A., & Morgan, P. (1978). The linear relation between temperatures based on the silica content of groundwater and regional heat flow: a new heat flow map of the United States. *Pure and Applied Geophysics*, 117(1-2), 227-241.
- Swanberg, C. A., & Morgan, P. (1980). The silica heat flow interpretation technique: assumptions and applications. *Journal of Geophysical Research: Solid Earth*, 85(B12), 7206-7214.
- Sweet, J. N. (1978). *Pressure effects on thermal conductivity and expansion of geologic materials*. MSc Thesis, Sandia National Laboratories, California.

- Sweet, J. N., Roth, E. P., & Moss, M. (1987). Thermal conductivity of Inconel 718 and 304 stainless steel. *International Journal of Thermophysics*, 8(5), 593-606.
- Şalk, M., Pamukçu, O., & Kaftan, İ. (2005). Determination of the Curie point depth and heat flow from magsat data of western Anatolia. *Journal of Balkan Geophysical Society*, 8, 149-160.
- Şengör, A. C. (1979). *Türkiye'nin neotektoniğinin esasları*. Department of Geological Sciences, State University of New York.
- Şengör, A.M.C. (1980). Mesozoic-Cenozoic tectonic evolution of Anatolia and surrounding regions. *Bulletin Bureau de Recherches Géologiques et Minières, France*, 115, 1–137.
- Şengör, A.M.C. (1987). Cross-faults and differential stretching of hanging walls in regions of low-angle normal faulting: examples from western Turkey, in: Coward M.P., Dewey J.F., Hancock P.L. (Eds.), *Continental Extensional Tectonics. Geological Society Special Publication*, 28, 575–589.
- Şengör, A. M. C., Görür, N., & Şaroğlu, F. (1985). Strike-slip faulting and related basin formation in zones of tectonic escape: Turkey as a case study. In K. T. Biddle, & N. Christie-Blick, (Eds.) *Strike-slip faulting and basin formation* (227-264). *Society of Economic Paleontologists and Mineralogists Special Publication*.
- Şengör, A.M.C., White, G., & Dewey, J.F. (1979). Tectonic evolution of the Bitlis Suture, southeastern Turkey: implications for the tectonics of the Eastern Mediterranean Rapp. Comm. *International Mer Méditerranée*, 25/26. 95–97.
- Şengör, A.M.C., & Yılmaz, Y. (1981). Tethyan evolution of Turkey: A plate tectonic approach. *Tectonophysics*, 75, 181–241.
- Şengör, A. M. C., Yılmaz, Y., & Sungurlu, O. (1984). Tectonics of the Mediterranean Cimmerides: nature and evolution of the western termination of Palaeo-Tethys. *Geological Society, London, Special Publications*, 17(1), 77-112.

- Şensoy, S., Demircan, M., Ulupınar, U., Balta, İ. (2008). Türkiye iklim atlas. *Turkish State Meteorological Service (DMI)*, Ankara.
- Tester, J. W., Anderson, B. J., Batchelor, A. S., Blackwell, D. D., DiPippo, R., Drake, E. M., et al. (2006). The future of geothermal energy. *Impact of Enhanced Geothermal Systems (EGS) on the United States in the 21st Century*, Massachusetts Institute of Technology, Cambridge, MA, 372.
- Tezcan, A. K. (1979). Geothermal studies, their present status and contribution to heat flow contouring in Turkey. In *Terrestrial heat flow in Europe* (283-292). Springer Berlin Heidelberg.
- Tezcan, A. A., & Turgay, I. (1989). *Türkiye ısı akısı haritası*. MTA, Jeofizik Etütleri Daire Başkanlığı, Ankara.
- Tezcan, A. K. & Turgay, M. I. (1991). Heat flow and temperature distribution in Turkey. *Geothermal atlas of Europe*. Gotha: Herman Haack Verlag.
- Tezcan, A.K. (1995). Geothermal explorations and heat flow in Turkey. In *Terrestrial heat flow and geothermal energy in Asia* (23-42). Rotterdam: August Aime Balkema.
- Thakur, M., Blackwell, D. D., & Erkan, K. (2012). The Regional thermal regime in Dixie Valley, Nevada, USA. *Geothermal Resources Council Transactions*, 36, 59-67.
- Thienprasert, A., & Raksaskulwong, M. (1984). Heat flow in northern Thailand. *Tectonophysics*, 103(1-4), 217-233.
- Tonani, F. B. (1980). Some remarks on the application of geochemical techniques in geothermal exploration. In *Advances in European Geothermal Research* (428-443). Springer Netherlands.
- The Scientific and Technological Research Council of Turkey (TUBITAK) report No: 113R019 (2016). *Development of a temperature-depth measurement system and investigations on the last two-century climate change in Turkey*, İstanbul.

- Truesdell, A.H., (1976). GEOTHERM, a geothermometric computer program for hot spring systems. *Proceedings of Second United Nations Symposium on the Development and Use of Geothermal Resources*, 831–836.
- Tüfekçi, N., Süzen, M. L., & Güleç, N. (2010). GIS based geothermal potential assessment: A case study from Western Anatolia, Turkey. *Energy*, 35(1), 246-261.
- Ünalın, G., & Öngür, T., (1979). Geothermal gradient and temperature investigation at 1000 m depth at some of basins of Turkey. *Geocome-1 1st Geological Congress of the Middle East*, 637-648.
- Van Hinsbergen, D.J.J., Hafkenscheid, E., Spakman, W., Meulenkaup, J.E., & Wortel, R. (2005). Nappe stacking resulting from subduction of oceanic and continental lithosphere below Greece. *Geology*, 33, 325–328.
- Van Hinsbergen, D.J.J., Dekkers, M.J., Bozkurt, E., & Koopman, M. (2010). Exhumation with a twist: Paleomagnetic constraints on the evolution of the Menderes metamorphic core complex, western Turkey. *Tectonics*, 29(3), 1-33.
- Verma, M. P. (2000). Revised quartz solubility temperature dependence equation along the water–vapor saturation curve. *World Geothermal Congress*, 1927-1932.
- Verma, S. P., & Santoyo, E. (1997). New improved equations for NaK, NaLi and SiO₂ geothermometers by outlier detection and rejection. *Journal of Volcanology and Geothermal Research*, 79(1), 9-23.
- Verma, S. P., Quiroz-Ruiz, A., & Díaz-González, L. (2008). Critical values for 33 discordancy test variants for outliers in normal samples up to sizes 1000, and applications in quality control in Earth Sciences. *Revista Mexicana de Ciencias Geológicas*, 25(1), 82-96.
- Vilà, M., Fernández, M., & Jiménez-Munt, I. (2010). Radiogenic heat production variability of some common lithological groups and its significance to lithospheric thermal modeling. *Tectonophysics*, 490(3), 152-164.

- Warren, N. W., & Latham, G. V. (1970). An experimental study of thermally induced microfracturing and its relation to volcanic seismicity. *Journal of Geophysical Research*, 75(23), 4455-4464.
- Wyss, M., & McNutt, S. R. (1998). Temporal and three-dimensional spatial analyses of the frequency–magnitude distribution near Long Valley Caldera, California. *Geophysical Journal International*, 134(2), 409-421.
- Wyss, M., & McNutt, S. R. (1998). Temporal and three-dimensional spatial analyses of the frequency–magnitude distribution near Long Valley Caldera, California. *Geophysical Journal International*, 134(2), 409-421.
- Yazman, M. K., Güven, A., Ermiş, Y., Yılmaz, M., Özdemir, İ., Akçay, Y., et al. (1998). Alaşehir Grabeni'nin ve Alaşehir-1 Prospektinin Değerlendirme Raporu (yayımlanmamış), Türkiye Petrolleri Anonim Ortaklığı, Ankara.
- Yazman, M. K., Çopur, S., Özdemir, İ., İztan, Y. H., Sayılı, A., & Batı, Z. (2004). *Büyük Menderes Grabeni'nin (Germencik- Denizli arası) jeolojisi, petrol olanakları ve Nazilli-1 arama kuyusu*. Teknik rapor (No: 4546) (yayımlanmamış), Türkiye Petrolleri Anonim Ortaklığı, Ankara.
- Yavuz, A. B., Turk, N., & Koca, M. Y. (2005). Material properties of the Menderes Massif marbles from SW Turkey. *Engineering geology*, 82(2), 91-106.
- Yılmaz, Y., Genç, Ş.C., Gürer, F., Bozcu, M., Yılmaz, K., Karacık, et al. (2000). When did the Western Anatolian grabens begin to develop? In: Bozkurt, E. Winchester, J.A. & Piper J.A.D. (Ed), *Tectonics and Magmatism in Turkey and the Surrounding Area*. *Journal of Geological Society of London*, 173, 131–162.
- Yemen, Y. (1999). *Ege bölgesi ısı akısı dağılımı*. MSc. Thesis, Süleyman Demirel Üniversitesi, Isparta
- Yolsal, S., Kilinc, H., Çağlar, I., & Taymaz, T. (2005). The Relationship between heat flow regime and active tectonics inferred from seismological data in western Anatolia. *Proceedings World Geothermal Congress*.

Yusufođlu, H. (1996). Northern margin of the Gediz graben: age and evolution, west Turkey. *Turkish Journal of Earth Sciences*, 5(1), 11-23.

Zienkiewicz, O. C., & Cheung, K. (1965). Finite elements in the solution of field problems. *Engineer*, 200, 507–510.

Zoth, G., & Haenel, R. (1988). Appendix. In *Handbook of terrestrial heat-flow density determination* (449-468). Netherlands: Springer.

